A Model-based Framework for Optimal Systems Integration of Adsorption Chillers

Ein modellgestützter Ansatz für die optimale Systemintegration von Adsorptionskältemaschinen

Von der Fakultät für Maschinenwesen der
Rheinisch-Westfälischen Technischen Hochschule Aachen
zur Erlangung des akademischen Grades eines
Doktors der Ingenieurwissenschaften
genehmigte Dissertation

vorgelegt von

Andrej Gibelhaus

Berichter: Univ.-Prof. Dr.-Ing. André Bardow
Univ.-Prof. Dr.-Ing. Dirk Müller

Tag der mündlichen Prüfung: 17.03.2021

Aachener Beiträge zur Technischen Thermodynamik Band 31

Andrej Gibelhaus
A Model-based Framework for Optimal Systems Integration of Adsorption Chillers
Ein modellgestützter Ansatz für die optimale Systemintegration von Adsorptionskältemaschinen

ISBN: 978-3-95886-406-1

Bibliografische Information der Deutschen Bibliothek
Die Deutsche Bibliothek verzeichnet diese Publikation in der Deutschen Nationalbibliografie; detaillierte bibliografische Daten sind im Internet über http://dnb.ddb.de abrufbar.

Herstellung & Vertrieb:

1. Auflage 2021
© Wissenschaftsverlag Mainz GmbH - Aachen
Süsterfeldstr. 83, 52072 Aachen
Tel. 0241 / 87 34 34 00
www.Verlag-Mainz.de

ISSN: 2198-4832

Satz: nach Druckvorlage des Autors
Umschlaggestaltung: Druckerei Mainz

printed in Germany
D82 (Diss. RWTH Aachen University, 2021)

Danksagung

Die vorliegende Arbeit entstand im Rahmen meiner Tätigkeit als wissenschaftlicher Mitarbeiter am Lehrstuhl für Technische Thermodynamik der Rheinisch-Westfälischen Technischen Hochschule Aachen. Ein besonderer Dank gilt meinem Doktorvater Univ.-Prof. Dr.-Ing. André Bardow für das entgegengebrachte Vertrauen und die Betreuung der Promotion. Seine andauernde Motivation und die fruchtbaren Diskussionen haben entscheidend zum erfolgreichen Abschluss dieser Arbeit beigetragen. Weiterhin danke ich Univ.-Prof. Dr.-Ing. Dirk Müller für die Übernahme des Koreferats und sein Interesse an meiner Arbeit sowie Univ.-Prof. Dr.-Ing. Klaus Radermacher für die Übernahme des Prüfungsvorsitzes und die angenehme Leitung der Prüfung.

Mein herzlicher Dank gilt allen Kolleginnen und Kollegen am Lehrstuhl für Technische Thermodynamik für die außergewöhnliche und freundschaftliche Arbeitsatmosphäre, die maßgeblich zu meiner tollen Zeit am Lehrstuhl beigetragen hat. Insbesondere danke ich meiner Arbeitsgruppe Sorptionstechnologie: Franz Lanzerath danke ich für Einarbeitung und Betreuung in den ersten Jahren. Heike Schreiber danke ich für ihre hilfsbereite Art und Meltem Erdogan für Tipps bei experimentellen Arbeiten. Uwe Bau möchte ich für die großartige Vorarbeit und den immer hilfreichen Austausch auch über die Arbeit hinaus danken. Stefan Graf danke ich für sein Engagement für viele großartige Freizeitaktivitäten mit der Arbeitsgruppe und Jan Seiler für die tolle gemeinsame Zeit im Büro. Dominik Tillmanns danke ich für seine stets gute Laune und Mirko Engelpracht für seinen unermüdlichen Einsatz im Labor. Marten Entrup und Matthias Henninger danke ich für das Hochhalten der Adsorptionskältemaschinen Fahne. Patrik Postweiler möchte ich für die großartige Master-Thesis und die Zusammenarbeit danach danken. Außerhalb meiner Arbeitsgruppe gilt ein großer Dank Leif Kröger für die unzähligen Stunden am und außerhalb des Lehrstuhls.

Darüber hinaus danke ich auch allen Studenten, die ich während meiner Zeit am Lehrstuhl betreuen durfte: Tanaphum Tangkrachang, Ruth Seeger, Tobias Gülker, Julian Lützow, Toni Busch, Leo Holzhauer, Patrik Dossow und Christoph Höges haben durch ihre Arbeiten zum Gelingen dieser Arbeit beigetragen.

Weiterhin möchte ich auch allen fest angestellten Mitarbeitern am Lehrstuhl danken, die den Lehrstuhl am Laufen halten und das familiäre Umfeld prägen. Besonderer Dank gilt

Prof. Dr.-Ing. Hans-Jürgen Koß für seine herzliche Art und die fachmännischen Fahrrad Beratungen. Eva Frach, Katrin Roßbruch und Dr.-Ing. Thorsten Brands danke ich für die Unterstützung bei allen Vertragsangelegenheiten und Iris Wallraven für die Organisation des Promotionsverfahrens. Gregor Migas danke ich für das Lösen sämtlicher IT-Probleme und für seinen ansteckenden Sportsgeist. Thomas Bungert, Edgar Brauers und Djuro Dragas möchte ich für die praktische Unterstützung bei dem einen oder anderen Nebenprojekt danken.

Ein großer Dank gilt meiner Familie, die mich während meiner gesamten Zeit begleitet und unterstützt hat: Ich danke meinen Eltern für ihr Vertrauen, ihre Zuversicht und ihre Unterstützung, auf die ich in jeder Lebenslage zählen konnte. Meiner Frau Regina danke ich ganz herzlich für ihre Unterstützung, ihre unfassbare Geduld und ihre Fähigkeit mich stets aufzumuntern. Ich bin unendlich dankbar dich so lange an meiner Seite zu haben und freue mich auf unseren nächsten Lebensabschnitt. Nicht zuletzt danke ich meinem Sohn Vincent, der es immer schafft mir ein Lächeln zu entlocken und die Arbeit vergessen zu machen. Danke für alles!

Aachen, im März 2021 *Andrej Gibelhaus*

'All models are wrong, but some are useful.'

George E. P. Box (1919-2013)

Contents

List of Figures

List of Tables

Notation

Latin symbols

a	annuity	
A	area	m^2
A	adsorption potential	J/kg
c	specific heat capacity	$\mathrm{J/(kg\,K)}$
c	specific costs	$\mathrm{EUR/(kW\,h)}$
C	heat capacity	J/kg
C	Sieder-Tate constant	
C	Costs	EUR
$\dot{C}$	heat capacity flow	W/K
d	diameter	m
D	diffusion coefficient	m^2/s
f	function	
$F'(\tau\alpha)_{\mathrm{en}}$	zero loss efficiency	
G	irradiation	$\mathrm{W/m}^2$
h	specific enthalpy	J/kg
h	heat transfer coefficient	$\mathrm{W/(m}^2\,\mathrm{K)}$
i	specific investment costs	EUR/kW
i	interest rate	%
L	length	m
m	mass	kg
$\dot{m}$	mass flow rate	kg/s
n	lifetime	a
n	number	
p	constant parameter	
p	pressure	bar
P	power	W
$\dot{q}$	specific heat flow rate	$\mathrm{W/m}^3$

Q	thermal energy	J
$\dot{Q}$	heat flow rate	W
r	radius	m
R	universal gas constant	J/(kg K)
t	time	s
T	temperature	°C or K
u	specific internal energy	J/kg
u	control variables	
U	internal energy	J
U	overall heat transfer coefficient	W/(m^2 K)
v	velocity	m s
V	volume	m^3
$\dot{V}$	volume flow rate	m^3/s
w	loading	g/g
W	filled pore volume	m^3/kg
W	work	J
x	differential state	
x	space dimension	m
z	algebraic state	

Greek symbols

α	thermal expansion coefficient	1/K
Δ	difference	
ϵ	effectiveness	
ζ	resistance coefficient	
η	efficiency	
λ	thermal conductivity	J/(m K)
μ	chemical potential	J/mol
ξ	friction factor	
ρ	density	kg/m^3
τ	operating hours	h
Φ	objective function	

Subscripts and superscripts

0	nominal

A	adsorber
AC	adsorption chiller
ad	adsorbed phase
ads	adsorption
air	air
alone	stand-alone
amb	ambient
annual	annual
ap	aperture
ax	axial
bed	adsorbent bed
bond	bonding difference
C	condenser
chill	chilling
coll	collector
comp	compressor
cond	condensation
cool	cooling
cooler	cooling tower
cycle	cycle
des	desorption
drive	driving
E	evaporator
eff	effective
el	electrical
evp	evaporation
eq	equilibrium
eq	equivalent
ext	external
fan	fan
fl	heat exchanger fluid
FL	full load
GC	gas cooler
h	hydraulic
heat	heating
helix	helix
high	high level
hx	heat exchanger
hyb	hybrid
i	index parameter

i	inner
in	inlet
inf	inflation
init	initial
int	interest
int	internal
invest	investment
irr	irradiation
is	isentropic
iso	isosteric
j	index parameter
liq	liquid
loss	loss
low	low level
m	mean
maint	maintenance
max	maximal
meas	measured
min	minimal
model	model
o	outer
op	operating
opt	optimal
out	outlet
p	isobaric
P	pump
particle	particle
peak	peak
port	port
rad	radial
ref	reference
refrig	refrigeration
reject	heat rejection
sat	saturated
sim	simulated
sor	adsorbent
ST	Sieder-Tate
sup	superheating
surface	surface
tot	total

v	vapor phase
v	isochoric
waste	waste heat

Abbreviations and Acronyms

COP	coefficient of performance (J/J)
CV	coefficient of variation
DAE	differential algebraic equation
disc	discretized
EER	energy efficiency ratio
GHG	greenhouse gas
GWP	global warming potential
HX	heat exchanger
IEA	International Energy Agency
LDF	linear driving force
NTU	number of transfer units
ODE	ordinary differential equation
PDE	partial differential equation
PF	plug-flow
R&D	research and development
RMSD	root mean square deviation
SCP	specific cooling power (W/kg)
SHC	solar heating and cooling
SR	size ratio
s.t.	subject to
VLE	vapor-liquid equilibrium

Kurzfassung

Der weltweite Kühlbedarf nimmt zu und stellt dadurch eine Herausforderung für die Netzstabilität und die Emissionsziele dar. Adsorptionskältemaschinen können dieser Herausforderung begegnen, indem sie Strom durch thermische Energie substituieren. Obwohl Adsorptionskältemaschinen hauptsächlich durch thermische Energie angetrieben werden, zeigen Erfahrungen aus der Praxis, dass die Stromeinsparungen oft kaum ausreichen, um den Bedarf der Peripherie, z.B. Pumpen und Lüfter, zu kompensieren. Daher ist eine intelligente Systemintegration entscheidend. Die Systemintegration ist anspruchsvoll, da folgende Aspekte zusammenkommen: (1) intrinsische Dynamik; (2) enge Interaktion zwischen den Systemkomponenten; und (3) starker Einfluss der Auslegung, Steuerung und Betriebsbedingungen. Diese Aspekte führen zu einer Vielzahl an Freiheitsgraden, die eine einfache Auslegung und Steuerung erschweren.

Um die genannten Herausforderungen anzugehen, stellt diese Arbeit Modelle und Methoden zur optimalen Systemintegration von Adsorptionskältemaschinen bereit. Zunächst wird ein Modell entwickelt, das genau genug ist, um relevante Eigenschaften auf Systemebene abzubilden, aber gleichzeitig numerisch effizient genug ist für modellgestützte Optimierungen. Die Modellgüte wird durch eine Kalibrierung und Validierung für zwei verschiedene Adsorptionskältemaschinen demonstriert, eine Ein-Bett Anlage im Labormaßstab und eine kommerzielle Zwei-Bett Anlage.

Anschließend wird das Modell für zwei Bereiche der Systemintegration verwendet: die Integration in Hybridsysteme und die Integration innerhalb der Peripherie. Als Beispiel für die Integration in Hybridsysteme wird eine Adsorptionskältemaschine in einen CO_2-Kompressionskältekreislauf integriert, um effizient Kälte mit natürlichen Kältemitteln bereitzustellen. Für das Hybridsystem wird ein hohes Energieeinsparungspotenzial identifiziert, das durch eine optimale Auslegung und Steuerung voll ausgeschöpft werden kann. Die demonstrierte Integration in Hybridsysteme dient gleichzeitig als Beispiel für eine konzeptionelle Integration, die das Potenzial einer bestimmten Anwendung quantifiziert.

Für die Integration innerhalb der Peripherie, wird eine optimierungsbasierte Methode vorgestellt zur detaillierten Dimensionierung und Steuerung aller Systemkomponenten inklusive der Peripherie. Die vorgestellte Methode wird exemplarisch für ein solarthermisch angetriebenes Adsorptionskältesystem demonstriert und liefert jeweils eine energetisch und eine wirtschaftlich optimale Auslegung und Steuerung. Zusammenfassend stellt die Arbeit einen umfassenden Ansatz für die optimale Systemintegration von Adsorptionskältemaschinen bereit: von der Modellvalidierung über die konzeptionelle Integration bis hin zur detaillierten Auslegung und Steuerung.

Abstract

The global demand for cooling increases and poses a challenge for the stability of electrical grids and the emission targets. Thermally-driven adsorption chillers can meet this challenge by substituting electricity with thermal energy. However, although adsorption chillers are primarily driven by thermal energy, practical experience shows that the electricity savings often hardly compensate the electricity demand of the auxiliaries, such as pumps and fans. Thus, smart systems integration is crucial. Systems integration of adsorption chillers is challenging due to several features: (1) intrinsic dynamics; (2) close interaction between various system components; and (3) strong coupling of design, control, and operating conditions. These features lead to a variety of degrees of freedom, which make it difficult to use simple design and control rules for systems integration.

To move towards optimal systems integration of adsorption chillers, this thesis provides appropriate models and methods. First of all, a model of an adsorption chiller is developed, which is accurate enough to consider quantities needed on system level, but also computationally sufficiently efficient for model-based optimizations. To demonstrate the model accuracy, the model is calibrated and validated for two types of adsorption chillers, a lab-scale one-bed adsorption chiller and a commercial two-bed adsorption chiller.

Subsequently, the presented model is used for two areas of systems integration: the integration in hybrid systems and the integration within the auxiliaries. To exemplify the integration in a hybrid system, an adsorption chiller is integrated into a CO_2 vapor compression cycle to efficiently provide refrigeration with natural refrigerants only. The exemplified integration identifies a significant potential for energy savings, which can be fully exploited by optimal design and control of the hybrid system. The demonstrated integration in hybrid systems is also an example for a conceptual integration, which quantifies the potential of a specific application.

To integrate the adsorption chiller within the auxiliaries, an optimization-based method is presented for detailed sizing and control of all system components including auxiliaries. The presented method is demonstrated for a solar-thermally-driven adsorption chiller system and determines both, an energetically and an economically optimal design and control. In summary, the thesis provides a comprehensive framework for optimal systems integration of adsorption chillers: from model validation over conceptual integration to detailed design and control.

CHAPTER 1

Introduction

Limiting global warming is one of the major challenges of the 21st century (United Nations, 2015). Limiting global warming to a maximal increase of the global average temperature below 2 °C (desirable below 1.5 °C) compared to pre-industrial levels, requires a drastic reduction of the worldwide greenhouse gas (GHG) emissions (Intergovernmental Panel on Climate Change, 2018). Refrigeration significantly contributes to global GHG emissions since more than 17 % of the world's electricity demand are used for refrigeration (Coulomb, 2016). While GHG emissions from electricity production could be avoided by integrating renewable energies, 14-35 % of the total GHG emissions of refrigeration result from the leakage of the refrigerants (Wu et al., 2013). The leakage has a high contribution to GHG emissions due to the high global warming potential (GWP) of commonly used refrigerants (Beshr et al., 2016). To reduce the emissions from leakage, low-GWP refrigerants are needed (Ciconkov, 2018).

Thermally-driven adsorption chillers combine the utilization of both, natural low-GWP refrigerants, such as water (Choudhury et al., 2013), and environmentally friendly driving energies, such as waste-heat or renewable heat sources (Meunier, 2013). Thus, adsorption chillers have the potential to provide a sustainable alternative to conventional vapor-compression chillers (Choudhury et al., 2013). However, adsorption chillers are often criticized for poor performance (Li et al., 2015; Meunier, 2013) and high investment costs (Eisentraut and Brown, 2014) compared to conventional chillers. To tackle both points of criticism, a lot of effort was put into improving the adsorption chiller itself in the past years by exploring new working pairs (Aristov, 2013), designing the heat exchanger (Freni et al., 2015), sizing the components (Lanzerath et al., 2015), developing advanced cycles (Li et al., 2015), and optimizing the control (Bau et al., 2019; Gräber et al., 2011). Nevertheless, adsorption chillers remain a niche technology in refrigeration (Mugnier and Jakob, 2015).

In practice, adsorption chillers often suffer from a poor system-level performance (Jaehnig and Thuer, 2011): Although adsorption chillers are primarily driven by thermal energy, auxiliaries, such as pumps and fans, are still required at system-level to provide and to reject the thermal energy. These auxiliaries can consume a significant amount of electricity (Speerforck and Schmitz, 2015), which diminishes the main advantage of adsorption chillers to replace electricity by thermal energy. As a result, the electrical efficiency of adsorption chiller systems is often only marginally higher than that of conventional vapor compression chillers (Weber et al., 2014).

To address these issues and to support wider market penetration of adsorption chillers, the International Energy Agency started Task 48 of the solar heating and cooling (SHC) programme. The main objective of Task 48 was to assist in the development of a strong and sustainable market for thermally-driven chillers by considering all main system components (International Energy Agency, 2015). In the position paper of Task 48, leading experts in the field concluded (Mugnier, 2015):

> "The components for solar thermally driven cooling have reached a high level of maturity. Instead, the main technical problems today lie at the system level in the proper design and operational control of fully integrated systems. Both, public and private R&D efforts are needed to further improve solar thermally driven cooling at the system level."

This thesis addresses the conclusion of the experts by moving towards optimal systems integration of adsorption chillers. For this purpose, we[1] pursue a model-based approach and employ mathematical optimization.

Structure of the thesis

In this thesis, we aim at improving the use of adsorption chillers by focusing on the systems integration, i.e., the interaction between the different system components. Therefore, we cover three important topics of systems integration: 1) development and validation of efficient models, 2) integration in hybrid systems, and 3) integration within the auxiliaries. Adsorption chillers are a representative class of adsorption-based technologies. Most of the developed models and methods are transferable to other adsorption-based technologies, such as heat pumps, heat transformers, and thermal storage units.

In Chapter 2, we present the state of the art in systems integration of adsorption chillers by introducing the working principle and the main characterization measures, describing available modeling approaches, and reviewing integration in hybrid systems as well as

[1] This thesis is written in the *pluralis modestiae* to avoid the excessive use of passive voice.

integration within the auxiliaries. Based on the state of the art, we derive the main conclusions and outline the contributions of the thesis.

In Chapter 3, we present an efficient and accurate adsorption chiller model suitable for systems integration. In particular, we propose an operator splitting approach to avoid the computationally expensive discretization of the heat exchangers of the adsorption chiller. The proposed approach allows us to achieve the accuracy of an experimentally validated, state-of-the-art model but with a considerable increase in computational efficiency. To demonstrate the applicability of the proposed model, we calibrate and validate the model for two types of adsorption chillers: a lab-scale one-bed adsorption chiller and a commercial two-bed adsorption chiller.

In Chapter 4, we demonstrate the integration in hybrid systems by integrating an adsorption chiller into a CO_2 vapor compression cycle to provide low temperature refrigeration efficiently and with natural refrigerants only. Thereby, we can quantify the potential of the hybrid system to evaluate if a more detailed investigation is promising.

In Chapter 5, we propose an optimization-based method for the detailed design and control of the adsorption chiller system, including the auxiliaries. The proposed method allows for the integrated optimization of design and control of adsorption chiller systems. Thereby, we can identify the optimal system for a specific application regarding a defined objective (e.g., energy efficiency or economy). We demonstrate the proposed method for a solar-thermally-driven adsorption chiller system.

Finally, we summarize the main results and conclusions of this thesis and derive possible future research topics in Chapter 6.

CHAPTER 2

State of the art in systems integration of adsorption chillers

In this chapter, we provide an overview of the state of the art in systems integration of adsorption chillers. The system is defined, in the context of this thesis, as the combination of adsorption chillers and connected components needed for operation on the application level, such as heat source, heat sink, and auxiliaries, such as pumps and fans. Here, adsorption chillers represent an exemplary class of adsorption-based technologies. Thus, most of the presented methods and models can be transferred to other adsorption-based technologies, such as heat pumps, heat transformers, and thermal storage.

First of all, we briefly provide the fundamentals of adsorption chillers. For this purpose, we introduce the working principle and the main performance indicators used for characterization in Section 2.1. Second, we review modeling approaches to describe both, the adsorption phenomenon and the adsorption chiller in Section 2.2. Afterwards, we present the state of the art in systems integration of adsorption chillers. For this purpose, we divide the systems integration into two main topics: (1) The integration of adsorption chillers with other technologies in hybrid systems is presented in Section 2.3. (2) The integration of the main system components and auxiliaries such as heat source, heat-rejection unit, and pumps is presented in Section 2.4. Finally, we conclude the main issues and outline the contribution of this thesis in Section 2.5.

2.1 Working principle and characterization

Adsorption chillers use thermal energy as a driving source to provide useful chilling. For this purpose, adsorption chillers employ the physical principle of adsorption. In Section 2.1.1, the adsorption phenomenon and the relevant terminology are introduced. In Section 2.1.2, we explain the working principle of an adsorption chiller employing a simple adsorption chiller cycle. In Section 2.1.3, we derive the main performance indicators used to characterize adsorption chillers.

2.1.1 Adsorption phenomenon

Adsorption describes a process where a fluid in vapor or liquid phase (adsorptive) attaches to the surface of a solid (adsorbent) as schematically shown in Figure 2.1. In the following, adsorption from the vapor phase is considered only, as it is the relevant process in adsorption chillers. The attached fluid in the adsorbed phase is called adsorbate, while the combination of adsorbent and adsorbate is referred to as the working pair (Figure 2.1). Physical adsorption is a reversible process caused by forces of the surface atoms, such as van-der-Waals forces and electrostatic interaction (Ruthven, 1984). The reverse process is called desorption.

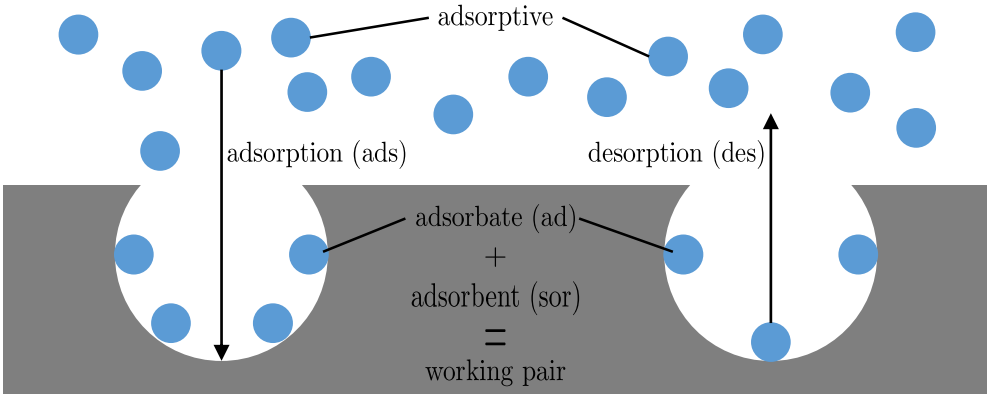

Figure 2.1: Terminology to describe the adsorption process and the states of the working fluid based on Keller and Staudt (2005). Figure based on Schnabel (2009).

The relative amount of adsorbate m_{ad} per mass of adsorbent m_{sor} is defined by the loading of the working pair w:

$$w = \frac{m_{\mathrm{ad}}}{m_{\mathrm{sor}}}. \tag{2.1}$$

Adsorption or desorption occur until the adsorptive and the adsorbate reach thermodynamic equilibrium (also called adsorption equilibrium), i.e. thermal (equal temperatures $T_{\mathrm{v}} = T_{\mathrm{ad}}$), mechanical (equal pressures $p_{\mathrm{v}} = p_{\mathrm{ad}}$) and chemical (equal chemical potentials $\mu_{\mathrm{v}} = \mu_{\mathrm{ad}}$)

equilibrium. The adsorption equilibrium is uniquely described by two independent state variables (commonly loading w, pressure p, or temperature T) according to Gibbs' phase rule (cf. Frolov and Mishin (2015)):

$$f(w, p, T) = 0. \tag{2.2}$$

Traditionally, the loading is expressed as a function of the pressure p and the temperature T (Ruthven, 1984):

$$w = w(p, T). \tag{2.3}$$

Adsorption is an exothermic process, as the energy level of the adsorbate is below the energy level of the adsorptive. Consequently, desorption is an endothermic process. The heat, either released during adsorption or needed for desorption, corresponds to the difference of specific enthalpy Δh_{ads} between the adsorptive (h_{v}) and the adsorbate (h_{ad}):

$$\Delta h_{\mathrm{ads}} = h_{\mathrm{v}} - h_{\mathrm{ad}}. \tag{2.4}$$

This enthalpy difference (also called specific enthalpy of adsorption) is an important property for technical applications, as it influences the performance (Ziegler, 2009). To determine the specific enthalpy of adsorption (Equation (2.4)), the specific enthalpy of the adsorptive is derived from the fluid properties $h_{\mathrm{v}}(p, T)$, while the specific enthalpy of the adsorbate is a property of the working pair. Thus, the specific enthalpy of the adsorbate h_{ad} can be expressed as a function of two state variables. Commonly, the temperature and loading are chosen as the independent state variables (Núñez, 2001):

$$h_{\mathrm{ad}} = h_{\mathrm{ad}}(T, w). \tag{2.5}$$

The calculation of the adsorption equilibrium (Equation (2.2)) and the specific enthalpy of the adsorbate (Equation (2.5)) requires a modeling approach, which is discussed in Section 2.2.1.

2.1.2 Simple adsorption chiller cycle

The basic principle of an adsorption chiller is similar to that of the (technically more popular) vapor-compression chiller:

1. A refrigerant is evaporated at a low pressure level to absorb heat at a low temperature level, providing useful cooling.
2. Subsequently, the evaporated refrigerant needs to be compressed to a higher pressure level to allow for condensation at a higher temperature level, rejecting heat to a heat sink (e.g., environment).
3. The cycle is closed by returning the condensed refrigerant to the evaporator.

The main difference between a conventional vapor-compression chiller and an adsorption chiller is the compression of the refrigerant. While the vapor-compression chiller uses mechanical energy to compress the refrigerant from the low to the high pressure level, the adsorption chiller employs thermal compression via adsorption. For this purpose, the evaporated refrigerant is adsorbed by the adsorbent at the low pressure level. Subsequently, the adsorbate is compressed to the high pressure level and desorbed by heating the working pair.

Commonly, a heat exchanger is employed to transfer heat to or from the working pair. The combination of the heat exchanger and working pair is called adsorber. In the same way, heat exchangers are also employed to vaporize or condense the refrigerant, corresponding to the evaporator and the condenser, respectively. Thus, the technically simplest configuration of an adsorption chiller consists of three components (adsorber, evaporator, and condenser), which are connected (e.g., by valves) to exchange the refrigerant (Figure 2.2). The corresponding simple adsorption chiller cycle consists of four phases: (1) adsorption, (2) isosteric heating, (3) desorption, and (4) isosteric cooling. These phases are illustrated by the configuration of the components in Figure 2.2 and by the thermodynamic cycle in Figure 2.3.

Generally, the adsorption chiller cycle is determined by four temperature levels:

1. the low temperature level of the evaporator, defined by the cooling application T_{cool},
2. the medium temperature level of the condenser, defined by the heat sink to reject the enthalpy of condensation $T_{\mathrm{reject}}^{\mathrm{cond}}$,
3. the medium temperature level of the adsorber in the adsorption phase, defined by the heat sink to reject the enthalpy of adsorption $T_{\mathrm{reject}}^{\mathrm{ads}}$, and
4. the high temperature level of the adsorber in the desorption phase, defined by the heat source to provide driving energy T_{heat}.

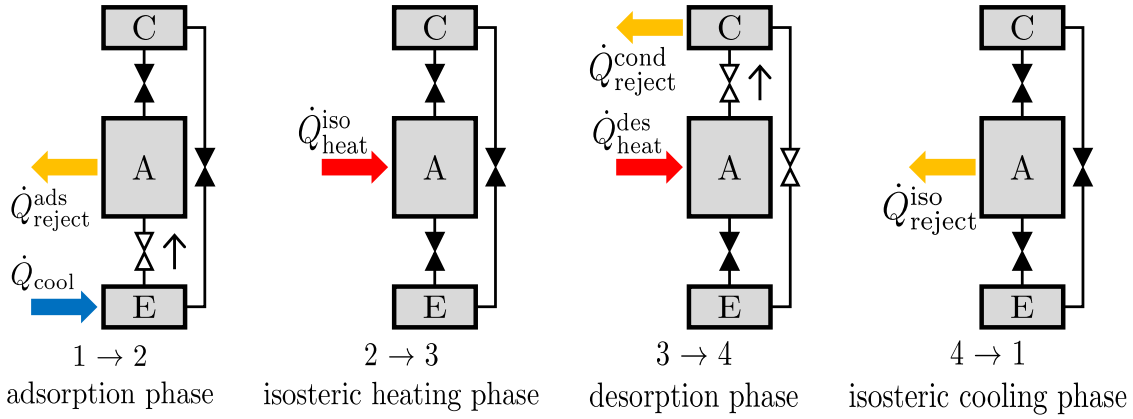

Figure 2.2: Phases of a simple adsorption chiller cycle with corresponding heat and mass flows in each component: Evaporator (E), Adsorber (A), and Condenser (C). Figure based on Lanzerath (2013).

In most technical applications, these four temperature levels are reduced to three levels (Ziegler, 2009), since the same heat sink (usually environment) is used for both, condensation and adsorption ($T^{\text{cond}}_{\text{reject}} = T^{\text{ads}}_{\text{reject}} = T_{\text{reject}}$). Therefore, we focus on a cycle with three temperature levels (i.e., $T_{\text{cool}}, T_{\text{reject}}, T_{\text{heat}}$) in the following.

1-2 Adsorption phase:

In this phase, the actual cooling heat flow $\dot{Q}_{\text{cool}}$ is absorbed by the evaporator. The absorbed heat evaporates the refrigerant at the low pressure level $p_{\text{sat}}(T_{\text{cool}})$, defined by the temperature of the cooling application T_{cool}. The evaporated refrigerant is adsorbed by the adsorber, as the evaporator is connected to the adsorber by an open valve (Figure 2.2). In the ideal cycle, the adsorption process is isobaric at the pressure level of the evaporator $p_{\text{sat}}(T_{\text{cool}})$ (Figure 2.3), which means that the refrigerant adsorbed from the vapor phase is immediately compensated by the evaporation. As adsorption is exothermic, the adsorber has to be cooled ($\dot{Q}^{\text{ads}}_{\text{reject}}$) to reject the released enthalpy of adsorption (cf. Section 2.1.1, Equation (2.4)). The adsorption phase ends, when the working pair reaches the heat-rejection temperature T_{reject}, defined by the heat sink (commonly environment). Thus, equilibrium state 2 (end of adsorption phase) is determined by the pressure of the evaporator $p_{\text{sat}}(T_{\text{cool}})$ and the heat-rejection temperature T_{reject}. Consequently, the maximal loading results from the adsorption equilibrium (Equation (2.2)) as function of the low pressure level and the heat-rejection temperature ($w_{\text{max}}(p_{\text{sat}}(T_{\text{cool}}), T_{\text{reject}})$).

2-3 Isosteric heating phase:

After the adsorption phase, the adsorbate needs to be compressed to the high pressure level $p_{\text{sat}}(T_{\text{reject}})$ of the condenser, defined by the temperature of the heat sink T_{reject}. This compression is realized by heating the adsorber ($\dot{Q}^{\text{iso}}_{\text{heat}}$) with closed valves to

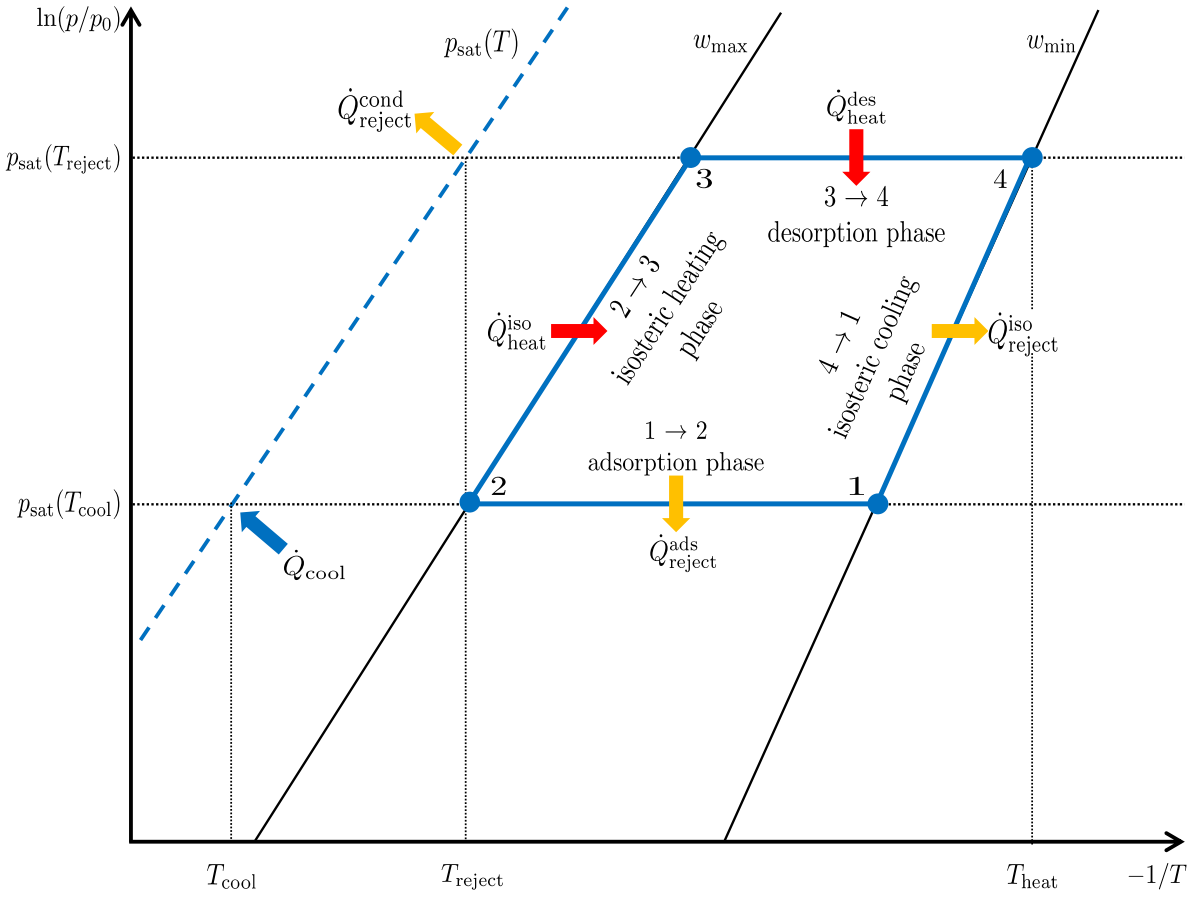

Figure 2.3: Ideal adsorption chiller cycle in an Arrhenius diagram. The transitions between the equilibrium states (1)-(4) correspond to the phases of the adsorption chiller (cf. Figure 2.2). Figure based on Núñez (2001).

both, evaporator and condenser. As both valves are closed, no significant ad- or desorption occurs so that the loading remains constant, while the temperature and the pressure of the adsorbate increase according to the equilibrium of the working pair (Equation (2.2)). Therefore this step results in isosteric heating at maximal loading w_{max}. The isosteric heating ends, when the adsorbate pressure reaches the pressure of the condenser ($p_{ad}(w_{max}, T^{iso}_{heat}) = p_{sat}(T_{reject})$) at equilibrium state 3. Technically, this pressure condition can be realized by a flap valve.

3-4 Desorption phase:

As soon as the pressure of the adsorber has reached the pressure of the condenser, the regeneration of the adsorber starts. For this purpose, the valve between the adsorber and the condenser opens (Figure 2.2), while the adsorber is further heated ($\dot{Q}^{des}_{heat}$) to

desorb the refrigerant and to further heat up the adsorber. The desorbed refrigerant is cooled and condensed in the condenser, rejecting the heat flow $\dot{Q}^{\mathrm{cond}}_{\mathrm{reject}}$. In the ideal cycle, the desorption process is isobaric at the pressure level of the condenser ($p_{\mathrm{sat}}(T_{\mathrm{reject}})$) (Figure 2.3). The isobaric desorption means that the refrigerant desorbed to the vapor phase is immediately condensed. The desorption phase ends when the working pair reaches the temperature of the heat source (T_{heat}). Thus, the pressure of the condenser $p_{\mathrm{sat}}(T_{\mathrm{reject}})$ and the heating temperature T_{heat} define the equilibrium state 4 and the minimal loading $w_{\mathrm{min}}(p_{\mathrm{sat}}(T_{\mathrm{reject}}), T_{\mathrm{heat}})$ according to the adsorption equilibrium (Equation (2.2)).

4-1 Isosteric cooling phase:

In the last step, the adsorbate needs to be expanded to the low pressure level of the evaporator $p_{\mathrm{sat}}(T_{\mathrm{cool}})$ again. Therefore, the adsorber is cooled ($\dot{Q}^{\mathrm{iso}}_{\mathrm{reject}}$) with closed valves to evaporator and condenser. As during the isosteric heating, no refrigerant enters or leaves the adsorber (constant loading). At the same time, the temperature and pressure of the adsorbate decrease according to the adsorption equilibrium (Equation (2.2)), resulting in an isosteric cooling at minimal loading w_{min}. The isosteric cooling ends, when the adsorbate pressure equals the pressure of the evaporator ($p_{\mathrm{ad}}(w_{\mathrm{min}}, T^{\mathrm{iso}}_{\mathrm{reject}}) = p_{\mathrm{sat}}(T_{\mathrm{cool}})$) at equilibrium state 1. Technically, this pressure condition is also usually realized by a flap valve.

During the cycle, the refrigerant is transferred from the evaporator to the condenser via the adsorber. To close the cycle, the liquid refrigerant has to be returned to avoid accumulation in the condenser or a dry-out in the evaporator. The refrigerant reflux is realized by a connection between the condenser and the evaporator, e.g., valve or drain to allow for periodic or continuous reflux, respectively.

Since the adsorber periodically cycles between adsorption and desorption temperature, the chiller operation is discontinuous, and the cooling heat flow $\dot{Q}_{\mathrm{cool}}$ is only provided during the adsorption phase. To allow for a quasi-continuous cooling, technical applications usually employ multi-bed chillers with at least two adsorbers, which are operated out of phase (Teng et al., 2016). Thus, always one adsorber is in the adsorption phase to provide cooling while the other adsorber is regenerated in the desorption phase.

2.1.3 Characterization of adsorption chillers

Adsorption chillers are typically characterized by two performance indicators, (1) the efficiency and (2) the power density (Demir et al., 2008). The efficiency of adsorption chillers is measured by the coefficient of performance (COP), which is defined as the ratio of the provided energy for cooling Q_{cool} (benefit) to the required driving energy for heating

Q_{heat} (effort):

$$\text{COP} = \frac{Q_{\text{cool}}}{Q_{\text{heat}}}. \tag{2.6}$$

The driving energy Q_{heat} consists of the energy inputs during the isosteric heating phase ($Q_{\text{heat}}^{\text{iso}}$) and during the desorption phase ($Q_{\text{heat}}^{\text{des}}$), cf. Section 2.1.2:

$$Q_{\text{heat}} = Q_{\text{heat}}^{\text{iso}} + Q_{\text{heat}}^{\text{des}}. \tag{2.7}$$

The COP considers only the total amounts of energies transferred during a cycle, but not the duration of the cycle.

To account for the duration of the cycle, the power density is measured by the specific cooling power (SCP):

$$\text{SCP} = \frac{\overline{\dot{Q}}_{\text{cool}}}{m_{\text{ref}}} = \frac{Q_{\text{cool}}^{\text{cycle}}}{\Delta t_{\text{cycle}} m_{\text{ref}}}, \tag{2.8}$$

where $Q_{\text{cool}}^{\text{cycle}}$ is the cooling energy transferred during one cycle and Δt_{cycle} is the duration of the cycle (cycle time). The SCP refers the average cooling power $\overline{\dot{Q}}_{\text{cool}}$ to a reference weight m_{ref}, to provide a scale-independent number. A frequently employed reference weight is the mass of the adsorbent m_{sor} (Freni et al., 2015; Qian et al., 2013; Wang et al., 2005), but there are also other reference weights in literature, such as the total mass of the adsorption chiller (Frazzica et al., 2014). Instead of a reference weight, also a reference volume is sometimes employed in the so-called volumetric cooling power (VCP) if the application is restricted by the volume (Sharafian and Bahrami, 2014). As reference volumes, e.g., the volume of the adsorber (Sapienza et al., 2011) or the total volume of the adsorption chiller (Núñez et al., 2007) are used. The reference measure should be chosen according to the preferences of the application (volume or mass restrictions) since the reference measure affects the design choices (Bau, 2018).

For adsorption chillers, COP and SCP are competing performance indicators. The competing behavior has been comprehensively discussed in literature (Bau, 2018; Miyazaki and Akisawa, 2009; Sapienza et al., 2011): On the one hand, the maximal COP is achieved if the adsorption chiller cycle approaches the equilibrium states (Section 2.1.2), since the maximal loading difference is reached and the cooling energy is maximal. However, approaching equilibrium requires long cycle times, since heat and mass transfer resistances limit the adsorption process. Long cycle times, on the other hand, reduce the SCP, as the power at the beginning of the cycle is higher than at the end of the cycle due to the low driving forces when approaching equilibrium (Aristov et al., 2008).

Therefore, adsorption chillers are typically characterized by a Pareto frontier, which describes the trade-off between COP and SCP, including the maximal values of both (Bau, 2018; Leong and Liu, 2004b; Metcalf et al., 2012). A Pareto frontier represents the optimal

operating range of an adsorption chiller. A specific operating point can be adjusted by the cycle time: Short cycle times lead to the maximal SCP (full load), but minimal COP (the first endpoint of the Pareto frontier). With increasing cycle times, the SCP decreases (part load), while the COP increases until the minimal SCP and the maximal COP are reached (the second endpoint of the Pareto frontier).

For systems integration, COP and SCP are not sufficient to characterize the adsorption chiller, since the isolated consideration of only these two performance indicators results in misleading conclusions: For low-cost driving heat, such as waste-heat- or solar-heat, the SCP seems much more important than the COP, as the driving energy is free of charge (Leong and Liu, 2004b). However, although adsorption chillers are primarily driven by thermal energy, also electrical energy is required for auxiliaries, such as the heat-rejection unit, pumps, and control units (Weber et al., 2014). Thus, the COP is crucial even for zero-cost driving heat, since a poor COP causes a high demand for electrical energy, due to two reasons (Ziegler, 2009):

1. A poor COP means that a high amount of driving heat has to be provided via pumps.
2. A high amount of driving heat results in a high amount of waste heat, which has to be rejected by the heat-rejection unit.

In particular, the electrical energy demand of the heat-rejection unit is crucial, since the thermal COP of adsorption chillers is much lower (usually 0.25-0.66) than the COP of vapor-compression chillers (usually 3-4) (Demir et al., 2008). Consequently, much more waste heat has to be rejected in adsorption chiller systems.

Thus, an additional performance indicator is needed for the electrical efficiency of adsorption chillers. The electrical efficiency is defined by the energy efficiency ratio (EER), which relates the provided energy for cooling Q_{cool} to the total demand of electrical energy W_{el} (Nienborg et al., 2017):

$$\mathrm{EER} = \frac{Q_{\mathrm{cool}}}{W_{\mathrm{el}}}. \tag{2.9}$$

On the system level, the EER is a critical performance indicator, since the EER determines the operating costs and allows to compare adsorption chillers to competing technologies, such as vapor-compression chillers. The EER competes with both other performance indicators (COP and SCP): On the one hand, high volume flows in the heat exchangers improve the heat transfer and, consequently, the COP and the SCP. On the other hand, high volume flows in the heat exchangers cause high demand for electrical energy and, thereby, decrease the EER. Thus, the EER needs to be considered for systems integration.

2.2 Modeling approaches

In this section, we present and discuss modeling approaches for adsorption chillers. First, we present the required models to describe the adsorption process. In particular, we present the model of Dubinin to describe adsorption equilibrium (Section 2.2.1) and the linear-driving-force (LDF) model to describe adsorption kinetics (Section 2.2.2). Second, we discuss available model classes for adsorption chillers, pointing out their advantages and disadvantages regarding systems integration (Section 2.2.3).

2.2.1 Adsorption equilibrium

As a basis for each adsorption model, the adsorption equilibrium of the working pair is required. To describe the adsorption equilibrium (Equation (2.2)), several models are proposed in the literature, e.g., the classical isotherm model of Langmuir (1918) and the extended BET-model (Brunauer et al., 1938) are among the most popular approaches. Comprehensive overviews are given in Kast (1988) and Do (1998). To describe the adsorption on microporous adsorbents, the model of Dubinin (1967) has proven most suitable to fit experimental data (Núñez, 2001). As microporous adsorbents, such as zeolites, fine-porous silica gels, and activated carbon, are commonly used in adsorption chillers, the equilibrium of the working pair is often modeled by the approach of Dubinin (Allouhi et al., 2014; Riffel et al., 2010; Zhao et al., 2012). Thus, we also employed the model of Dubinin in this thesis.

The model of Dubinin (1967) was particularly developed for microporous adsorbents. This model assumes the filling of the micropores as main adsorption mechanism instead of the coverage of plane surfaces, as assumed in most prior models for non-porous and macroporous adsorbents. Dubinin defines the filled pore volume W as a volumetric loading, defined by the loading w and the density of the adsorbate $\rho_{\mathrm{ad}}(T)$, which is only a function of the temperature T:

$$W = \frac{w}{\rho_{\mathrm{ad}}(T)}. \tag{2.10}$$

The density of the adsorbate $\rho_{\mathrm{ad}}(T)$ can often be approximated well by the density of the boiling liquid for temperatures below the boiling point at atmospheric pressure (Dubinin, 1960). As a driving force, the adsorption potential A is defined following the potential theory of Polanyi (Polanyi, 1916, 1932) as a function of the temperature T and the pressure p:

$$A = R\ T\ \ln\frac{p_{\mathrm{sat}}(T)}{p}, \tag{2.11}$$

where R is the ideal gas constant and $p_{\mathrm{sat}}(T)$ is the saturation pressure.

A key idea of Dubinin's theory is that the adsorption equilibrium can be described by a single characteristic curve, which is the pore volume W as a function of the adsorption potential A:

$$W = W(A). \tag{2.12}$$

This idea is based on the main assumption of the theory that the characteristic curve is temperature invariant. The temperature invariance means that for a constant pore volume W the adsorption potential A is independent of the temperature $\left(\left(\frac{\partial A}{\partial T}\right)_W = 0\right)$. Thus, the originally three-dimensional adsorption equilibrium (Equation (2.2)) is transformed to a two-dimensional equilibrium (Equation (2.12)), which is one of the main benefits of the Dubinin theory. At the same time, the assumption of the temperature invariance is also a main point of criticism, as it is not based on a fundamental theory but empirical observations (Núñez, 2001). However, the temperature invariance has been frequently proven by experiments for working pairs typically employed in adsorption chillers, e.g., zeolites and silica gels (Goldsworthy, 2014; Núñez, 2001; Schawe, 1999).

The adsorption potential A is defined as the difference between the chemical potentials of the liquid and the adsorbed phase. Therefore, the adsorption potential can be interpreted as the difference in free enthalpy for a reversible, isothermal transition from the liquid to the adsorbed phase. Consequently, the enthalpy difference between the liquid and the adsorbed phase (bonding enthalpy Δh_{bond}) can be directly derived from the characteristic curve:

$$\Delta h_{\mathrm{bond}} = A - T\alpha \left(\frac{\partial A}{\partial \ln W}\right)_T, \tag{2.13}$$

where α is the coefficient of thermal expansion, which can be calculated from the density of the adsorbate (Núñez, 2001). Note that this expression of the bonding enthalpy is also based on the assumed temperature invariance of the characteristic curve. The detailed derivation of the bonding enthalpy and a discussion on the assumption of the temperature invariance is given by Núñez (2001). Finally, the specific enthalpy of the adsorbate h_{ad} (Equation (2.5)) results from the specific enthalpy of the liquid phase h_{liq} reduced by the bonding enthalpy Δh_{bond}:

$$h_{\mathrm{ad}} = h_{\mathrm{liq}} - \Delta h_{\mathrm{bond}} = h_{\mathrm{liq}} - A + T\alpha \left(\frac{\partial A}{\partial \ln W}\right)_T. \tag{2.14}$$

Thus, all required equilibrium properties (cf. Section 2.1.1) can be calculated from a single characteristic curve. There are mainly two approaches to describe the characteristic curve (Equation (2.12)): The first approach is based on physically motivated functions to link the adsorption equilibrium to microscopic properties, such as the pore geometry. The most popular physically motivated functions are the approaches of Dubinin-Radushkevich (Bering et al., 1966), Dubinin-Asthakov (Dubinin and Astakhov, 1971), and Dubinin-Stöckli

(Dubinin and Stoeckli, 1980). However, these physically motivated functions often are not able to describe real working pairs sufficiently accurate (Hauer, 2002). For this reason, the second approach to describe the characteristic curve is based on empirical functions, which can fit experimental data accurately (Núñez, 2001; Schawe, 1999). To assure physical consistency, the empirical functions have to fulfill some criteria, e.g., the functions have to be continuously differentiable and strictly decreasing (Hauer, 2002; Núñez, 2001).

In this thesis, we use an empirical function to describe the characteristic curve, as we want to model a real adsorption chiller with possibly high accuracy to be used for systems integration (cf. Chapter 3). The implementation of the characteristic function in the adsorption chiller model is described in Section 3.1.2.

2.2.2 Adsorption kinetics

Besides the adsorption equilibrium, dynamic models of the adsorption phenomenon additionally require a model for the adsorption kinetics. The adsorption kinetics can be limited by inter- and intra-particle resistances (Ruthven, 1984). For technical applications, particularly for packed-bed adsorption chillers, it has been shown that intra-particle resistances dominate the inter-particle resistances (Raymond and Garimella, 2011).

Generally, the intra-particle mass transfer in the adsorbent can be described by Fick's first law of diffusion, where different diffusion mechanisms can occur, e.g., molecular, Knudsen, and surface diffusion (Ruthven, 1984). Due to the complex and hardly measurable diffusion effects, the linear-driving-force (LDF) approach has been established to model the adsorption kinetics for technical applications (Sircar and Hufton, 2000). The LDF approach summarizes all diffusion mechanisms into one proportionality factor for a linear loading difference as driving force (Ruthven, 1984). For spherical particles, the proportionality factor is commonly determined by the approach of Glueckauf (1955), as function of an effective diffusion coefficient D_{eff} and the radius of the particle r_{particle}:

$$\frac{\mathrm{d}\overline{w}}{\mathrm{d}t} = \frac{15 D_{\text{eff}}}{r_{\text{particle}}^2}(w_{\text{surface}} - \overline{w}). \tag{2.15}$$

This LDF approach can be derived from Fick's first law of diffusion, assuming a homogeneous temperature of the spherical adsorbent particle and omitting any angular dependencies and higher-order terms (Liaw et al., 1979). The derived Equation (2.15) describes the change of the average loading $\overline{w}$ (adsorption rate $\frac{\mathrm{d}\overline{w}}{\mathrm{d}t}$) as function of the difference between the loading at the particle surface w_{surface} and the average loading $\overline{w}$ itself. The surface loading w_{surface} is also referred to as equilibrium loading, as the average loading evolves towards this surface loading to reach equilibrium. The surface loading (or equilibrium loading) is determined from the adsorption equilibrium (Section 2.2.1) using

the temperature of the adsorbent and the pressure of the vapor surrounding the adsorbent particle.

The LDF approach is still discussed controversially in the literature (Aristov, 2020): The LDF approach is criticized for overestimating the adsorption uptake at short cycle times and for underestimating the uptake at long cycle times compared to Fick's Diffusion (Aristov et al., 2006; Raymond and Garimella, 2011). However, the higher accuracy of Fick's diffusion model does usually not justify the significantly higher computational effort, particularly for adsorption chiller simulations on system-level (Dalibard, 2017). Therefore, the LDF approach is commonly used to model the adsorption kinetics in adsorption chillers and shows good agreement with experimental data (Lanzerath et al., 2015; Lee et al., 2020; Wang et al., 2015).

2.2.3 Adsorption chiller models

Modeling of adsorption chillers is a key to understand and interpret observed phenomena, to design components and systems, to predict performance and trends, and to assist in optimization (Yong and Sumathy, 2002). However, modeling of adsorption chillers is a challenging task, due to the combination of the intrinsic dynamic nature (discontinuous operation) and the interaction of several components (adsorbers, evaporator, and condenser) that determine the performance (cf. Section 2.1.2). Due to this complexity, studies for systems integration often do not model the adsorption process explicitly, but use grey- or black-box models, e.g., based on performance maps (Buonomano et al., 2018; Palomba et al., 2018), polynomial regression analysis (Sawant et al., 2020), or artificial neural networks (Krzywanski et al., 2017; Lazrak et al., 2016). Although the grey- and black-box models are computationally very efficient, these models do not deliver any insights into the adsorption chiller process, and consequently, are not suitable to improve the adsorption chiller itself. For this reason, we focus on physics-based (white-box) models in this thesis.

A detailed consideration of all physical effects would result in a high computational effort (Pesaran et al., 2016), inappropriate for many practical applications, such as systems integration. Thus, there is a trade-off between model accuracy and computational efficiency for the modeling of adsorption chillers. Consequently, various models with different levels of complexity have been developed in the literature to address different applications. Several literature reviews (Pesaran et al., 2016; Sah et al., 2017; Teng et al., 2016; Yong and Sumathy, 2002) classify adsorption chiller models into three main classes with an increasing level of complexity: (1) thermodynamic equilibrium models, (2) lumped-parameter models, and (3) distributed-parameter model (heat and mass transfer models). In the following, the model classes are briefly presented and discussed regarding their application and their specific advantages and disadvantages. For more detailed information about the model

classes and a comprehensive overview of their application, we refer to the reviews mentioned above.

(1) Thermodynamic equilibrium models

Thermodynamic equilibrium models are based on the first- and second-law analysis of the adsorption chiller cycle (cf. Section 2.1.2), considering the equilibrium states for given process temperatures. The model equations are derived from steady-state energy balances of individual components for defined phases of the cycle (steady-state models). To exemplify the mathematical formulation, the thermal energy transferred to or from the adsorber bed Q is derived from the first law (steady-state energy balance):

$$\mathrm{d}U = h_{\mathrm{in/out}}\ \mathrm{d}m_{\mathrm{in/out}} + \mathrm{d}Q \tag{2.16}$$

$$\int C_{\mathrm{A}}\ \mathrm{d}T + m_{\mathrm{sor}} \int \underbrace{\left(\underbrace{h_{\mathrm{v}} - \Delta h_{\mathrm{ads}}}_{h_{\mathrm{ad}}} - \cancelto{\approx 0}{\frac{p_{\mathrm{ad}}}{\rho_{\mathrm{ad}}}} \right)}_{u_{\mathrm{ad}}} \mathrm{d}w = m_{\mathrm{sor}} \int h_{\mathrm{in/out}}\ \mathrm{d}w + \int \mathrm{d}Q \tag{2.17}$$

$$\rightarrow Q = \int C_{\mathrm{A}}\ \mathrm{d}T + m_{\mathrm{sor}} \int \left(h_{\mathrm{ad}} - h_{\mathrm{in/out}} \right)\ \mathrm{d}w. \tag{2.18}$$

Here, $\mathrm{d}U$ is the change in internal energy and $h_{\mathrm{in/out}}\ \mathrm{d}m_{\mathrm{in/out}}$ is the incoming or leaving enthalpy flow. The total heat capacity of the adsorber bed C_{A} includes the heat capacities of both, the adsorbent and the adsorbate. Furthermore, the total heat capacity C_{A} can also include additional thermal masses, which are captured by the model, such as the heat exchanger. The specific internal energy of the adsorbate u_{ad} is calculated from the specific enthalpy of the adsorbate h_{ad} and the ratio of the adsorbent pressure and the adsorbent density $\frac{p_{\mathrm{ad}}}{\rho_{\mathrm{ad}}}$. This ratio $\frac{p_{\mathrm{ad}}}{\rho_{\mathrm{ad}}}$ is rather small compared to the enthalpies and, therefore, often neglected. The specific enthalpy of the adsorbate h_{ad} is decomposed into the specific enthalpy of the adsorptive h_{v} and the specific enthalpy of adsorption Δh_{ads}.

For a given process (e.g. simple adsorption chiller cycle, Section 2.1.2) and for a given equilibrium model (Section 2.2.1), Equation (2.18) can either be solved numerically or, under some assumptions, even analytically. Thus, thermodynamic equilibrium models can be described mathematically by a set of algebraic equations, which are the class easiest to solve numerically. However, the adsorption phenomenon is only described by the adsorption equilibrium (Section 2.2.1), while the adsorption kinetics (Section 2.2.2) are neglected. Neglecting losses due to the adsorption kinetics is a rough simplification for the behavior of real adsorption chillers. Therefore, this model class is mainly employed to evaluate and compare the potential of different applications, cycles, and working pairs, as illustrated in the following.

Thermodynamic equilibrium models have been used to assess the potential of adsorption-based solar cooling applications (Critoph, 1988) and to compare adsorption chillers to

compression chillers from an exergetic point of view (Meunier et al., 1998). Furthermore, cascading adsorption cycles (Douss and Meunier, 1989) and advanced heat and mass recovery cycles (Alam et al., 2004; Pons and Poyelle, 1999; Shelton et al., 1989) have been evaluated to quantify the theoretical potential and to derive limitations and improvements. Cacciola and Restuccia (1995) compared different working pairs for adsorption heat pumps, operating at specific climatic conditions. Recently, thermodynamic equilibrium models have been employed to assess the theoretical potential of new adsorbent composites (Calabrese et al., 2020) and mixtures as working fluid (Luberti et al., 2020).

The brief overview shows that thermodynamic equilibrium models are particularly useful to perform first evaluations of adsorption cycles and working pairs since these models are regarded as the simplest and computationally most efficient class. However, this model class only delivers upper limits of the efficiency for given working pairs and process conditions, since a process based on equilibrium states is assumed. These equilibrium states are hardly achieved in practical applications, due to the adsorption kinetics (Section 2.2.2), which would lead to very long cycle times and low power densities. As thermodynamic equilibrium models neglect adsorption kinetics, the power densities, as well as the efficiencies of real applications, cannot be predicted, which represents the main drawback of this model class. Therefore, thermodynamic equilibrium models are not suitable for systems integration.

(2) Lumped-parameter models

To tackle the main drawback of thermodynamic equilibrium models, lumped-parameter models have been developed to consider adsorption kinetics via overall, effective transport resistances. For this purpose, the time-resolved states (such as temperature, pressure, and loading) of individual components are derived from transient mass and energy balances (dynamic models). To exemplify the mathematical formulation, the time derivative of the temperature of the adsorber bed $\frac{\mathrm{d}T}{\mathrm{d}t}$ is derived from the first law (transient energy balance):

$$\frac{\mathrm{d}U}{\mathrm{d}t} = \dot{m}_{\mathrm{in/out}} h_{\mathrm{in/out}} + \dot{Q} \tag{2.19}$$

$$C_{\mathrm{A}} \frac{\mathrm{d}T}{\mathrm{d}t} + m_{\mathrm{sor}} \left(h_{\mathrm{ad}} - \cancel{\frac{p_{\mathrm{ad}}}{\rho_{\mathrm{ad}}}}^{\approx 0} \right) \frac{\mathrm{d}w}{\mathrm{d}t} = m_{\mathrm{sor}} h_{\mathrm{in/out}} \frac{\mathrm{d}w}{\mathrm{d}t} + \dot{Q} \tag{2.20}$$

$$C_{\mathrm{A}} \frac{\mathrm{d}T}{\mathrm{d}t} = m_{\mathrm{sor}} \left(h_{\mathrm{in/out}} - h_{\mathrm{ad}} \right) \frac{\mathrm{d}w}{\mathrm{d}t} + \dot{Q}. \tag{2.21}$$

The internal energy of the adsorber bed is expressed in the same way as in the energy balance of the thermodynamic equilibrium models (cf. Equation (2.17)). There are one-zone and multi-zone lumped-parameter models (Yong and Sumathy, 2002): In one-zone models, the entire adsorber is described by one energy balance (Equation (2.21)), where the total heat capacity C_{A} includes all thermal masses. In multi-zone models, several thermally-coupled balances are considered, e.g., for adsorber bed, heat exchanger, and

heat transfer fluid. The coupling between the balances is realized by the enthalpy flows and the heat flow $\dot{Q}$ (cf. Equation (2.21)), which can be described by convective heat transfer between the different zones. Furthermore, the energy balance of the adsorber bed (Equation (2.21)) is coupled to the mass balance by the adsorption rate $\frac{\mathrm{d}w}{\mathrm{d}t}$, which is described by a kinetic model, such as the linear driving force model (cf. Section 2.2.2). This coupling between energy and mass balance is often referred to as coupled heat and mass transfer of the adsorption process (Okunev et al., 2008).

Thus, lumped-parameter models are described mathematically by a set of coupled ordinary differential equations (ODE) for the transient balances, constrained by algebraic equations for adsorption equilibrium and fluid properties. In sum, the set of equations results in a differential-algebraic equations (DAE) system. The solution of the DAE system requires numerical methods, which make lumped-parameter models more complex than thermodynamic equilibrium models. Still, a quite efficient solution is possible, as various advanced numerical methods have been developed (Söderlind and Wang, 2006).

The main simplification of this model class is the neglect of the spatial resolution of individual components, e.g., of the adsorber-bed in Equation (2.21). Instead, spatially uniform states (such as temperature, pressure, and loading) are assumed. Nevertheless, the intrinsic dynamic behavior of adsorption chillers is captured, since both, the adsorption equilibrium and the adsorption kinetics are considered, allowing for more detailed insights into the adsorption process. Among the first, Sakoda and Suzuki (1986) and Sakoda and Suzuki (1984) developed and validated a lumped-parameter model of a solar-driven adsorption system to interpret the results of an experimental setup. After their work, this model class was widely used to estimate the performance of adsorption chillers for different control strategies, operating conditions, and component designs, as illustrated in the following.

As lumped-parameter models first allowed to capture the effect of finite cycle times, the influence of the cycle time on the performance of adsorption chillers was investigated (Chua et al., 2001) and allowed for optimization of the cycle time (Gräber et al., 2011). Furthermore, the influence of the operating temperatures on both performance indicators, COP and SCP, was resolved, e.g., to evaluate novel composite adsorbents (Gong et al., 2011; Tso et al., 2012) and multi-stage cycles (Hamamoto et al., 2005). Besides, also design effects were studied by varying the effective heat transfer resistance of the adsorber for different operating temperatures (Sharafian and Bahrami, 2015) or for different cycle times (Rezk and Al-Dadah, 2012). Moreover, Bau et al. (2017) developed a rigorous optimization framework to optimize both, adsorber design and control simultaneously.

The brief overview shows that lumped-parameter models are widely used to investigate and to optimize the design and the control of full-scale adsorption chillers because these dynamic models can resolve the trade-off between power density and efficiency. The main

advantage of lumped-parameter models is the good compromise between accuracy and computational efficiency: On the one hand, lumped-parameter can predict the performance indicators of real adsorption chillers with satisfying accuracy (Chen and Chua, 2020; Lee et al., 2020). On the other, lumped-parameter models are computationally very efficient, as even rigorous optimizations are feasible within a few minutes (Bau et al., 2017). Therefore, this model class is also popular for systems integrations (Nienborg et al., 2017; Santori et al., 2012; Verde et al., 2010). Nevertheless, the main drawback is that lumped-parameter models neglect the spatial resolution so that, e.g., the specific geometries of the components cannot be captured.

(3) Distributed-parameter models

The next level of detail is achieved by distributed-parameter models, which consider both, the temporal as well as the spatial resolution of the states in a component (Pesaran et al., 2016). For this purpose, the time- and space-resolved states of individual components can be derived from transient mass and energy balances for a differential control volume. To exemplify the mathematical formulation, the time derivative $\left(\frac{\partial T}{\partial t}\right)$ and the space derivative $(\nabla^2 T)$ of the temperature of the adsorber bed are given by the energy balance:

$$\left(\rho c_\mathrm{p}\right)_\mathrm{bed} \frac{\partial T}{\partial t} = k_\mathrm{bed} \nabla^2 T + \rho_\mathrm{bed} \left(h_\mathrm{in/out} - h_\mathrm{ad}\right) \frac{\partial w}{\partial t} + \dot{q}, \tag{2.22}$$

where $c_\mathrm{p,bed}$ is the specific heat capacity, ρ_bed is the density and k_bed is the thermal conductivity of the adsorber bed. The energy balance is derived similar to that of the lumped-parameter models (Equation (2.19)-(2.21)), but a differential control volume of the adsorber bed is used to include the spatial derivative. The adsorption rate $\frac{\partial w}{\partial t}$ also requires a kinetic model, such as Fick's diffusion or the linear driving force model (cf. Section 2.2.2). Within distributed-parameter models, the complexity varies depending on the dimensions of the spatial discretization (1-d, 2-d, or 3-d). The required dimension is usually derived from the desired level of detail and the geometry of the considered components, but also from the tolerated computational effort. As symmetries can often be exploited, there are 1-d discretizations, e.g., only in the radial direction of a circular adsorber bed (Restuccia et al., 2002), 2-d discretizations, e.g., in the radial and axial direction of a circular adsorber bed, but also 3-d discretizations in all directions (Niazmand et al., 2012). Also, different dimensions of discretizations for individual parts of the adsorber are used, e.g., a 1-d discretization of the heat exchanger and a 2-d discretization of the adsorber bed (Maggio et al., 2006). For this purpose, the individual parts of the adsorber, such as adsorber bed, heat exchanger, and heat transfer fluid, are described by separate balance equations, which are coupled by enthalpy flows, mass flows, and the specific heat flow $\dot{q}$.

Distributed-parameter models are described mathematically by a set of coupled partial differential equations (PDE). The solution of the PDE system requires additional numerical

methods for the discretization of the spatial derivatives, which further increase the complexity compared to the solution of lumped-parameter models. For the spatial discretization of the adsorber bed, different methods have been applied, such as the finite difference method (Zhang and Wang, 1999), the finite volume method (Mhimid, 1998) or the finite element method (Passos et al., 1989). Due to the spatial discretization, distributed-parameter models can distinguish between different transport mechanisms (e.g., convective and diffusive transport), and capture the specific geometry of components. Therefore, this model class is usually employed for a detailed investigation of the adsorption process, as illustrated in the following literature review.

For a better understanding of the adsorption process, distributed-parameter models can identify transport properties (Dawoud et al., 2007) and limiting transport mechanisms (Maggio et al., 2006). Furthermore, distributed-parameter models were applied to study the design choices of the adsorbent configuration, such as the particle diameter (Radu et al., 2017), the porosity of the bed (Leong and Liu, 2004a), and the thermal conductivity (Marletta et al., 2002). Another application field is the detailed investigation of the design choices of the adsorber, such as the fin spacing (Mahdavikhah and Niazmand, 2013; Sharafian et al., 2015), or of the bed thickness (Leong and Liu, 2006).

The brief overview shows that distributed-parameter models deliver a powerful tool for a profound analysis of the adsorption process and the detailed design of adsorbers. Distributed-parameter models allow for a better agreement with experimental data than lumped-parameter models because the spatial resolution is considered (Chua et al., 2004). However, the spatial resolution significantly increases the computational effort: The simulation of the adsorption/desorption process for a few grains can take up to 10 min (Freni et al., 2012). Even current studies often use simplifications of other components, such as ideal models of the evaporator and the condenser, to keep the computational effort low to allow for parameter variations (Cao and Chung, 2019; Scherle and Nieken, 2020; Yaïci and Entchev, 2019). Yaïci and Entchev (2019) reported a CPU time between 4 h and 8 h to simulate one operating point of an 3-d-discretized adsorber with (ideal) constant pressure boundaries for the evaporator and the condenser. Recently, Graf et al. (2020) predicted the performance of a full-scale adsorption chiller, using a 3-d-discretized adsorber bed, real models of the evaporator and the condenser, and transport coefficients from a small-scale experiment: on the one hand, the performance prediction was very accurate, but on the other hand, the high computational effort (up to 24 h for one simulation) prevents the use of the model for optimization. Thus, distributed-parameter models are too complex for systems integration, as even more component models have to be considered.

The discussion of the available model classes indicates that lumped-parameter models are currently most suitable and popular for systems integration, due to a good compromise

between accuracy and computational efficiency (Mohammed et al., 2019). However, although lumped-parameter models often predict the performance indicators of real systems with satisfying accuracy, several studies reported quantitative deviations between the dynamic simulations and measured data (Dalibard, 2017; Schicktanz and Núñez, 2009; Wu et al., 2000). In early studies, Douss et al. (1988) and Karagiorgas and Meunier (1987) already observed that the model and experiment deviate most strongly for the dynamic curves of the temperatures around the switches between the adsorption and the desorption phases (called thermal shock). The authors concluded that the lumped-parameter models are not able to capture the fast dynamics of the heat transfer fluid, which can be important for the control of adsorption chillers. Therefore, lumped-parameter models were expanded by 1-d discretized heat exchangers to resolve the temperature profile of the heat transfer fluid (Critoph, 1999). All other parts, such as the adsorber bed, are still described by lumped-parameter models. These so-called 1-d, lumped-parameter models represent a first step towards distributed-parameter models. However, 1-d, lumped-parameter models are mostly still considered as lumped-parameter models, since a key component, the adsorber bed, is still a lumped model (Pesaran et al., 2016). Nevertheless, the 1-d, lumped-parameter model gain significantly in accuracy compared to the original lumped-parameter models, while still providing high computational efficiency allowing for the optimization of a full-scale adsorption chillers (Bau, 2018). Wang and Chua (2007) compared a 1-d, lumped-parameter to a distributed-parameter model and reported a maximal deviation of 10 % for the prediction of the coefficient of performance and the cooling power. At the same time, the computational efficiency was significantly higher for the 1-d, lumped-parameter model. Therefore, 1-d, lumped-parameter models allow for efficient simulation of full-scale adsorption chillers (Aprile et al., 2020) and for systems integration (Palomba et al., 2019b, 2020). For example, Lanzerath et al. (2015) validated a 1-d, lumped-parameter model with experimental data from a lab-scale adsorption chiller. The agreement between model and experimental data was excellent and mostly even within the measurement uncertainties. However, an accurate fit between simulation and experiment required a fine discretization of the adsorber heat exchanger (Lanzerath, 2013), which, in turn, decreases the computational efficiency. For system-level optimizations (Nienborg et al., 2017) and model predictive control (Bau et al., 2019), high computational efficiency is crucial. To increase computational efficiency, the discretization resolution is usually reduced at the cost of accuracy. Thus, the discretization resolution of 1-d, lumped-parameter models still represents a trade-off between accuracy and computational efficiency.

2.3 Integration in hybrid systems

Adsorption chillers, as thermally-driven technology, often provide a promising solution for heat integration in hybrid systems (Hassan et al., 2020). Therefore, various hybrid cooling systems have been proposed and reviewed in literature (Askalany et al., 2012; Hassan et al., 2020; Kojok et al., 2016). Among hybrid systems, the combination of adsorption and vapor-compression technologies is promising, since the adsorption chiller can be efficiently integrated with the vapor-compression cycle to improve the overall performance (Palomba et al., 2020). Particularly, the combination of an adsorption chiller and a CO_2 vapor-compression cycle seems promising, since CO_2 is currently one of the most popular natural refrigerants in compression cycles (Zolcer Skačanová and Battesti, 2019). Furthermore, the transcritical CO_2 cycle offers excellent conditions for an adsorption chiller providing waste heat at temperatures around 100 °C and demand for heat rejection at ambient temperature (Sawalha, 2013). Thus, hybrid CO_2 vapor-compression systems are reviewed in more detail in the following.

CO_2 as refrigerant offers various advantages, such as global warming potential (GWP) of one, favorable thermodynamic and transport properties, low price, non-flammable properties, and suitability for low refrigeration temperatures (Bansal, 2012). However, a major drawback of CO_2 as refrigerant is the low efficiency at high ambient temperatures due to transcritical operation. This low efficiency results amongst others from high exergy losses of the non-isothermal heat release at high temperatures in the supercritical gas cooling step (Aprea and Maiorino, 2009; Aprea et al., 2013). To increase the efficiency at high ambient temperatures, either (1) the transcritical operation can be avoided (Sharma et al., 2014), or (2) the waste heat can be recovered (Sawalha, 2013).

(1) The transcritical operation can be avoided by cascade systems with a low and a high-temperature cycle (Colorado and Velázquez, 2013). The low-temperature cycle can be operated subcritically even at high ambient temperatures since the high-temperature cycle provides the heat sink for condensation. However, the high-temperature cycle not only requires additional electrical energy but commonly employs refrigerants with high GWP (Sharma et al., 2014). To reduce the consumption of electrical energy and to use environmentally friendly refrigerants only, thermally-driven sorption chillers have been proposed for the high-temperature cycle (Fernández-Seara et al., 2006). Thermally-driven sorption chillers use heat to provide cooling and, thus, can substitute electrical energy by waste- or renewable heat (Deng et al., 2011). Compression-sorption cascade systems with CO_2 in the low-temperature cycle and sorption chiller in the high-temperature cycle have been investigated in the literature comprehensively: There are theoretical studies proposing to drive the sorption chiller by waste heat, e.g., industrial waste heat (Chen et al., 2017; Colorado and Rivera, 2015; Jain et al., 2015). Other theoretical studies propose combined heat and power (CHP) systems to simultaneously provide mechanical power to the CO_2

cycle and thermal power to the sorption chiller (Fernández-Seara et al., 2006; Garimella et al., 2011; Marimón et al., 2011). Experimental studies of compression-sorption cascade systems have explored solar and waste heat to drive the sorption chiller (Cyklis, 2014; Vasta et al., 2018). These experimental studies reached electrical energy savings up to 50 % (Vasta et al., 2018). However, an external heat source was always required to drive the sorption chiller.

(2) The simplest way to recover the waste heat is to directly supply the heat, e.g., for heating of buildings (Nöding et al., 2016; Sarkar et al., 2008; Sawalha, 2013). However, finding a matching heat demand is challenging since the amount of waste heat is particularly high at high ambient temperatures. In contrast, the heating demand is generally low at high ambient temperatures. This mismatch between heat supply and demand motivates the use of a thermally-driven sorption chillers. A sorption chiller can recover the waste heat from the transcritical CO_2 cycle to generate additional cooling. The additional cooling can be integrated into the CO_2 cycle to increase the efficiency of the overall hybrid system (Graf et al., 2015).

Sorption chillers can be divided into absorption and adsorption chillers (Deng et al., 2011). Hybrid systems integrating an absorption chillers into a CO_2 cycle have been investigated in detail: Efficiency increases of 14-22 % compared to a stand-alone CO_2 cycle have been shown (Arora et al., 2011; Graf et al., 2015). However, absorption chillers also require electrical energy, which is often neglected when determining the efficiency. In some cases, the electrical energy demand of absorption chillers is only marginally lower than for compression chillers (Nienborg et al., 2017). Thus, the additional electrical energy demand can significantly reduce the efficiency increase by the hybrid systems.

Compared to absorption chillers, adsorption chillers offer some advantages: First, the electrical energy demand is lower for adsorption chillers (Helm, 2015). Second, adsorption chillers can employ low driving temperatures below 70 °C (Choudhury et al., 2013), which enables high heat recovery rates from the CO_2 cycle. Third, adsorption chillers commonly use environmentally friendly working pairs (Choudhury et al., 2013). Still, hybrid systems integrating an adsorption chiller into the CO_2 cycle have only been investigated once in the literature to the best of the authors' knowledge. In a pilot project, Gerber (2011) has integrated a commercially available adsorption chiller into an existing CO_2 cycle. This hybrid system achieved energy savings of 12 % in the CO_2 cycle at an ambient temperature of 25 °C. However, the additional energy demand of the adsorption chiller was almost 8 %, significantly reducing the net energy savings. Low net energy savings have been mainly attributed to a mismatch in size ratio between CO_2 cycle and adsorption chiller and suboptimal control parameters. Therefore, Gerber (2011) concludes that system design and control is crucial and that there is optimization potential in system design and control to achieve higher net energy savings.

2.4 Integration of main system components and auxiliaries

In practice, an adsorption chiller system not only consists of its main components adsorber, evaporator, and condenser, but also of various auxiliary components that are needed for operation, such as heat-rejection units, fans, and pumps: The design and control of all system components including the auxiliaries is crucial, since a poor electrical efficiency of adsorption chiller systems in practice is mainly due to two reasons (Weber et al., 2014): (1) a poor system design due to under- or oversizing of components, leading to an unbalanced system design with bottlenecks; and (2) a poor control due to sub-optimal choices of control parameters, leading to high electricity consumption for operation. So far, design and control of adsorption chiller systems have often been improved separately:

1. Regarding system design, the sizes of the main components, such as heat source and heat-rejection unit, are usually determined by design guidelines (Mugnier et al., 2017; Palomba et al., 2019a) or pre-design approaches based on steady-state calculations (Le Denn et al., 2013). These simple design approaches deliver a useful initial estimate for the system design but do not guarantee the optimal design for a specific application. For detailed design studies, dynamic simulations have been proposed (Henning et al., 2013). However, dynamic simulations can be very costly and time-consuming if many interdependent degrees of freedom have to be considered simultaneously. In particular, if control is included as a degree of freedom, studying all possible combinations leads to a high number of dynamic simulations.
2. Regarding system control, the control parameters, such as temperatures of the adsorption chiller circuits, pump speed, and fan speed, are usually set to nominal values in practice (Speerforck and Schmitz, 2015). These nominal values are not necessarily optimal for the specific application. Advanced control strategies have been developed to adapt both, the driving and the heat-rejection temperature of the adsorption chiller via three-way valves and via the fan speed of the heat-rejection unit (Albers et al., 2009). These advanced control strategies have shown to improve electrical efficiency by 35 % (Albers, 2014). More advanced control strategies can also adapt the volume flows of the heat transfer circuits via speed-controlled pumps (Dalibard et al., 2016). The adaption of the volume flows reduces the electricity consumption further by up to 25 % (Nienborg et al., 2017). Both of the presented advanced control strategies have been investigated for already existing systems with fixed system design.

However, system design and control are interdependent (Helm, 2015), as illustrated by the following example: An undersized heat-rejection unit requires higher volume flows of pumps and fans to release the required heat. The higher volume flows increase electricity

consumption. Accounting for this interdependency of system design and control requires an integrated optimization resulting in many degrees of freedom.

2.5 Conclusions and contribution of this thesis

From the state of the art described in the previous sections, the following conclusions are drawn:

(1) The common performance indicators, coefficient of performance (COP) and specific cooling power (SCP), are important to characterize adsorption chillers, but insufficient on system level (Section 2.1.3). On system level, the energy efficiency ratio (EER) is additionally required to consider the electrical efficiency of the system, which is crucial for the operating costs and the competitiveness with other technologies. Section 2.1.3 illustrates that all three performance indicators compete with each other on system level. Furthermore, these performance indicators do not only depend on the adsorption chiller alone, but also on the other system components, such as the heat-rejection unit. For this reason, systems integration of adsorption chillers needs to consider the connected system components and their interaction, which results in various degrees of freedom. To cope with these various degrees of freedom, a model-based systems integration offers a powerful and efficient tool.

(2) Modeling of adsorption chillers is well established and widely used to investigate the performance and to optimize design and control (Section 2.2.3). However, the choice of a suitable model is always dominated by a trade-off between model accuracy and computational efficiency and, therefore, results from the specific goals of the investigation. For systems integration, the classification in Section 2.2.3 indicates that lumped-parameter models are currently most popular. The extension to 1-d, lumped-parameter models can further increase the accuracy. However, the choice of the discretization resolution is still an open issue and leads again to the trade-off between accuracy and computational efficiency. For complex applications such as systems integration, high computational efficiency is often achieved by coarse discretization, which causes a poor accuracy. Currently, a system-level adsorption chiller model is lacking, which provides the satisfying accuracy of a finely discretized 1-d, lumped-parameter model but with enhanced computational efficiency suitable for model-based optimization.

(3) Hybrid systems are a promising application area for adsorption chillers, providing efficient solutions for heat integration (cf. Section 2.3). As a particularly promising hybrid system, Section 2.3 identifies the integration of an adsorption chiller into a CO_2 vapor-compression cycle. This hybrid system can efficiently provide low-temperature refrigeration with natural refrigerants only. However, a comprehensive assessment of such a hybrid system with optimized design and control is still missing.

(4) The design and control of the main system components, such as heat source and heat-rejection unit, but also of the auxiliaries, such as pumps and fans, is crucial to achieve a high electrical efficiency of the adsorption chiller system (cf. Section 2.4). Section 2.4 reviews that design and control of adsorption chiller systems are often considered separately, although there are interdependencies. An integrated design and control leads to many degrees of freedom and, thus, requires a computationally efficient, optimization-based approach.

Based on the four conclusions derived above, the main contribution of this thesis can be divided into the following three parts:

1) Development and validation of an efficient adsorption chiller model

To resolve the trade-off between accuracy and computational efficiency of 1-d, lumped-parameter models, we propose an alternative modeling approach for the discretized heat exchangers of adsorption chiller models in Chapter 3. The proposed approach avoids the discretization of the heat exchangers by applying operator splitting to the energy balance of the heat transfer fluid. Thereby, the computational efficiency of the adsorption chiller model can be significantly improved, while still providing the same accuracy as with finely discretized heat exchanger models. The proposed model is validated with experimental data to be used for systems integration in Chapter 4 and 5.

2) Integration of an adsorption chiller into a hybrid CO_2 refrigeration system

To assess the potential of a hybrid system combining an adsorption chiller and a CO_2 vapor compression cycle, we pursue a model-based approach in Chapter 4. The model-based approach allows to optimize design and control to exploit the full potential of the hybrid system. Thereby, the potential of the hybrid system can be quantified for specific conditions and the requirements for the adsorption chiller can be derived, such as needed electrical efficiency.

3) Integrated design and control of adsorption chiller systems

To allow for an integrated optimization of design and control of all system components and auxiliaries, we propose an efficient model-based method in Chapter 5. The proposed method employs dynamic optimization to identify both, optimal design and optimal control of all system components and auxiliaries for a problem-specific objective, such as electrical efficiency or total costs. Thereby, the proposed method delivers the optimal design and control of adsorption chiller systems for the considered application and allows to assess the practical performance.

A model-based framework for the optimal systems integration of adsorption chillers

In summary, this thesis also provides a model-based framework for the optimal systems integration of adsorption chillers. The framework consists of three main steps, which are demonstrated in the Chapters 3-5, respectively (Figure 2.4):

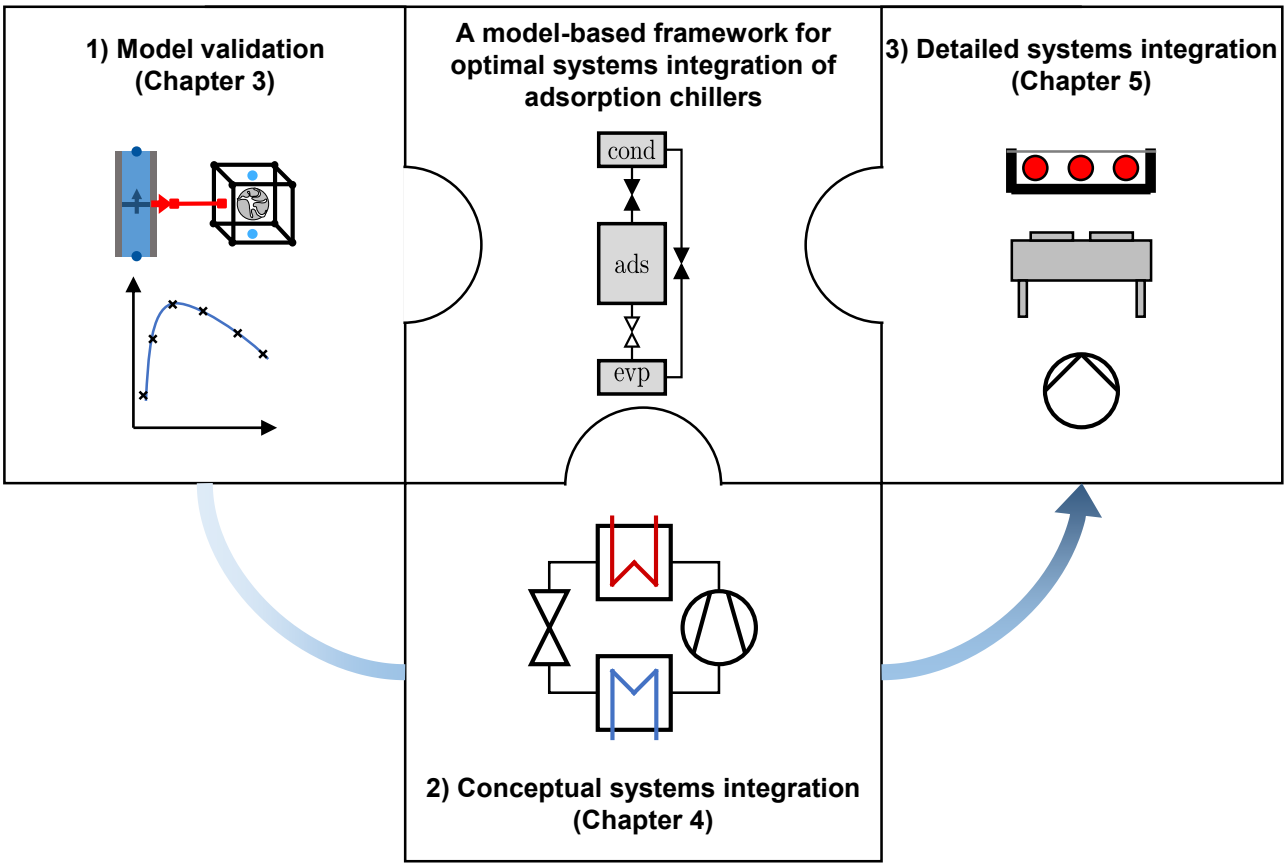

Figure 2.4: Main contribution of this thesis: A model-based framework for optimal systems integration of adsorption chillers; from 1) model validation (Chapter 3) over 2) conceptual systems integration (Chapter 4) to 3) detailed systems integration (Chapter 5).

1) **Model validation:** The basis for model-based systems integration is a reliable and efficient adsorption chiller model. To ensure the reliability, we propose to calibrate and validate the model developed in this thesis with experimental data of the considered adsorption chiller, as demonstrated in Chapter 3. Subsequently, the validated model can be used for the following systems integration steps.

2) **Conceptual integration:** Given the validated model and a systems of interest, we propose to start with a conceptual systems integration. The goal of the conceptual integration is to estimate the potential of the considered system and to evaluate if or

under which circumstances the integration of an adsorption chiller is potentially beneficial. For this purpose, the conceptual integration focuses on the interaction between the main technologies of the system, but does not consider all components and auxiliaries in detail. The conceptual integration is particularly useful for complex systems, such as hybrid systems, to avoid a too detailed problem before the potential of the system has been estimated. The conceptual integration quantifies the potential of the system to decide, if a more detailed consideration should be pursued. In Chapter 4, we demonstrate the conceptual integration for a hybrid refrigeration system.

3) **Detailed integration:** If the conceptual integration revealed a sufficiently high potential of the considered system, we propose to continue with the detailed systems integration. The goal of the detailed integration is the detailed optimization of design and control of the adsorption chiller system. For this purpose, the detailed integration focuses on the interaction of the adsorption chiller with all system components needed for operation, such as the heat source and heat-rejection unit, including the auxiliaries, such as pumps and fans. The detailed integration delivers the optimal design and control of all system components and auxiliaries. In Chapter 5, we present an optimization-based method for the detailed integration and demonstrate it for a solar-thermally-driven adsorption chiller system.

CHAPTER 3

Development and experimental validation of an efficient adsorption chiller model

In this chapter, we present and evaluate the adsorption chiller model employed in this thesis. We propose an alternative modeling approach for the heat exchangers to eliminate the influence of discretization, and to resolve the trade-off between accuracy and computational efficiency of 1-d, lumped-parameter models. For this purpose, the proposed approach applies operator splitting to the transport equation of the heat transfer fluid, instead of discretizing the convective term. Applying operator splitting allows for an efficient, analytical solution of the convective heat transfer.

The proposed modeling approach for the heat exchangers is inspired by a thermo-hydraulic pipe model, which is based on a plug-flow approach (Heijde et al., 2017). This plug-flow-based pipe model has been successfully employed to avoid the discretization of the hydraulics in district heating and cooling networks (Oppelt et al., 2016; Sartor and Dewalef, 2017). Heijde et al. (2017) showed a good agreement between the plug-flow-based pipe model and both, experimental data as well as a finely discretized pipe model, for a step response to a change in the inlet temperature. At the same time, the simulation of the plug-flow-based model was up to 68 times faster compared to the finely discretized model. Thus, the plug-flow-based pipe model seems very suitable to model the fast dynamics in the heat exchangers of adsorption chillers.

This chapter is structured as follows: First, we introduce the plug-flow-based adsorption chiller model in Section 3.1. Second, we describe the calibration and validation method in Section 3.2. The method is employed in Section 3.3 to compare the proposed model with both, experimental data from a lab-scale one-bed adsorption chiller and a 1-d, lumped-parameter model. Afterwards, we validate the plug-flow-based model for a commercial

two-bed adsorption chiller in Section 3.4 to demonstrate the applicability of the model to other adsorption chiller types. Finally, we investigate the validity range of the proposed modeling approach in Section 3.5. The main results are summarized in Section 3.6.

3.1 Modeling

The adsorption chiller models has three main components: Adsorber, evaporator, and condenser (Figure 3.1). Each component consists of sub-models for the heat exchanger and the adsorber bed or the vapor liquid equilibrium (VLE). Here, the models are implemented

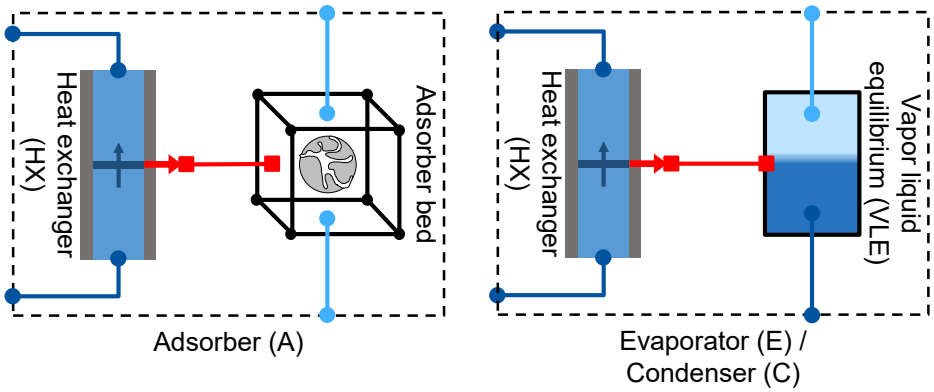

Figure 3.1: Scheme of the three main components of an adsorption chiller: Adsorber (A), Evaporator (E), and Condenser (C). The models of the evaporator and the condenser are identical. Each component consists of a heat exchanger (HX), which is thermally connected to the adsorber bed or the vapor liquid equilibrium (VLE).

within the commercial software environment Dymola (Dassault Systèmes, 2020) using the Modelica language (Modelica Association, 2017), as presented in the following sections. All fluid properties are calculated with the TILMedia library (Schulze, 2013), which uses data from Refprop (Lemmon et al., 2013). For the refrigerant water, the equation of state from Wagner and Pruß (2002), and auxiliary models for the thermal conductivity and the viscosity from Huber et al. (2009, 2012) are employed. The presented models are available in our open-source library SorpLib published on GitLab (Institute of Technical Thermodynamics, RWTH Aachen, 2020) or will be added in the future.

3.1.1 Plug-flow-based heat exchanger

The heat exchanger is a key component of the adsorption chiller. An accurate representation of the heat exchanger typically requires a model with spatial discretization in one dimension. Here, we avoid the spatial discretization by a plug-flow-based approach. The plug-flow-

based approach is inspired by the thermo-hydraulic pipe model proposed by Heijde et al. (2017) to describe pipes in heating networks. Here, the thermo-hydraulic pipe model is adapted for adsorption chillers to describe the heat transfer between the heat transfer fluid and the thermally connected models, i.e., the adsorber bed and the VLE volume. Figure 3.2 shows the scheme and the sub-models of the heat exchanger, which are described in the following.

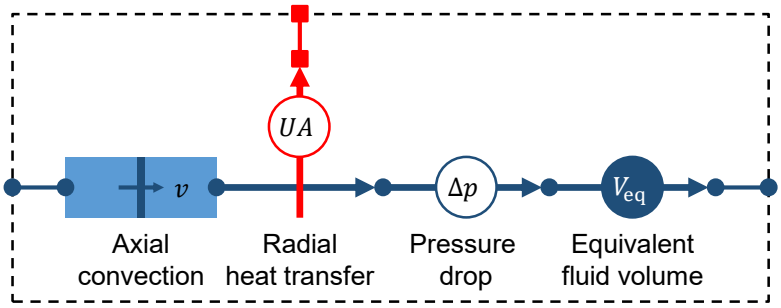

Figure 3.2: Scheme of the plug-flow-based heat exchanger model. The model consists of four sub-models, which are computed sequentially: 1) axial convection, 2) radial heat transfer, 3) pressure drop, and 4) equivalent fluid volume. The red squares are heat ports to share the temperature and heat flow information with the connected model. The blue circles are fluid ports to share specific enthalpy, pressure and mass flow information with connected models.

Since liquid water is used as heat transfer fluid in the heat exchangers, the flow is modeled as incompressible. Thus, the mass balance for each sub-model results from the continuity equation as:

$$\dot{m}_{\mathrm{fl,in}} - \dot{m}_{\mathrm{fl,out}} = 0, \tag{3.1}$$

where $\dot{m}_{\mathrm{fl,in}}$ is the entering and $\dot{m}_{\mathrm{fl,out}}$ is the leaving mass flow. Thus, the heat exchanger can be described as incompressible, 1-d convective flow (Batchelor, 2000). Neglecting axial diffusion and internal sources due to dissipation (cf. (Roetzel et al., 2020)), the energy balances of the fluid and the heat exchanger wall read:

$$m_{\mathrm{fl}} \frac{\partial h_{\mathrm{fl}}}{\partial t} + m_{\mathrm{fl}} v_{\mathrm{fl}} \frac{\partial h_{\mathrm{fl}}}{\partial x} = -hA_{\mathrm{i}} \left(T_{\mathrm{fl}} - T_{\mathrm{wall}}\right) \tag{3.2}$$

$$m_{\mathrm{wall}} c_{\mathrm{wall}} \frac{\partial T_{\mathrm{wall}}}{\partial t} = hA_{\mathrm{i}} \left(T_{\mathrm{fl}} - T_{\mathrm{wall}}\right) - hA_{\mathrm{o}} \left(T_{\mathrm{wall}} - T_{\mathrm{port}}\right), \tag{3.3}$$

where m_{fl} is the mass, h_{fl} is the specific enthalpy, v_{fl} is the velocity, and T_{fl} is the temperature of the fluid. The mass, the specific heat capacity, and the temperature of the heat exchanger wall are given by ρ_{wall}, c_{wall}, and T_{wall}, respectively. The independent variables are the time t and the axial coordinate x. To describe the heat transfer, the inner heat transfer

value [1] hA_i and the outer heat transfer value hA_o are used. The temperature at the heat port T_port represents the temperature of the thermally connected component at the outer side of the heat exchanger wall (cf. Figure 3.2).

To solve Equations 3.2 and 3.3, the classical finite-volume approach approximates the spatial derivative $\left(\frac{\partial h_\mathrm{fl}}{\partial x}\right)$ by spatial discretization of the heat exchanger using a backward difference (upwind) scheme (Roetzel et al., 2020). The spatial discretization leads to a ordinary differential equations system, which can be large and computationally expensive for a fine discretization.

Instead of spatial discretization, the plug-flow-based approach applies some simplifications and operator splitting (Heijde et al., 2017): First, we neglect the delay of the heat transfer from the fluid to the heat port due to the heat exchanger wall ($\frac{\partial T_\mathrm{wall}}{\partial t} \approx 0$ in Equation (3.3)). For adsorption chillers, this delay by the heat exchanger wall is often small, because of its lower thermal mass and faster heat transfer than of the connected thermal mass (adsorber bed or VLE volume). Thereby, Equations 3.2 and 3.3 simplify to:

$$m_\mathrm{fl}\,\frac{\partial h_\mathrm{fl}}{\partial t} + m_\mathrm{fl} v_\mathrm{fl}\,\frac{\partial h_\mathrm{fl}}{\partial x} = -UA\,(T_\mathrm{fl} - T_\mathrm{port}) \tag{3.4}$$

with the overall heat transfer value through the wall UA:

$$UA = \frac{hA_\mathrm{i} \cdot hA_\mathrm{o}}{hA_\mathrm{i} + hA_\mathrm{o}}. \tag{3.5}$$

Second, we apply operator splitting (MacNamara and Strang, 2016) to Equation (3.4). Thereby, the total specific enthalpy change of the fluid over the heat exchanger Δh_fl (Equation (3.4)) is split into 1) the specific enthalpy change due to axial convection $\Delta h_\mathrm{fl}^\mathrm{ax}$ and 2) the specific enthalpy change due to radial heat transfer $\Delta h_\mathrm{fl}^\mathrm{rad}$:

$$\Delta h_\mathrm{fl} = \Delta h_\mathrm{fl}^\mathrm{ax} + \Delta h_\mathrm{fl}^\mathrm{rad}. \tag{3.6}$$

Both specific enthalpy changes are calculated sequentially (cf. Figure 3.2).

Axial convection

The axial convection describes the axial fluid transport through the heat exchanger due to the flow but without the radial heat transfer:

$$\frac{\partial h_\mathrm{fl}^\mathrm{ax}}{\partial t} + v_\mathrm{fl}\,\frac{\partial h_\mathrm{fl}^\mathrm{ax}}{\partial x} = 0. \tag{3.7}$$

[1] In this thesis, the product of the heat transfer coefficient h and the heat transfer area A is referred to as heat transfer value hA to avoid long expressions.

Radial heat transfer

The radial heat transfer describes the convective heat transfer between the fluid and the thermally connected component. To compute this heat transfer, the Lagrangian approach is used to allow for an analytical solution of the outlet temperature of the fluid (Heijde et al., 2017; Oppelt et al., 2016): The Lagrangian approach attaches the coordinate system to a moving fluid particle flowing through the heat exchanger. Due to the attached coordinate system, there is no spatial distribution in the energy balance of a moving fluid volume of infinitesimal length δx:

$$m_{\mathrm{fl}} \, \frac{dh_{\mathrm{fl}}^{\mathrm{rad}}}{dt} \, \delta x = -UA \left(T_{\mathrm{fl}} - T_{\mathrm{port}}\right) \, \delta x. \tag{3.8}$$

Expressing the specific enthalpy change by the temperature change and rearranging Equation (3.8) leads to:

$$\int_{T_{\mathrm{fl,in}}^{\mathrm{rad}}}^{T_{\mathrm{fl,out}}^{\mathrm{rad}}} \frac{m_{\mathrm{fl}} c_{\mathrm{fl}}}{UA} \, \frac{\mathrm{d}T_{\mathrm{fl}}^{\mathrm{rad}}}{T_{\mathrm{fl}}^{\mathrm{rad}} - T_{\mathrm{port}}} = -\int_{t_{\mathrm{in}}}^{t_{\mathrm{out}}} \mathrm{d}t. \tag{3.9}$$

The integral on the left of Equation (3.9) can be solved analytically under the following assumptions:

1. The temperature dependency of both, the overall heat transfer coefficient U and the fluid properties (ρ_{fl} and c_{fl}) is negligible within the integration range ($T_{\mathrm{fl,in}}^{\mathrm{rad}}$ and $T_{\mathrm{fl,out}}^{\mathrm{rad}}$).
2. Each entering fluid particle is exposed to a constant temperature T_{port} while flowing through the heat exchanger.

With these assumptions, Equation (3.10) delivers the analytical solution for the outlet temperature $T_{\mathrm{fl,out}}^{\mathrm{rad}}$:

$$T_{\mathrm{fl,out}}^{\mathrm{rad}}(t_{\mathrm{out}}) = T_{\mathrm{port}}(t_{\mathrm{in}}) + \left(T_{\mathrm{fl,in}}^{\mathrm{rad}}(t_{\mathrm{in}}) - T_{\mathrm{port}}(t_{\mathrm{in}})\right) \, \exp\left[-\frac{UA}{m_{\mathrm{fl}} c_{\mathrm{fl}}} \, \left(t_{\mathrm{out}} - t_{\mathrm{in}}\right)\right]. \tag{3.10}$$

The assumptions made above apply well for adsorption chillers, since the flow velocity of the heat transfer fluid is high while the heat transfer to the thermally connected components adsorbent and VLE volume is generally poor, due to the porous adsorbent and the near-vacuum conditions. For this reason, the temperature change of the thermally connected component is small for the propagation time of a fluid particle. To test this assumption, the Stanton number St can be used:

$$\mathrm{St} = \frac{\mathrm{Nu}}{\mathrm{Pe}} = \frac{\mathrm{Nu}}{\mathrm{Re\ Pr}} = \frac{U}{v \rho_{\mathrm{fl}} c_{\mathrm{fl}}} = \frac{\text{radial convective heat transfer}}{\text{axial convective heat transfer}}. \tag{3.11}$$

The Stanton number (St) can be expressed as the ratio of the Nusselt number (Nu) and the Péclet number (Pe), which is the product of the Reynolds number (Re) and the Prandtl number (Pr). The Nusselt number (Nu) in the numerator describes the ratio of radial heat transfer to diffusive heat transfer. The Péclet number (Pe) in the denominator describes the ratio of axial convection to diffusive heat transfer. Thus, the Stanton number (St) can be interpreted as the ratio of radial heat transfer to axial convection. A small Stanton number means that the radial heat transfer to the thermally connected component is low compared to the axial convection due to fluid motion. Consequently, a small Stanton number supports that the assumption of a small temperature change of the connected component for the propagation time of the fluid particle should hold. In Section 3.5, the validity of this assumption is tested for typical Stanton numbers.

In Equation (3.10), the propagation time of the outflowing fluid particles is needed, i.e. the difference between outflow and inflow time $t_{\mathrm{out}} - t_{\mathrm{in}}$. As the outlet temperature is calculated at the outlet of the heat exchanger, the outflow time of the fluid particles t_{out} corresponds to the current simulation time t. The corresponding inflow time of the fluid particles t_{in} is regarded as property of the fluid, which is transported according to the axial convection equation (same as for the specific enthalpy in Equation (3.7)):

$$\frac{\partial t_{\mathrm{in}}}{\partial t} + v_{\mathrm{fl}} \, \frac{\partial t_{\mathrm{in}}}{\partial x} = 0. \tag{3.12}$$

Both axial convection equations (3.7 and 3.12) are efficiently solved by the Modelica operator *spatialDistribution()*, which keeps track of the spatial distribution of the transported property, by suitable sampling, interpolation, and shifting of the stored distribution. For more details about the implementation of the operator, the reader is referred to the language specifications of Modelica (Modelica Association, 2017).

Heat transfer correlations

To calculate the outlet temperature in Equation (3.10), the overall heat transfer value UA is needed. The overall heat transfer value can be used as a calibration parameter to calibrate the model to experimental data (Heijde et al., 2017). To account for the dependence of the heat transfer coefficient on the mass flow, we follow the approach of Lanzerath (2013) and decompose the overall heat transfer value (UA) into the flow-dependent inner heat transfer value (hA_{i}) and the outer heat transfer value (hA_{o}) (cf. Equation (3.5)). While the outer heat transfer value (hA_{o}) is used as calibration parameter of the model, the inner heat transfer coefficient is calculated based on empirical correlations from literature. For this purpose, the inner heat transfer coefficient h_{i} results from the Nusselt number (Nu):

$$h_{\mathrm{i}} = \mathrm{Nu} \, \frac{\lambda_{\mathrm{fl}}}{d_{\mathrm{h}}}, \tag{3.13}$$

where λ_{fl} is the thermal conductivity of the heat transfer fluid, and d_{h} is the hydraulic diameter of the heat exchanger. The required Nusselt number is expressed as a function of the Reynolds number (Re) and the Prandtl number (Pr). The corresponding functions are derived from empirical correlations for specific heat exchanger types.

In this thesis, the heat exchangers of the considered adsorber and evaporator are realized as finned tubes (cf. Appendix B). To model the inner transfer coefficient inside the tubes, we employ the Sieder-Tate correlation (Sieder and Tate, 1936), as one of the most popular correlations for turbulent pipe flows. Furthermore, the correlation allows to consider inner structures of a tube by adapting the Sieder-Tate constant C_{ST} (Thome, 2010). Compared to the original Sieder-Tate correlation, we neglected the viscosity coefficient, which considers the changing viscosity of the fluid due to the temperature difference between the center of the tube and the tube wall. Here, this temperature difference is small due to the high inner and the poor outer heat transfer coefficients of the heat exchangers, cf. Lanzerath (2013). Consequently, the simplified Sieder-Tate correlation reads:

$$\mathrm{Nu} = C_{\mathrm{ST}} \mathrm{Re}^{0.8} \mathrm{Pr}^{1/3}, \qquad \begin{array}{c} 10\,000 < \mathrm{Re} \\ 0.7 < \mathrm{Pr} < 16\,000 \end{array} \tag{3.14}$$

where C_{ST} is the Sieder-Tate constant, which accounts for different tube structures.

The heat exchanger of the condenser is realized as a helix (cf. Appendix B). To model the inner heat transfer coefficient in the helix, we employ the correlation developed by Schmidt (1967). This correlation considers the improved heat transfer coefficient due to the centrifugal forces in the coils of the helix. In the Schmidt correlation, we also neglect the correction factor to account for changing viscosity of the fluid in the radial direction, as discussion above. Thus, the simplified Schmidt correlation reads:

$$\mathrm{Nu} = \frac{\zeta/8 \ \mathrm{Re} \ \mathrm{Pr}}{1 + 12.7\sqrt{\zeta/8}\left(\mathrm{Pr}^{2/3} - 1\right)}, \qquad 22\,000 < \mathrm{Re} \tag{3.15}$$

where ζ is the resistance coefficient, which is calculated as function of the diameter of the tube helix d_{helix}:

$$\zeta = \frac{0.3164}{\mathrm{Re}^{0.25}} + 0.03 \left(\frac{d_{\mathrm{h}}}{d_{\mathrm{helix}}}\right)^{0.5}. \tag{3.16}$$

Pressure drop correlation

The pressure drop in each heat exchanger is calculated with the Darcy-Weisbach equation (Brown, 2002):

$$\Delta p = \xi \frac{L}{d_{\mathrm{h}}} \frac{\rho_{\mathrm{fl}}}{2} v^2, \tag{3.17}$$

where L is the length of the heat exchanger, and ξ is the friction factor, which can be used as a calibration parameter.

Equivalent fluid volume

The delay of the heat transfer due to the heat exchanger wall was neglected in energy balance in Equation (3.4). However, the thermal mass of the heat exchanger wall needs to be accounted for in the overall energy balance of the heat exchanger model. This thermal mass is important, since the heat exchanger wall of the adosrber is cycled between adsorption and desorption temperature. Consequently, the energy needed to heat the heat exchanger wall, e.g., influences the coefficient of performance of the adsorption chiller (cf. Equation (2.6)). To account for the thermal mass of the heat exchanger wall, we add an equivalent, ideally mixed fluid volume at the end of the heat exchanger model, which has the same thermal mass as the heat exchanger wall (Figure 3.2). The energy balance of the equivalent fluid volume reads:

$$V_{\mathrm{eq}}\rho_{\mathrm{fl}}\frac{\mathrm{d}h_{\mathrm{fl}}^{\mathrm{eq}}}{\mathrm{d}t} = \dot{m}_{\mathrm{fl}}\left(h_{\mathrm{fl,in}}^{\mathrm{eq}} - h_{\mathrm{fl}}^{\mathrm{eq}}\right), \tag{3.18}$$

where V_{eq} is the geometric volume of the fluid. This geometric volume is calculated from the thermal mass of the heat exchanger wall:

$$V_{\mathrm{eq}} = \frac{m_{\mathrm{wall}}c_{\mathrm{wall}}}{\rho_{\mathrm{fl}}c_{\mathrm{fl}}}, \tag{3.19}$$

where m_{wall} is the mass and c_{wall} is the specific heat capacity of the heat exchanger wall.

The position of the equivalent fluid volume at the end of the heat exchanger has an additional advantage for the numeric solution of the model: When the heat exchangers are connected to other system models, the equivalent fluid volume hydraulically separates the connected models and, thus, avoids systems of non-linear equations (Heijde et al., 2017).

3.1.2 Adsorber bed

The adsorber bed includes the adsorbent and the adsorbate. To model the adsorber bed, we use a lumped-parameter approach based on the work of Lanzerath et al. (2015). The lumped-parameter model assumes a homogenous temperature, loading, and pressure inside the adsorber bed. Figure 3.3 illustrates the structure of the model, which is explained in the following.

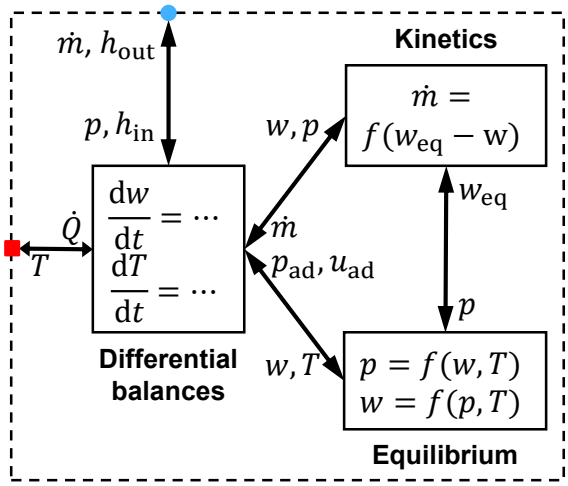

Figure 3.3: Interaction between the sub-models of the adsorber bed. The arrows indicate the flow of information between the sub-models. The red square is a heat port to share the temperature T and heat flow $\dot{Q}$ information with the connected model. The blue circle is a fluid port to share mass flow $\dot{m}$, specific enthalpy h, and pressure p information with the connected model.

Differential balances

The adsorber bed model contains two differential balances, which describe the time-dependent changes of the differential states, namely the loading w (mass balance):

$$m_{\text{sor}} \frac{\text{d}w}{\text{d}t} = \dot{m}_{\text{in/out}}, \tag{3.20}$$

and the temperature T (energy balance):

$$m_{\text{sor}} \left(c_{\text{sor}} + w c_{\text{ad}}\right) \frac{\text{d}T}{\text{d}t} = \dot{m}_{\text{in/out}} \left(h_{\text{in/out}} - u_{\text{ad}}\right) + \dot{Q}. \tag{3.21}$$

On the left of Equation (3.21), m_{sor} and c_{sor} denote the mass of the adsorbent and the specific heat capacity of the adsorbent, respectively. The specific heat capacity of the adsorbate c_{ad} is approximated by the specific heat capacity of the liquid phase (Chakraborty et al., 2007).

On the right of Equation (3.21), the flows are derived from the connected models and the sub-models (cf. Figure 3.3): The incoming specific enthalpy h_{in} and the heat flow $\dot{Q}$ result from the connected models. To calculate the incoming or the leaving mass flow ($\dot{m}_{\text{in/out}}$), the kinetics model is employed, while the internal energy of the adsorbate u_{ad} is derived from the equilibrium model. Finally, the leaving specific enthalpy h_{out} is calculated by the fluid properties of the adsorptive as a function of the current temperature T of

the adsorber bed and the pressure of the adsorbate p_{ad}, which is also calculated by the equilibrium model.

Equilibrium model

The task of the equilibrium model is to fully describe the state of the working pair, given two of three states (temperature, pressure, or loading). Within the adsorber bed model, the equilibrium model delivers the pressure of the adsorbate p_{ad} and the internal energy of the adsorbate u_{ad} for the differential balances, and the equilibrium loading w_{eq} for the kinetic model (cf. Figure 3.3). In this thesis, the equilibrium is described by the model of Dubinin (1967) (cf. Section 2.2.1). However, any other equilibrium model can also be implemented in the adsorber bed model.

For given temperature (T) and loading (w) from the differential balances (Equations 3.20 and 3.21), the pressure of the adsorbate p_{ad} can be derived by calculating the filled pore volume $W(w,T)$ (Equation (2.10)) and using the inverse of the characteristic curve ($W^{-1}(A) = A(W)$) (cf. Equation (2.11)):

$$p_{\mathrm{ad}} = p_{\mathrm{sat}}(T)\ \exp\frac{-A(W)}{RT}. \tag{3.22}$$

The specific internal energy of the adsorbate u_{ad} is also calculated by the equilibrium model as:

$$u_{\mathrm{ad}} = h_{\mathrm{ad}} - \frac{p_{\mathrm{ad}}}{\rho_{\mathrm{ad}}}, \tag{3.23}$$

where the specific enthalpy of the adsorbate h_{ad} results from the model of Dubinin (Equation (2.5)) and the density of the adsorbate ρ_{ad} is approximated by the density of the liquid phase (cf. Section 2.2.1).

To determine the equilibrium loading w_{eq}, the temperature of the adsorber bed T and the pressure at the fluid port p (cf. Figure 3.3) are used to calculate the adsorption potential $A(T,p)$ (Equation (2.11)). The adsorption potential allows to calculate the filled pore volume using the characteristic curve $W(A)$ (Equation (2.12)) and delivers the equilibrium loading w_{eq} (cf. Equation (2.10)):

$$w_{\mathrm{eq}} = W\ \rho_{\mathrm{ad}}. \tag{3.24}$$

In this thesis, we use a characteristic curve of the working pair silica gel 123 / water, which was experimentally determined by Schawe (1999), since both investigated adsorption chillers employ this working pair. The corresponding function and the experimentally determined coefficients are shown in Appendix A.

Kinetics model

The kinetics model delivers the mass flow $\dot{m}_{\mathrm{in/out}}$ adsorbed or desorbed by the adsorber bed for the differential balances (cf. Figure 3.3). For this purpose, the adsorption rate in the mass balance (Equation (3.20)) is described by the linear driving force (LDF) approach (cf. Section 2.2.2) and delivers the mass flow $\dot{m}_{\mathrm{in/out}}$ as function of the equilibrium loading w_{eq} and the current loading w:

$$\dot{m}_{\mathrm{in/out}} = m_{\mathrm{sor}} \frac{15 D_{\mathrm{eff}}}{r_{\mathrm{particle}}^2} \left(w_{\mathrm{eq}} - w \right), \tag{3.25}$$

where D_{eff} is the effective diffusion coefficient and r_{particle} is the particle radius. The effective diffusion coefficient D_{eff} summarizes all transport resistances between the vapor phase and the adsorbate, and is used as a calibration parameter of the model in the following.

3.1.3 VLE volume

To describe the refrigerant in the evaporator and the condenser, we use a lumped-parameter model of a VLE volume, which is also based on the work of Lanzerath et al. (2015). In the VLE model, the refrigerant is assumed to be always in the two-phase region. Furthermore, the liquid phase and the vapor phase are always in thermodynamic equilibrium.

The VLE model contains two differential balances, which describe the time-dependent changes of the differential states, namely the density ρ (mass balance):

$$V \frac{\mathrm{d}\rho}{\mathrm{d}t} = \dot{m}_{\mathrm{in}} - \dot{m}_{\mathrm{out}}, \tag{3.26}$$

and the temperature T (energy balance):

$$V \left(u + \rho \left(\frac{\partial u}{\partial \rho} \right)_T \right) \frac{\mathrm{d}\rho}{\mathrm{d}t} + V \rho c_v \frac{\mathrm{d}T}{\mathrm{d}t} = \dot{m}_{\mathrm{in}} h_{\mathrm{in}} - \dot{m}_{\mathrm{out}} h_{\mathrm{out}} + \dot{Q}, \tag{3.27}$$

where V is the geometric volume of the evaporator or the condenser, and c_v is the specific isochoric heat capacity of the refrigerant.

The partial derivative of the internal energy u with respect to the density ρ can be formulated as (Tummescheit, 2002):

$$\left(\frac{\partial u}{\partial \rho} \right)_T = \frac{1}{\rho^2} \left(-p + T \frac{\mathrm{d}p}{\mathrm{d}T} \right). \tag{3.28}$$

As the refrigerant is in the two-phase region, the derivative of the pressure with respect to the temperature results from the Clausius-Clapeyron equation:

$$\frac{\mathrm{d}p}{\mathrm{d}T} = \frac{\Delta h_\mathrm{v}}{T\left(v_\mathrm{v} - v_\mathrm{liq}\right)}, \tag{3.29}$$

where Δh_v is the specific enthalpy of vaporization, v_v is the specific volume of the vapor phase, and v_liq is the specific volume of the liquid phase.

The entering and leaving mass flows ($\dot{m}_\mathrm{in}$ and $\dot{m}_\mathrm{out}$), the incoming specific enthalpy h_in, and the heat flow $\dot{Q}$ result from the connected models. The leaving specific enthalpy h_out results either from the specific enthalpy of the saturated vapor at the vapor port or from the specific enthalpy of the boiling liquid at the liquid port.

3.2 Calibration and validation method

In this section, we present the calibration and validation method based on Lanzerath (2013), which is applied to determine the calibration parameters of the adsorption chiller model (outer heat transfer values and effective diffusion coefficient, cf. Section 3.1), and to evaluate the accuracy of the model.

3.2.1 Statistical measures

The calibration of the model aims at optimizing the agreement between simulation and measurement for a defined calibration cycle by estimating the unknown calibration parameters. The agreement between simulation and measurement is evaluated for characteristic quantities of the model. As characteristic quantities, we use the heat flows of the adsorption chiller, since the heat flows determine the main performance indicators (COP, SCP and EER, cf. Section 2.1.3). We quantify the agreement between the simulated heat flows $\dot{Q}^\mathrm{i}_\mathrm{sim}$ and the measured heat flows $\dot{Q}^\mathrm{i}_\mathrm{meas}$ over a time period Δt with the root-mean-square deviation $\mathrm{RMSD_i}$ of each component (i $\in$ [evaporator, condenser, adsorber]):

$$\mathrm{RMSD_i} = \sqrt{\frac{1}{\Delta t}\int_0^{\Delta t}\left(\dot{Q}^\mathrm{i}_\mathrm{meas} - \dot{Q}^\mathrm{i}_\mathrm{sim}\right)^2 \mathrm{d}t}. \tag{3.30}$$

To consider the different amounts of energy transferred in each component, we weight each $\mathrm{RMSD_i}$ with the corresponding average heat flow of the component ($Q^\mathrm{i}_\mathrm{meas}/\Delta t$). The weighted $\mathrm{RMSD_i}$ results in the coefficient of variation of each component ($\mathrm{CV_i}$):

$$\mathrm{CV_i} = \frac{\mathrm{RMSD_i}}{Q^\mathrm{i}_\mathrm{meas}/\Delta t} = \frac{1}{Q^\mathrm{i}_\mathrm{meas}/\Delta t}\sqrt{\frac{1}{\Delta t}\int_0^{\Delta t}\left(\dot{Q}^\mathrm{i}_\mathrm{meas} - \dot{Q}^\mathrm{i}_\mathrm{sim}\right)^2 \mathrm{d}t}, \tag{3.31}$$

and the average coefficient of variation of the entire adsorption chiller $\left(\overline{\mathrm{CV}}\right)$:

$$\overline{\mathrm{CV}} = \frac{1}{3}\sum_{\mathrm{i}} \mathrm{CV}_{\mathrm{i}} = \frac{1}{3}\sum_{\mathrm{i}} \left(\frac{1}{\dot{Q}^{\mathrm{i}}_{\mathrm{meas}}/\Delta t} \sqrt{\frac{1}{\Delta t}\int_0^{\Delta t} \left(\dot{Q}^{\mathrm{i}}_{\mathrm{meas}} - \dot{Q}^{\mathrm{i}}_{\mathrm{sim}}\right)^2 \mathrm{d}t} \right). \tag{3.32}$$

The coefficient of variation (CV) characterizes the accuracy of the model. Therefore, the calibration step minimizes the CV by estimating the calibration parameters, as described below.

3.2.2 Application to the adsorption chiller

The presented adsorption chiller model in Section 3.1 has four calibration parameters:

1. the three outer heat transfer values of the heat exchangers adsorber $(hA)^{\mathrm{A}}_{\mathrm{o}}$, evaporator $(hA)^{\mathrm{E}}_{\mathrm{o}}$, and condenser $(hA)^{\mathrm{C}}_{\mathrm{o}}$, cf. Section 3.1.1, and
2. the effective diffusion coefficient D_{eff}, cf. Section 3.1.2.

The four calibration parameters are not independent, since the heat transfer resistances and the mass transfer resistance are connected in series (cf. (Lanzerath, 2013)). Thus, a lower heat transfer coefficient can be compensated by a higher mass transfer coefficient, and vice versa. To allow for an independent estimation of the outer heat transfer values of the condenser $(hA)^{\mathrm{C}}_{\mathrm{o}}$, and of the evaporator $(hA)^{\mathrm{E}}_{\mathrm{o}}$, we use a two-step calibration approach, as illustrated in Figure 3.4. Only the heat transfer value of the adsorber $(hA)^{\mathrm{A}}_{\mathrm{o}}$ and the effective diffusion coefficient D_{eff} cannot be identified independently due to the lack of an additional measurable quantity (cf. (Lanzerath, 2013)).

In the first step of the calibration approach, the condenser (1a) and the evaporator (1b) are calibrated separately. Both calibrations (1a and 1b) proceed in the same way and, therefore, are summarized as the first step. We use the three measured quantities at the model boundaries as input, namely the inlet temperature $T_{\mathrm{in,meas}}$, the volume flow $\dot{V}_{\mathrm{meas}}$, and the vapor pressure in the VLE volume p_{meas}. With the measured inputs, we simulate the outlet temperature $T_{\mathrm{out,sim}}$ to simulate the heat flow $\dot{Q}_{\mathrm{sim}}$. Having the simulated heat flow, the CV values of the condenser and evaporator (Equation (3.31)) are minimized by estimating the respective heat transfer value ($(hA)^{\mathrm{C}}_{\mathrm{o}}$ and $(hA)^{\mathrm{E}}_{\mathrm{o}}$).

In the second step of the calibration approach, the adsorber is calibrated in the entire adsorption chiller model. The heat transfer values of the condenser ($(hA)^{\mathrm{C}}_{\mathrm{o}}$) and the evaporator ($(hA)^{\mathrm{E}}_{\mathrm{o}}$) are fixed as determined in the first calibration step. For the calibration of the adsorber, the measured inlet temperatures $T_{\mathrm{in,meas}}$ and the measured volume flows $\dot{V}_{\mathrm{meas}}$ of all heat exchangers are used as inputs at the model boundaries. Subsequently, the calculated and the measured heat flows of all heat exchangers are used to minimize the $\overline{\mathrm{CV}}$

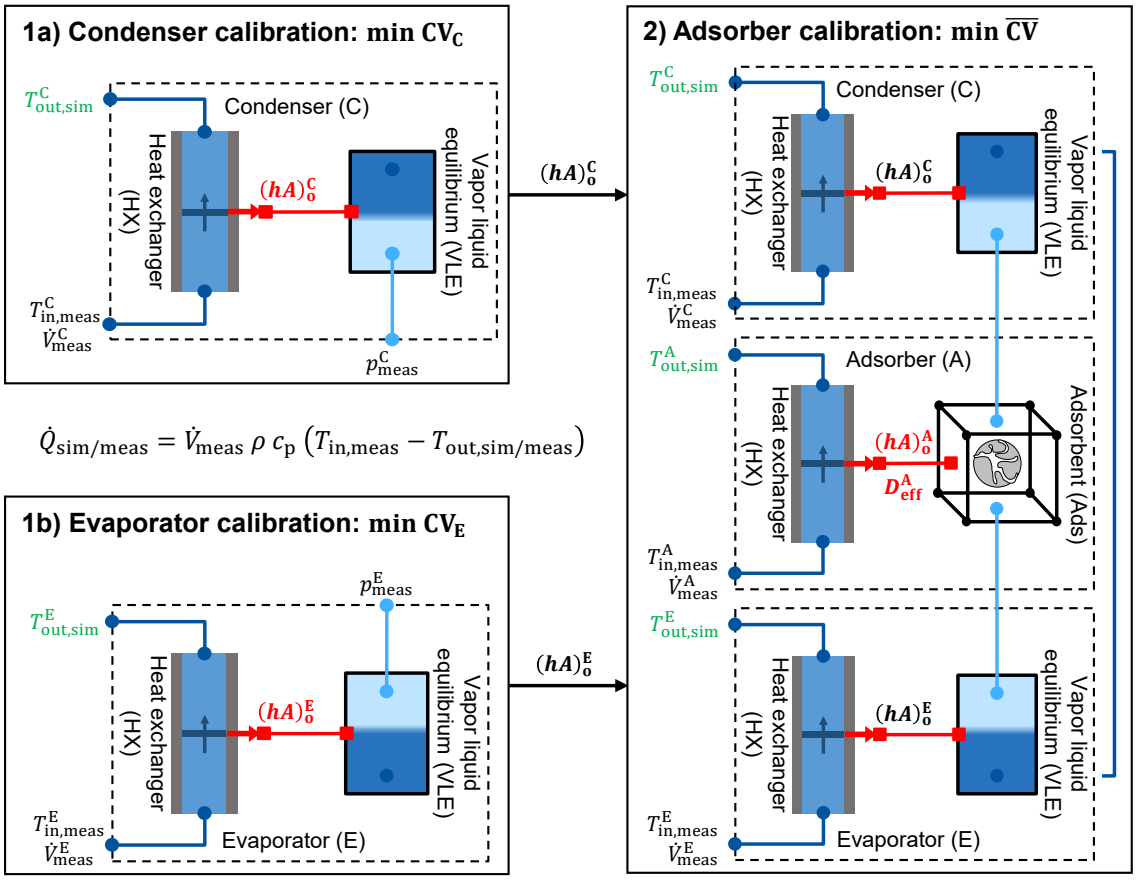

Figure 3.4: Two-step calibration approach for the adsorption chiller model. The inputs and outputs of the models are classified by a color code: measured quantities are black, simulated quantities are green and calibration parameters are red.

(Equation (3.32)) by estimating both remaining calibration parameters of the adsorber: the outer heat transfer value $(hA)^{A}_{o}$) and the effective diffusion coefficient D_{eff}.

To solve the optimization problems in both calibration steps (minimize CV_i and $\overline{CV}$), we use the calibration function of the Dymola design library (Dassault Systèmes, 2020), which transforms the dynamic optimization problem into a non-linear programming problem (NLP) and applies a sequential quadratic programming (SQP) algorithm to solve the NLP (Nocedal and Wright, 2006).

After the calibration step, all calibration parameters are fixed for the validation step. In the validation step, the model accuracy ($\overline{CV}$) is evaluated for varying operating conditions (i.e., inlet temperatures and cycle times).

3.3 Comparison of the plug-flow-based and the discretized adsorption chiller model

To evaluate the plug-flow-based adsorption chiller model, we calibrate and validate (Section 3.2) the model with experimental data, which was generated with a lab-scale one-bed adsorption chiller (Lanzerath, 2013; Lanzerath et al., 2015). The scheme of the adsorption chiller model corresponds to Figure 3.4. Lanzerath et al. (2015) also used their experimental data for the validation of a 1-d, lumped-parameter model (discretized model), which serves as a reference model in the following. Thereby, we can directly compare the plug-flow-based model to an experimentally validated state-of-the-art model, regarding both, accuracy (agreement with experimental data) and computational efficiency (simulation time). A brief description of the considered adsorption chiller test-stand and the corresponding parametrization of the models is given in Appendix B.

As the discretized model trades-off accuracy and computational efficiency depending on the discretization resolution, we consider two cases of the discretized model in the following:

1. A fine discretization of 40 cells in the adsorber, and 10 cells in the evaporator and the condenser. Lanzerath (2013) determined this fine discretization resolution empirically since a finer discretization had no further significant impact on the simulation results. Therefore, the fine discretization serves as the reference model to achieve high accuracy.
2. A coarse discretization of 5 cells in the adsorber, and 2 cells in the evaporator and the condenser. We have chosen this coarse discretization to achieve a similar computational efficiency with the discretized model as with the plug-flow-based model. Therefore, the coarse discretization serves as the reference model to achieve high computational efficiency.

For a further discussion of the discretization resolution, the reader is referred to Appendix C.

The reflux connection between the condenser and the evaporator is modeled by a closeable drain, which returns the liquid refrigerant above a defined filling level from the condenser to the evaporator. The connections between the adsorber and both, the evaporator and the condenser are modeled as manually closeable valves. Note that in contrast to the discretized model of Lanzerath (2013), we neglect the flow resistances between adsorber and the evaporator / the condenser, as the flow resistances are very small compared to the diffusion resistance. Thus, the flow resistances only marginally affect the model output, but increase the simulation time since iterations are needed to calculate the intermediate pressures between the flow and the diffusion resistances. In the following, both models

(discretized and plug-flow-based) are simulated without flow resistances, to allow for a sound comparison between both modeling approaches.

3.3.1 Calibration

To calibrate the adsorption chiller model, we apply the two-step calibration approach (Figure 3.4) for the calibration cycle used by Lanzerath (2013):

1. evaporator inlet temperature of 10 °C,
2. condenser and adsorption inlet temperature of 35 °C,
3. desorption inlet temperature of 90 °C, and
4. adsorption and desorption time of 900 s.

The estimated calibration parameters of the plug-flow-based adsorption chiller model are shown in Table 3.1 and compared to those of the discretized model (cf. Lanzerath (2013)).

Table 3.1: Comparison of the estimated calibration parameters for the plug-flow-based and the discretized adsorption chiller model.

	Discretized model	**Plug-flow-based model**	**Deviation**
Heat transfer value of evaporator $(hA)_{\mathrm{o}}^{\mathrm{E}}$	176 W/K	169 W/K	−4 %
Heat transfer value of condenser $(hA)_{\mathrm{o}}^{\mathrm{C}}$	3174 W/K	2005 W/K	−37 %
Heat transfer value of adsorber $(hA)_{\mathrm{o}}^{\mathrm{A}}$	331 W/K	257 W/K	−22 %
Effective diffusion coefficient D_{eff}	$1.8 \times 10^{-10}\,\mathrm{m^2/s}$	$2.41 \times 10^{-10}\,\mathrm{m^2/s}$	34 %

The estimated heat transfer value of the evaporator is practically identical for both models (deviation of 4 %). In contrast, the estimated heat transfer coefficient of the condenser has the largest deviation between the two models with 37 %. However, the heat transfer coefficient of the condenser barely impacts the simulation results since the outer heat transfer in the condenser is not limiting the process (cf. resistance analysis by Bau (2018)). Thus, its exact value is hard to estimate, as the optimum is very flat. Even if using the heat transfer value estimated by Lanzerath (2013) in the plug-flow-based model (3174 W/K instead of 2005 W/K), the coefficient of variation of the adsorption chiller only changes

less than 1 %. The deviations of the heat transfer value of the adsorber and the effective diffusion coefficient can be explained by the linear dependency between both parameters, as also mentioned by Lanzerath (2013): A higher diffusion coefficient compensates a lower heat transfer coefficient and vice versa. Thus, Lanzerath (2013) gives a range for both parameters with $(hA)_{\mathrm{o}}^{\mathrm{A}} = 250\,\mathrm{W/K}...480\,\mathrm{W/K}$ and $D_{\mathrm{eff}} = 1.3 \times 10^{-10}\,\mathrm{m^2/s}...2.7 \times 10^{-10}\,\mathrm{m^2/s}$, which includes both parameter values identified for the plug-flow-based model (cf. Table 3.1). Nevertheless, using the parameters of Lanzerath (2013) in the plug-flow-based model would worsen the coefficient of variation of the adsorption chiller by 16 %. Thus, a separate calibration of the plug-flow-based model is important to achieve a good model accuracy.

All estimated heat transfer coefficients are higher for the plug-flow-based model than for the discretized model (Table 3.1). We expect that this systematic difference is due to two reasons: 1) The plug-flow-based model assumes a constant temperature at the outer side of the heat exchanger for each entering fluid particle (cf. Section 3.1.1). This assumption leads to a higher driving force for the heat transfer, since the temperature at the outer side is changing in reality due to the heat transfer. To compensate this higher driving force, the estimated heat transfer coefficient for the plug-flow-based model is lower. 2) In the discretized model an upwind discretization scheme is applied (cf. Roetzel et al. (2020)). The upwind scheme uses the leaving temperature of each fluid cell to calculate the heat transfer. Thereby, the driving force is underestimated for a finite discretization, since the driving force of the entering fluid is higher than that of the leaving fluid in each cell. To compensate the lower driving force, the estimated heat transfer coefficient for the discretized model is higher.

Using the estimated calibration parameters from Table 3.1, Figure 3.5 shows the excellent agreement between the experimental data and the simulations of both models (plug-flow-based and finely discretized) for the calibration cycle. Figure 3.5 shows that the plug-flow-based model leads to practically identical results as the finely discretized model. The $\overline{\mathrm{CV}}$-value (Equation (3.32)) of the plug-flow-based model is even slightly lower (13.5 %) than the $\overline{\mathrm{CV}}$-value of the finely discretized model (13.6 %). Thus, both models provide the same accuracy. However, the simulation of the plug-flow-based model is three times faster than the simulation of the finely discretized model. The coarsely discretized model achieves a similar simulation time as the plug-flow-based model, but the $\overline{\mathrm{CV}}$-value increases by 71 % to 23.1 %.

Still, there are some deviations between the models and the experimental data, which are discussed in the following: The peak of the heat flow of the evaporator at the beginning of the cycle (Figure 3.5 (a) at 100-200 s) is slightly overestimated by the models. We expect that the overestimation results from two effects:

1. On the one hand, the LDF approach, used to model the adsorption kinetics, is known to overestimate the uptake at short cycle times (cf. Section 2.2.2).

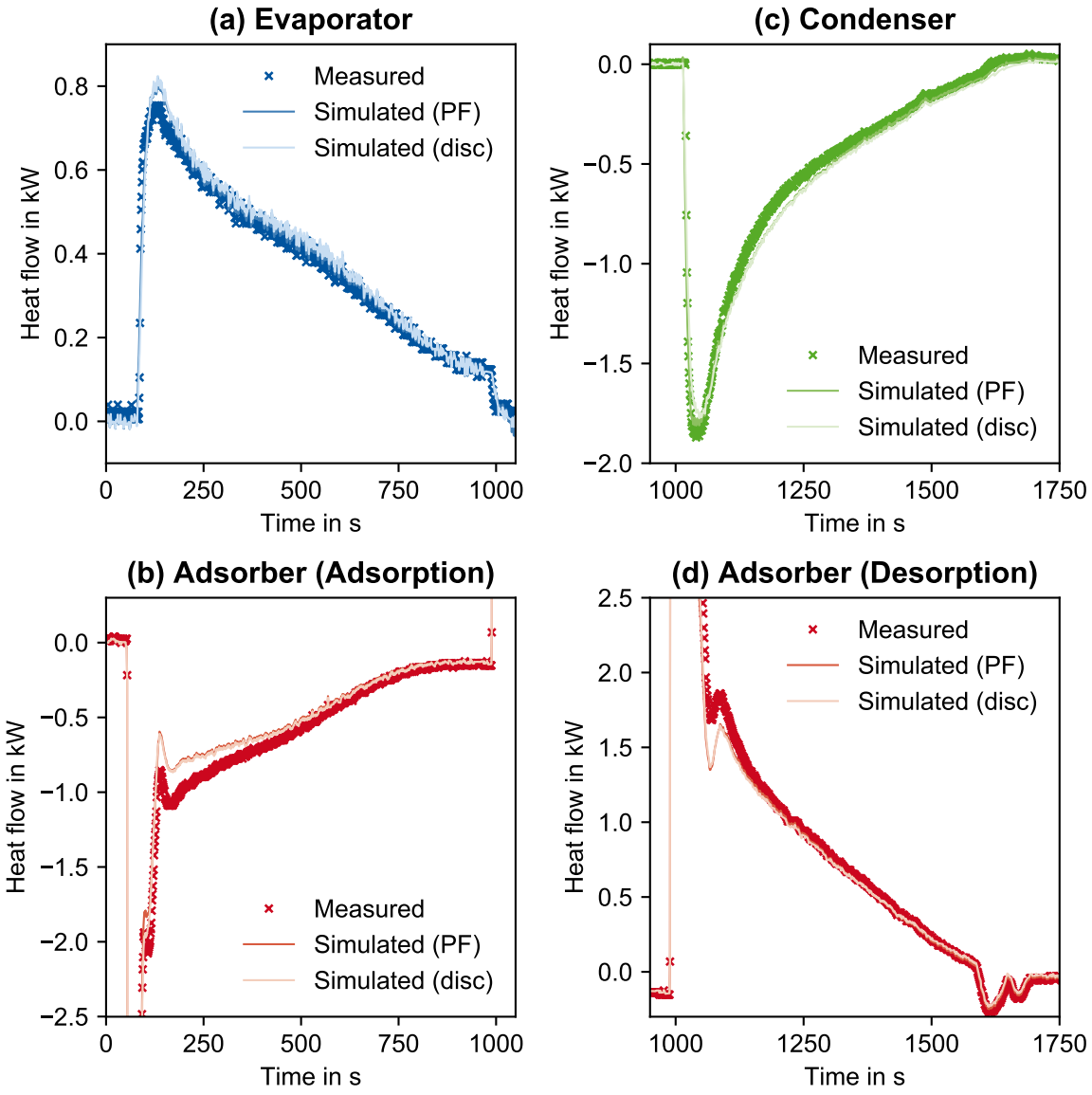

Figure 3.5: Measured and simulated heat flows of the lab-scale one-bed adsorption chiller (Lanzerath, 2013) in the calibration cycle. The simulated heat flows of both models, plug-flow-based (PF) and discretized (disc), are practically identical and, therefore, hard to distinguish. The y-axis of the heat flow of the adsorber is cut off at 2.5 kW since the exchange of hot and cold heat transfer fluid inside the heat exchanger causes a very high peak, that is one order of magnitude higher than the heat flows shown.

2. On the other hand, neglecting the flow resistance between the evaporator and the adsorber might also overestimate the refrigerant vapor flow.

Both effects lead to an overestimation of the heat flow, as more refrigerant is vaporized

in the models. As the overestimation arises in both models, we expect that this model inaccuracy does not result from the proposed plug-flow-based approach.

Furthermore, the model slightly underestimates the heat flows of the adsorber in adsorption phase (Figure 3.5 (b) at 100-400 s) and desorption phase (Figure 3.5 (d) at 1000-1200 s). We expect that the underestimation of the heating and rejecting heat flows results from additional thermal masses of the adsorption chiller or of the test-stand, which are also cycled between adsorption and desorption temperature but are not included in the model. The model of the adsorber only includes the thermal masses of the heat exchanger and the adsorber bed. However, there are also additional thermal masses, such as piping between the heat exchangers and the temperature sensors, fasteners, or casing parts of the adsorber, which are also heated during the desorption process and cooled during the adsorption process. These additional thermal masses are not included in the current model but can be added in future work to improve the agreement with the experimental data further. Note that this underestimation of the heating and the rejecting heat flow in the adsorber also arises in the discretized model. Therefore, we also expect that this model inaccuracy is not specific for the proposed plug-flow-based approach.

3.3.2 Validation

To validate the plug-flow-based adsorption chiller model, we fix the calibration parameters determined for the calibration cycle (Section 3.3.1) and evaluate the model accuracy for changed operating conditions (inlet temperature and adsorption/desorption time). The changed operating conditions are summarized in the seven validation cycles in Table 3.2.

For the validation cycles from Table 3.2, Figure 3.6 compares the plug-flow-based model to the discretized model regarding both, accuracy and computational efficiency. The average coefficient of variation ($\overline{\mathrm{CV}}$) of the plug-flow-based model is between 9.3 % and 30.4 % for all validation cycles. Lanzerath (2013) also stated a similar range of $\overline{\mathrm{CV}}$-values between 12.6 % and 27.4 % for his finely discretized model. Furthermore, Lanzerath (2013) showed that even for a $\overline{\mathrm{CV}}$-value of 27.4 % the simulated and the measured heat flows showed a good qualitative agreement and the performance indicators coefficient of performance and specific cooling power were almost predicted within the measurement uncertainties. Thus, the similar $\overline{\mathrm{CV}}$-range of the plug-flow-based model indicates that the calibrated model is also able to predict different operating points than the calibration cycle.

Regarding the accuracy, the plug-flow-based and the finely discretized model are equivalent, with a slight benefit for the plug-flow-based model (Figure 3.6 (a)): The $\overline{\mathrm{CV}}$-values are almost equal for the calibration cycle (C) and for the validation cycles V4 and V7. For the validation cycles V1, V2 and V6 the $\overline{\mathrm{CV}}$-values of the plug-flow-based model are even lower by 24.5 %, 10.8 % and 27 %, respectively. Only in the validation

Table 3.2: Variation of the operating conditions (inlet temperatures and adsorption/desorption time) for the validation cycles of the lab-scale, 1-bed adsorption chiller (Lanzerath, 2013). The varied condition compared to the calibration cycle (first line) is bold.

Desorption inlet temperature in °C	**Condenser / adsorption inlet temperature in** °C	**Evaporator inlet temperature in** °C	**Adsorption / desorption time in** s
90	35	10	900
90	35	10	**450**
90	35	10	**1800**
90	35	**5**	900
90	35	**20**	900
70	35	10	900
110	35	10	900
90	**25**	10	900

cycles V3 and V5 the plug-flow-based model has higher $\overline{\text{CV}}$-values by 7.3 % and 11.2 %, respectively.

Regarding computational efficiency, the plug-flow-based model significantly outperforms the finely discretized model, as the simulation time is reduced by 65 %-70 % in all cycles (Figure 3.6 (b)). To achieve the computational efficiency of the plug-flow-based model, the discretization resolution of the discretized model has to be reduced by 75 % (coarsely discretized model). However, the coarsely discretized model worsens the accuracy by increasing the $\overline{\text{CV}}$-values between 13.2 % in the validation cycle V5 and 129.6 % in the validation cycle V1 compared to the plug-flow-based model.

To emphasize the quality of the plug-flow based model, Figure 3.7 compares the predicted performance indicators of the adsorption chiller (coefficient of performance COP and specific cooling power SCP, cf. Section 2.1.3) to those of the accurate, finely discretized model and the measured values. The predicted performance indicators are mostly within the measurement uncertainties. The largest deviation from the measured values for both performance indicators (COP and SCP) can be observed in the validation cycle V4, where the simulated values are slightly outside the measurement uncertainty. Nevertheless, the plug-flow-based model is closer to the measured values than the finely discretized model in the validation cycle V4: The deviation from the measured COP is 15.6 % for the finely discretized model and 13.3 % for the plug-flow-based model. The deviation from the measured SCP is 11.7 % for the finely discretized model and 9.5 % for the plug-flow-based model.

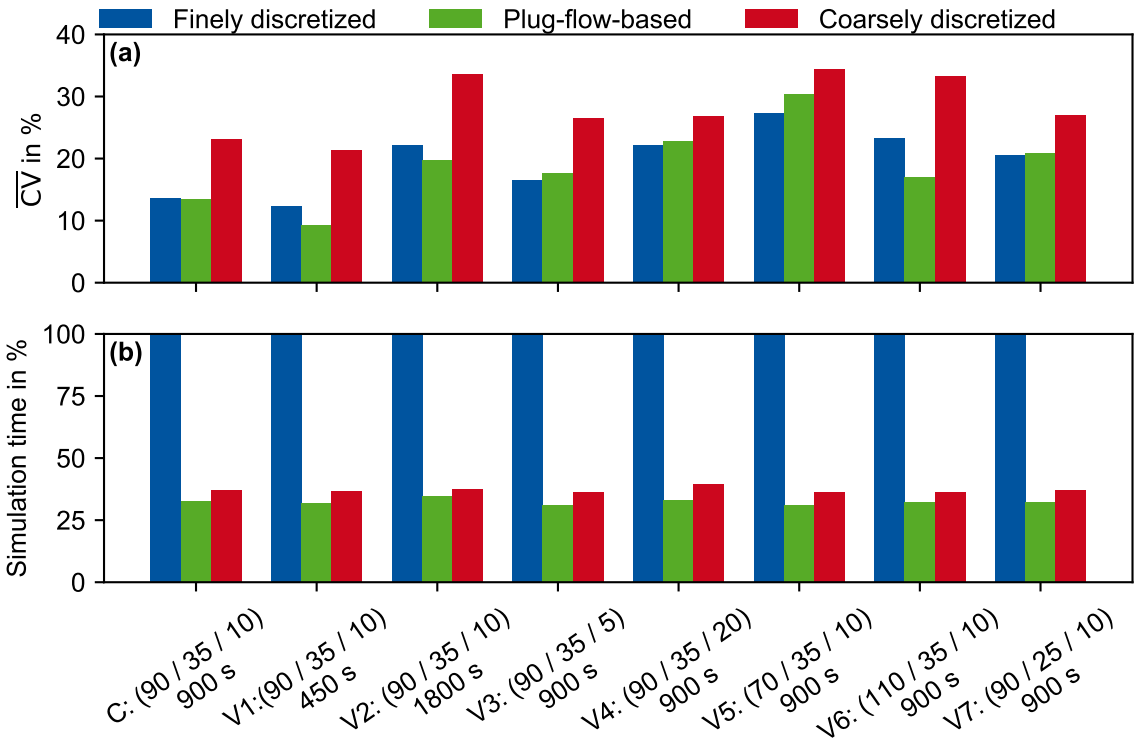

Figure 3.6: Comparison of the plug-flow-based and the discretized model of the lab-scale adsorption chiller for the calibration cycle (C) and the validation cycles (V1-V7) (Table 3.2). (a) Evaluation of the accuracy by the average coefficient of variation $\overline{CV}$ (Equation (3.32)). (b) Evaluation of the computational efficiency by the relative simulation time referred to the finely discretized model.

While the specific cooling power of the adsorption chiller is both, under- and overestimated by the models, the COP is overestimated systematically. This systematic overestimation of the COP results from the underestimation of the heat flow of the heating circuit (Figure 3.5) due to the additional thermal masses of the test stand not considered in the model (cf. discussion in Section 3.3.1). To improve the accuracy of the model further, the additional thermal masses can be added to the model in future work. Note that the same systematic overestimation of the COP arises in both models (Figure 3.7) and thus, is not a specific drawback of the proposed plug-flow-based approach.

The results show that the plug-flow-based adsorption chiller model has practically the same accuracy as the finely discretized model but significantly improves the computational efficiency by up to 70 %. The improved computational efficiency results from the drastic reduction of differential equations since the discretized model needs to solve the energy balance in each fluid and wall cell. Therefore, the finely discretized model has 88 %

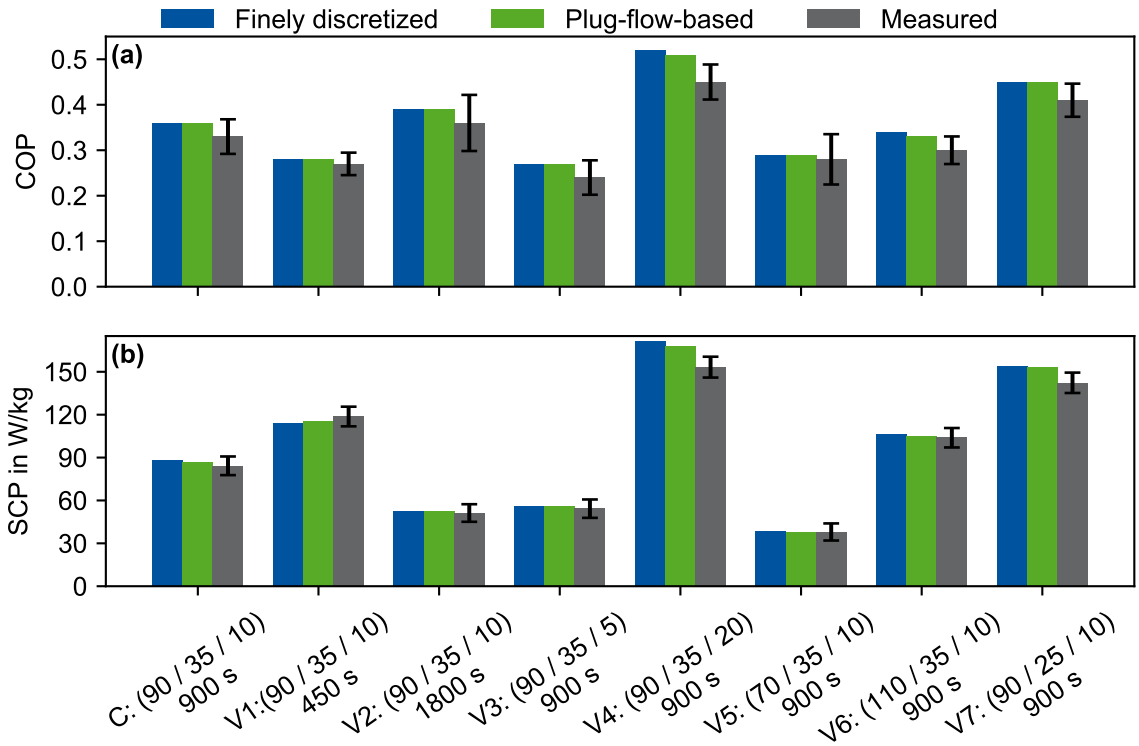

Figure 3.7: Prediction of the performance indicators of both models, the plug-flow-based and the finely discretized, and comparison to the measured values: (a) coefficient of performance COP and (b) specific cooling power SCP. The measurement uncertainties are indicated by black bars.

more differential equations (126 differential equations) than the plug-flow-based model (15 differential equations).

3.4 Model validation for a commercial two-bed adsorption chiller

In this section, we want to demonstrate the applicability of the proposed plug-flow-based model (Section 3.1) to other adsorption chillers. For this purpose, we used experimental data of the commercial adsorption chiller *Invensor LTC 30 e plus* (Invensor GmbH, 2020) and applied the calibration and validation method from Section 3.2 to this chiller.

The commercial adsorption chiller consists of two adsorber beds to allow for quasi-continuous operation. To describe the two-bed adsorption chiller, we added a second identical adsorber to the model. Furthermore, we modeled the connections between the heat exchangers of the model and the three hydraulic circuits as defined by the manufacturer (Figure 3.8). The adsorption chiller has connections for three hydraulic circuits, which are

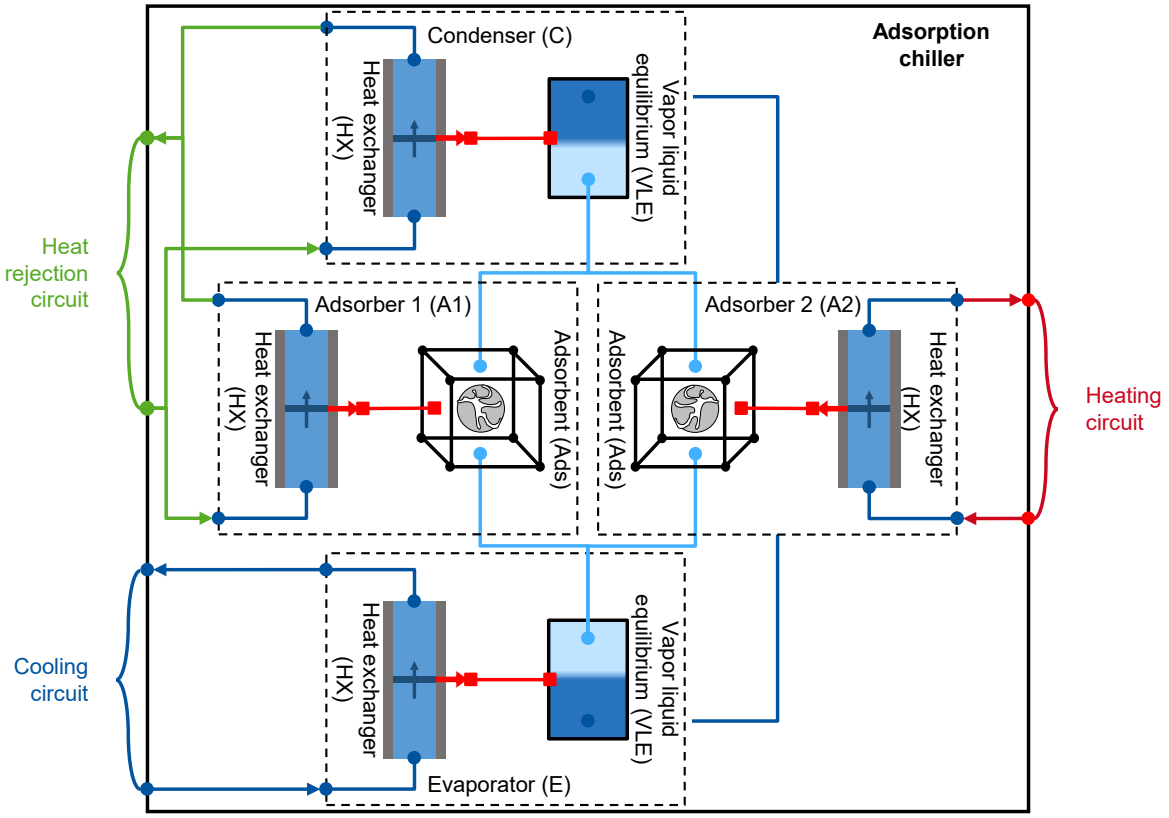

Figure 3.8: Scheme of the two-bed adsorption chiller model. The model consists of two adsorbers (A1 and A2), one evaporator (E) and one condenser (C). In the illustrated connection of the hydraulic circuits, adsorber 1 is in adsorption phase and adsorber 2 is in desorption phase.

needed for operation (Figure 3.8):

1. The heating circuit provides the driving power from a heat source.
2. The heat rejection circuit rejects the waste heat to a heat sink.

3. The cooling circuit provides useful cooling power for the cooling application.

To continuously operate the chiller, one adsorber is always connected to the heating circuit (desorption phase) while the other adsorber is connected to the heat rejection circuit (adsorption phase). Thereby, one adsorber always adsorbs the evaporated refrigerant from the evaporator to continuously provide cooling power. The two phases (desorption and adsorption) have equal duration and are periodically switched between both adsorbers. The duration of the phases is determined by an internal control algorithm of the manufacturer. In the model, the duration of the phases given as fixed input, which is taken from the measurement data. The evaporator and the condenser are always connected to the cooling circuit and the heat rejection circuit, respectively. In the adsorption phase both, the condenser and the adsorber reject heat to the heat rejection circuit. Therefore, both components are connected in parallel. Thus, the heat rejection circuit is split into two flows, one for the adsorber and one for the condenser. The splitting ratio is also determined internally and, therefore, also given as an input to the model.

The refrigerant connections between the adsorbers and the evaporator / the condenser are modeled by flap valves:

1. The refrigerant can only flow from the evaporator to the adsorber, if the evaporator pressure is higher than the adsorber pressure, while the other flow direction is always closed.
2. The refrigerant can only flow from the adsorber to the condenser, if the adsorber pressure is higher than the condenser pressure, while the other flow direction is also closed.

The reflux between the condenser and the evaporator is modeled by a drain, which keeps the filling level of the condenser constant by returning the condensed refrigerant to the evaporator.

3.4.1 Calibration

The calibration step estimates the calibration parameters of the model, namely the outer heat transfer values of the heat exchangers and the effective diffusion coefficient, cf. Section 3.2.2. As calibration cycle, we use the nominal operating point defined by the manufacturer (temperature triple 85 / 27 / 18):

1. heating temperature of 85 °C,
2. heat rejection temperature of 27 °C and
3. cooling temperature of 18 °C.

The manufacturer provided time-resolved measurement data within a cooperation project,

for which a non-disclosure agreement applied. Therefore, time-resolved data shown in the following is normalized.

Figure 3.9 shows the excellent agreement between the measured and the simulated heat flows for the calibration cycle. The $\overline{\mathrm{CV}}$-value of the model in the calibration cycle is

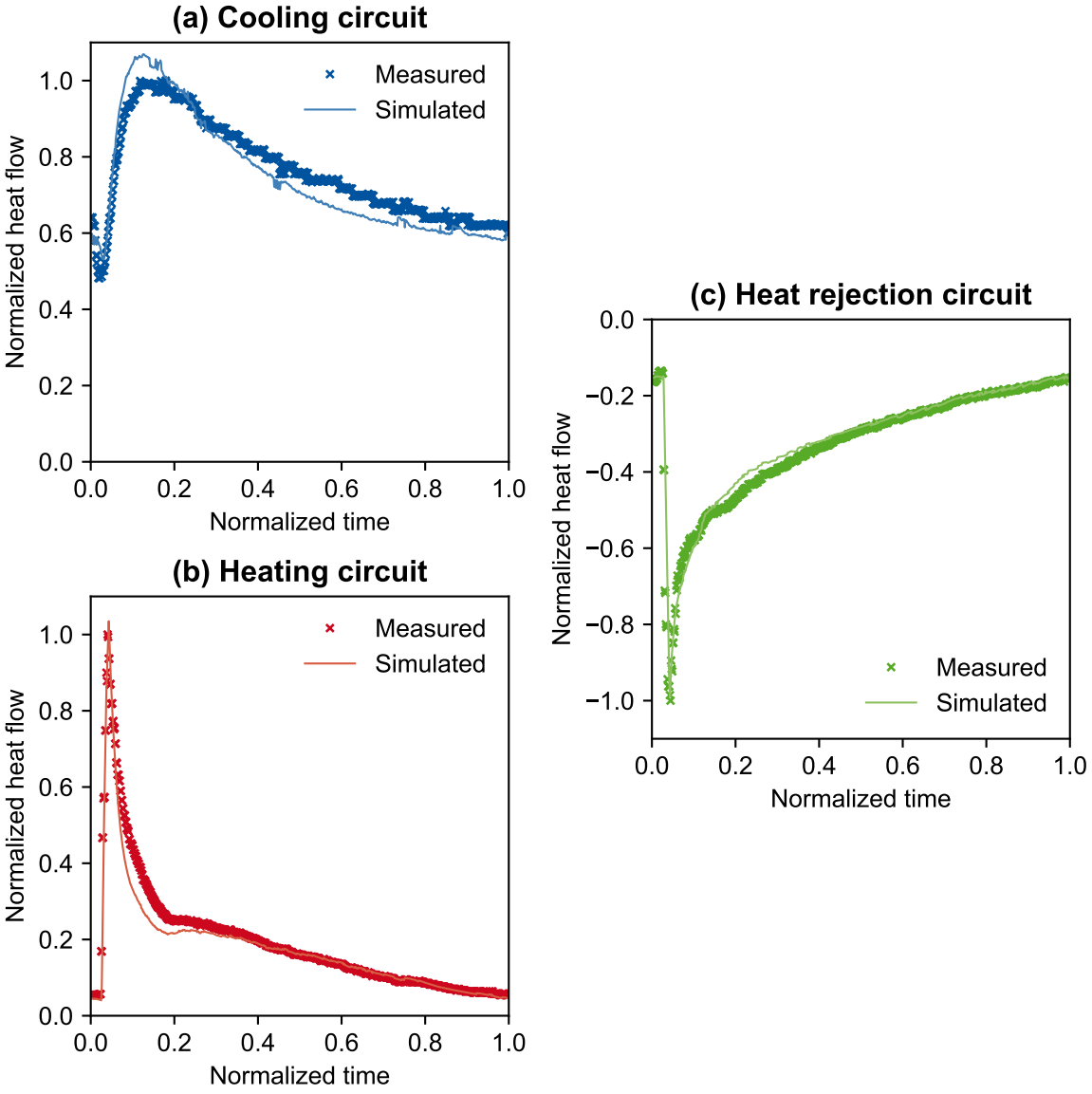

Figure 3.9: Measured and simulated heat flows of the commercial two-bed adsorption chiller *Invensor LTC 30 e plus* (Invensor GmbH, 2020) in the calibration cycle. The axes are normalized by their maximal value.

13 %, which is even slightly lower than for the lab-scale adsorption chiller in Section 3.3.1 (13.5 %). Nevertheless, there are some deviations between the model and the experimental data: (1) The model slightly overestimates the peak of the heat flow of the cooling circuit

at the beginning of the cycle (Figure 3.9 (a) at normalized time between 0.1-0.2). (2) The model slightly underestimates the heat flow of the heating circuit (Figure 3.9 (b) at normalized time between 0.1-0.2) and the heat flow of the heat rejection circuit (Figure 3.9 (c) at normalized time between 0.2-0.4). Both deviations also arose for the lab-scale one-bed adsorption chiller. For a discussion of these deviations the reader is referred to Section 3.3.1.

3.4.2 Validation

Next, we validate the model by varying the operating conditions of the adsorption chiller and evaluating the accuracy of the calibrated model with fixed calibration parameters. The varied operating conditions of the validation cycles are summarized in Table 3.3. Note

Table 3.3: Variation of the operating conditions (inlet temperatures and volume flows) for the validation cycles of the *Invensor LTC 30 e plus* adsorption chiller (Invensor GmbH, 2020). The varied conditions compared to the calibration cycle (first line) are bold.

Heating circuit inlet temperature in °C	**Heat rejection circuit inlet temperature in** °C	**Cooling circuit inlet temperature in** °C	**Volume flows**
85	27	18	nominal
85	**25**	18	nominal
85	**25**	18	**halved**
65	27	18	nominal
75	27	**12**	nominal
75	**32**	18	nominal

that in contrast to the validation cycles in Table 3.2, there are following differences:

1. The cycle time is not manually varied, but determined by an internal control algorithm. Therefore, the cycle time is different in each validation cycle.
2. There are also simultaneous variations of more than one operating condition compared to the calibration cycle.
3. The variation of the volume flows in the hydraulic circuits is also considered. The nominal volume flows are given in the data-sheet of the adsorption chiller (Invensor

GmbH, 2020): 6300 l/h in the heating circuit, 11 400 l/h in the heat rejection circuit, and 6600 l/h in the cooling circuit.

Figure 3.10 shows the accuracy of the calibrated model for the validation cycles. The

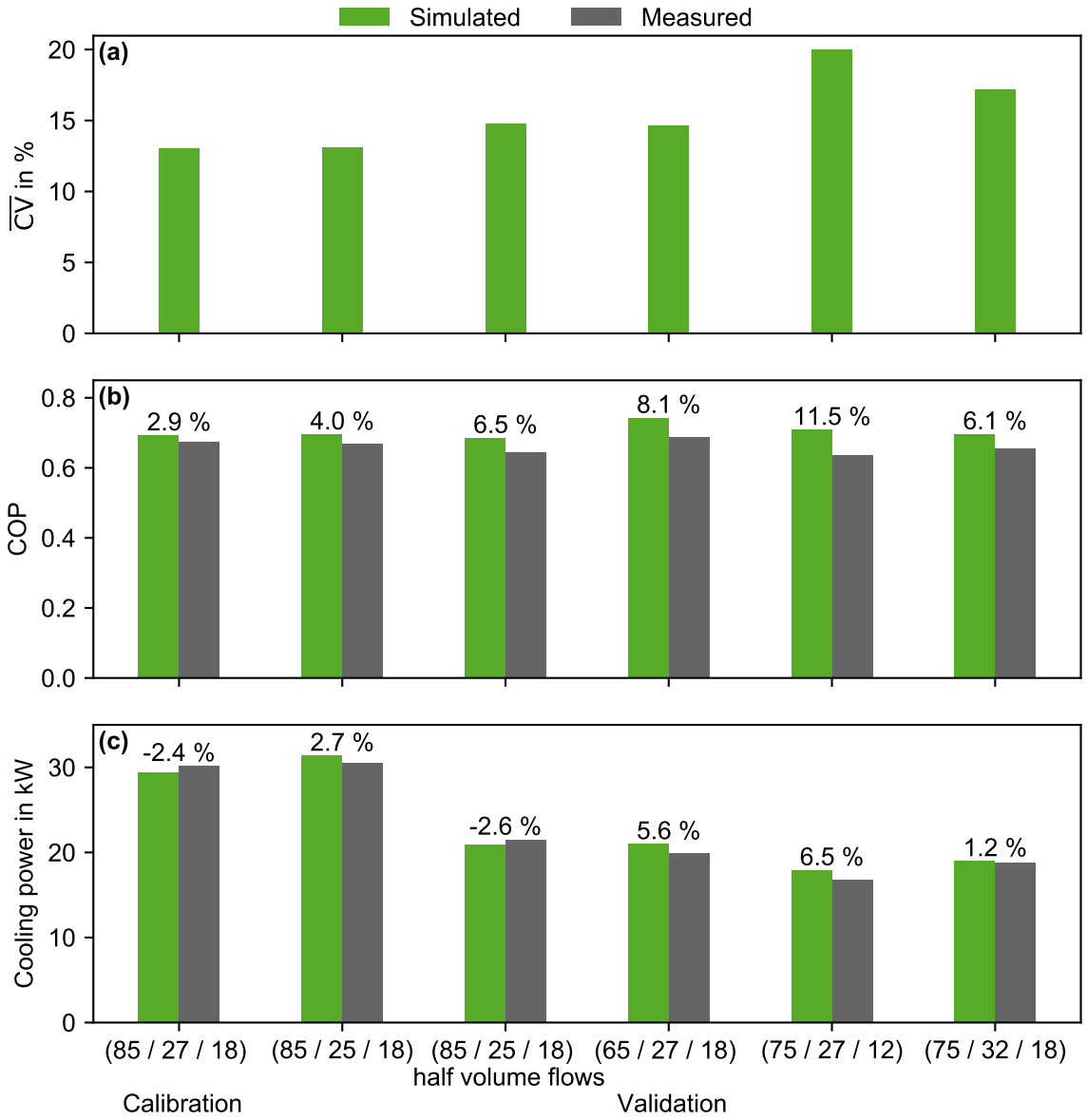

Figure 3.10: Validation of the plug-flow-based model of the *Invensor LTC 30 e plus* adsorption chiller (Invensor GmbH, 2020) for all measured cycles (Table 3.3). (a) Evaluation of the accuracy by the average coefficient of variation $\overline{CV}$ (Equation (3.32)). Comparison between the measured and the simulated values of (b) the coefficient of performance COP and (c) the average cooling power. The deviations between simulated and measured values are given above the bars.

average coefficient of variation $\overline{CV}$ for all validation cycles is between 13.1 % and 20 %

(Figure 3.10 (a)), which results in a maximal increase of the $\overline{\mathrm{CV}}$ by 54 % compared to the calibration cycle (13 %). This increase of the $\overline{\mathrm{CV}}$ in the validation cycles is even lower than for the models of the lab-scale adsorption chiller in Section 3.3.2 (increase of up to 100 %). The absolute values of the $\overline{\mathrm{CV}}$ are also in the same range as for the model of the lab-scale adsorption chiller (Section 3.3.2).

Furthermore, the coefficient of performance COP and the average cooling power are also predicted very accurately: The deviation between the measured and the simulated value is between 2.9 % and 11.5 % for the COP (Figure 3.10 (b)) and between 1.2 % and 6.5 % for the average cooling power (Figure 3.10 (c)). These deviations from the measured values are also even lower than for the models of the lab-scale adsorption chiller (Section 3.3.2). As the model of the lab-scale adsorption chiller was already quiet accurate (cf. Section 3.3.2 and Lanzerath (2013)), the results show that the plug-flow-based model can also describe the commercial two-bed adsorption chiller with high accuracy.

While the average cooling power of the adsorption chiller is both, under- and overestimated by the model, the COP is overestimated systematically. This systematic overestimation also arose for the lab-scale one-bed adsorption chiller. For a discussion of this overestimation the reader is referred to Section 3.3.2.

3.5 Validity of the plug-flow-based model

In this section, we further test the validity range of the plug-flow-based modeling approach. For this purpose, we focus on the adsorber as the key component of the adsorption chiller. We consider an adsorber with an ideal evaporator and condenser, as shown in Figure 3.11. The adsorber is parametrized according to the lab-scale adsorption chiller investigated in Section 3.3. Furthermore, the following analyzes also employ the calibration cycle from Section 3.3.

As discussed in Section 3.1.1, the proposed plug-flow-based heat exchanger model is based on the assumption that the temperature change of the thermally connected component is small for the propagation time of a fluid particle. This assumption can be tested with the Stanton number (Equation (3.11)). Therefore, we investigated the deviation between the simulated heat flows of the plug-flow-based adsorber and of the finely discretized adsorber as a function of the Stanton number (Figure 3.12). This deviation between both models is referred to as the error of the plug-flow-based model in the following. To quantify the error of the plug-flow-based model, we use the coefficient of variation (CV) of the adsorber (cf. Section 3.2.1). The discretization of the discretized adsorber was chosen to 100 cells to ensure that the simulation results are independent of the discretization. The influence of the discretization resolution on the simulation results is discussed further in Appendix C.

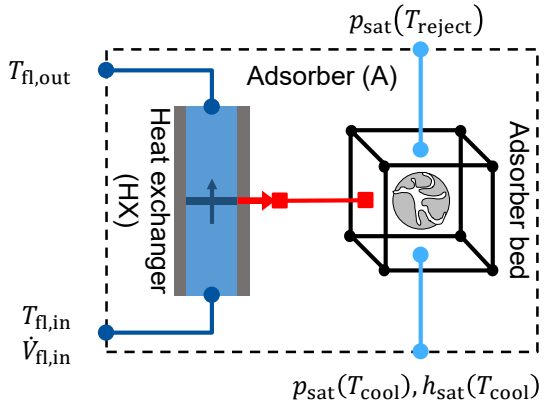

Figure 3.11: Scheme of the adsorber model with ideal evaporator and condenser. The ideal evaporator is modeled as constant saturation pressure and specific saturation enthalpy at cooling temperature ($p_{sat}(T_{cool})$ and $h_{sat}(T_{cool})$), and the ideal condenser is modeled as constant saturation pressure at cooling temperature ($p_{sat}(T_{cool})$). The inlet temperature of the heat transfer fluid $T_{fl,in}$, and the inlet volume flow $\dot{V}_{fl,in}$ are given as model inputs, while the outlet temperature of the heat transfer fluid $T_{fl,out}$ is delivered as output.

As expected, the error of the plug-flow-based adsorber increases with an increasing Stanton number (Figure 3.12), due to the worsening model assumption of a small temperature change of the connected adsorber bed for the propagation time of a fluid particle (cf. Section 3.1.1). For the same reason, the error of the plug-flow-based model decreases if the thermal mass of the adsorbent ($(mc)_{sor}$) increases compared to the heat transfer fluid ($(mc)_{fl}$) leading to the higher thermal inertia and, thus, slower temperature change.

In each case shown in Figure 3.12, the error of the plug-flow-based model is less than 50 % of the deviation between measurement and simulation: For the thermal mass ratio of 0.56 corresponding to the lab-scale adsorber (Section 3.3), the error of the plug-flow-based model is between 5.8 % for small Stanton numbers and 37.4 % for high Stanton numbers. For the doubled ratio of thermal masses (1.12), the error of the plug-flow-based model is between 4.7 % and 26.5 %, while for the halved ratio of thermal masses (0.28), the error of the plug-flow-based model is between 6.4 % and 46.5 %. For small Stanton numbers below 1×10^{-3}, the error of the plug-flow-based model is less than 14 % and very similar for all three ratios of thermal masses. In contrast, the error increases strongly for Stanton numbers above 1×10^{-3}. Furthermore, the error also increases for small mass ratios more strongly. Therefore, we recommend the use of the plug-flow-based model for Stanton numbers between 1×10^{-4} and 1×10^{-3} (green shading in Figure 3.12). Outside this range of Stanton numbers, we propose a case-specific analysis to decide whether the error of the plug-flow-based model is acceptable. However, we expect that most adsorption chillers will

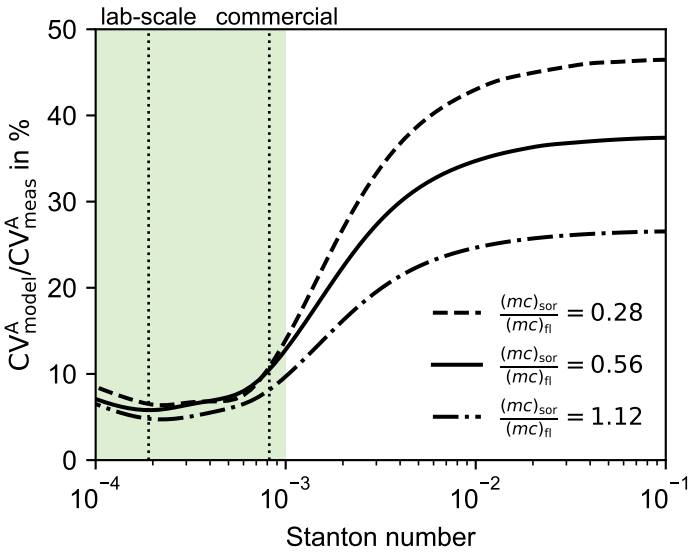

Figure 3.12: Error of the plug-flow-based model as a function of the Stanton number. The deviation is quantified by the normalized coefficient of variation of the adsorber (A) (CV^A): the CV^A between the plug-flow-based and the discretized adsorber model (CV^A_{model}) referred to the CV between the measurement and the simulation of the adsorber (CV^A_{meas}) in the calibration cycle (Section 3.3.1). The error of the plug-flow-based model is shown for three different thermal mass ratios of adsorbent ($(mc)_{sor}$) to heat transfer fluid ($(mc)_{fl}$). The thermal mass ratio of 0.56 corresponds to the lab-scale one-bed adsorption chiller (Section 3.3). Furthermore, the Stanton numbers of the lab-scale adsorber (Section 3.3) and of the commercial adsorber (Section 3.4) are shown. The green shading indicates our recommended range for the use of the plug-flow-based model.

be covered by the recommended range, as shown for the lab-scale (Section 3.3) and the commercial (Section 3.4) adsorption chiller in this thesis (Figure 3.12).

Note that for very small Stanton numbers (approximately below 2×10^{-4}), the error of the plug-flow-based model also slightly increases. The reason for this increase is that the thermal connection between the adsorber bed and the heat exchanger becomes very poor since the radial convective heat transfer is very small. Therefore, almost no heat is transferred to the adsorber bed and the model mainly describes the dynamics of the heat exchanger wall. However, the thermal inertia of the heat exchanger wall is not modeled precisely by the plug-flow-based model but approximated by an equivalent fluid volume. This approximation is based on the assumption that the dynamics of the wall are negligible compared to the dynamics of the adsorber bed (cf. Section 3.1.1). This approximation of the heat exchanger wall starts to become critical for very small Stanton numbers below 1×10^{-4}, since the adsorber bed practically does not participate in the heating and cooling process. However, we believe that the range of very small Stanton numbers below 1×10^{-4}

is irrelevant for technical applications of adsorption chillers, as the adsorber bed is almost thermally isolated from the heat exchanger leading to an inefficient process.

3.6 Summary

The spatial discretization of heat exchangers often leads to computationally expensive models of adsorption chillers. Here, we proposed an alternative modeling approach for the heat exchangers to improve computational efficiency while ensuring high accuracy. In the proposed approach, the discretization of the heat exchanger models is avoided by applying operator splitting to the convective transport equation of the heat transfer fluid leading to a plug-flow-based model.

The proposed model proved to be as accurate as a finely discretized model of a lab-scale one-bed adsorption chiller: The average coefficient of variation $\overline{\mathrm{CV}}$, which characterizes the deviation from experimental data, was similar for both models or even lower by up to 26 % for the plug-flow-based model. Furthermore, the plug-flow-based model was able to predict the main performance indicators of the adsorption chiller (coefficient of performance COP and specific cooling power SCP) more accurately than the discretized model: The deviation from measured COP was below 12 % for the plug-flow-based model, while the deviation was up to 16 % for the discretized model. The deviation from measured SCP was below 10 % for the plug-flow-based model, while the deviation was up to 12 % for the discretized model. At the same time, the computational efficiency of the plug-flow-based model was significantly higher by up to 70 % compared to the discretized model.

The applicability of the proposed model was also demonstrated for a commercial two-bed adsorption chiller. For the commercial two-bed adsorption chiller, the model also achieved similar good accuracy as for the lab-scale one-bed adsorption chiller: The average coefficient of variation $\overline{\mathrm{CV}}$ was in the same range as for the lab-scale adsorption chiller (below 20 % for all measured cycles). Furthermore, the coefficient of performance COP and the average cooling power were predicted very accurately with a maximal deviation below 12 % for the COP and below 7 % for the average cooling power.

Finally, the validity of the proposed plug-flow-based model was tested. We found that the plug-flow-based model is well suited in the range of Stanton numbers between 1×10^{-4} and 1×10^{-3} with deviations from a finely discretized model is below 14 % of the deviation from the measurement. Outside this range of Stanton numbers, we propose a case-specific analysis to test the model validity.

Overall, the proposed plug-flow-based modeling approach provides an accurate and computationally efficient alternative to the discretization of heat exchangers of adsorption

chiller models. The high computational efficiency makes the model well suited for addressing complex design and control optimizations of full-scale adsorption chiller systems.

CHAPTER 4

Integration into a hybrid system

In this chapter, we comprehensively assess the potential energy savings by a hybrid system integrating an adsorption chiller into a CO_2 vapor-compression cycle. For this purpose, we first discuss and present a suitable concept for the hybrid system. Secondly, we employ dynamic modeling and optimization methods to efficiently optimize control parameters, such as high pressure level of the CO_2 cycle and cycle time of the adsorption chiller as well as design parameters, such as the size ratio between adsorption chiller and CO_2 cycle. For the optimized hybrid system, we show the impact of the ambient temperature and the electrical energy demand of the adsorption chiller on the energy savings compared to a stand-alone CO_2 cycle. Finally, we present the annual energy savings for two case studies: (1) the first case study represents a warm climate in Athens, where 22 % of electrical energy can be saved; (2) the second case represents a moderate climate in Cologne, where 16 % of electrical energy can be saved.

This chapter is organized as follows: In Section 4.1, we discuss hybrid system concepts

---

Contents of this chapter have been reprinted from:

A. Gibelhaus, N. Fidorra, F. Lanzerath, U. Bau, J. Köhler, and A. Bardow. "Hybrid refrigeration by CO_2 vapour compression cycle and water-based adsorption chiller: An efficient combination of natural working fluids". *International Journal of Refrigeration* 103 (2019), pp. 204–214, with permission from Elsevier. Contributions of the author: Writing the draft as principal author, implementing the models, planning and conducting the simulations, and evaluating the results.

and derive a concept, which is investigated in the following sections. In Section 4.2, we introduce the modeling and optimization framework to assess the hybrid system systematically. Based on the systematic assessment, we present the energy savings by the hybrid system in Section 4.3 and, afterward, the summary in Section 4.4.

4.1 Hybrid system concept

In this section, we first discuss potential combinations of a CO_2 vapor compression cycle and a sorption chiller (cf. Section 2.3). The discussed combinations generally apply for both ab- and adsorption chillers. For this reason, we refer to sorption chillers in general in the discussion in Section 4.1.1. Based on the discussion, we derive a hybrid system concept, which we present in Section 4.1.2. For the following investigations, we only consider adsorption chillers due to the advantages mentioned in Section 2.3.

4.1.1 Combinations of CO_2 cycle and sorption chiller

Figure 4.1 shows the schematic layouts of the potential combinations of CO_2 vapor compression cycle and sorption chiller. For a detailed literature review and discussion of these combinations the reader is referred to Section 2.3. CO_2 cycles and sorption chillers are frequently combined in cascade systems (Colorado and Rivera, 2015; Vasta et al., 2018). In a cascade system, the sorption chiller absorbs the complete heat released from the CO_2 cycle $\dot{Q}_{\text{cool}}$ and releases it to the ambient $\dot{Q}_{\text{waste}}$ as shown in Figure 4.1 (a). Thus, the sorption chiller sets the high pressure level of the CO_2 cycle and enables subcritical operation even at high ambient temperatures. With such cascade systems, electrical energy savings up to 50 % have been reported compared to stand-alone CO_2 cycles (Vasta et al., 2018). However, sorption chillers of large capacities are required to absorb the complete heat released from the CO_2 cycle and, thus, a large amount of external driving heat $\dot{Q}_{\text{drive}}$ has to be available for the sorption chiller.

Instead of absorbing the entire heat from the CO_2 cycle, the sorption chiller can also only extend the heat-release step in the CO_2 cycle below the ambient temperature, resulting in a partially integrated hybrid system (cf. Figure 4.1 (b)): After heat release to the environment ($\dot{Q}_{\text{waste}}$) in a gas cooler, the sorption chiller can further cool the CO_2 ($\dot{Q}_{\text{cool}}$) even below ambient temperature (Mohammadi and Ameri, 2016; Salajeghe and Ameri, 2016). In this operation mode, the major part of the heat is rejected to the environment ($\dot{Q}_{\text{waste}}$), wherefore transcritical operation of the CO_2 cycle can usually not be avoided at high ambient temperatures. Still, the efficiency of the transcritical CO_2 cycle increases due to additional cooling by the sorption chiller ($\dot{Q}_{\text{cool}}$). However, an external heat source is still required to drive the sorption chiller ($\dot{Q}_{\text{drive}}$). Simultaneously, waste heat at high

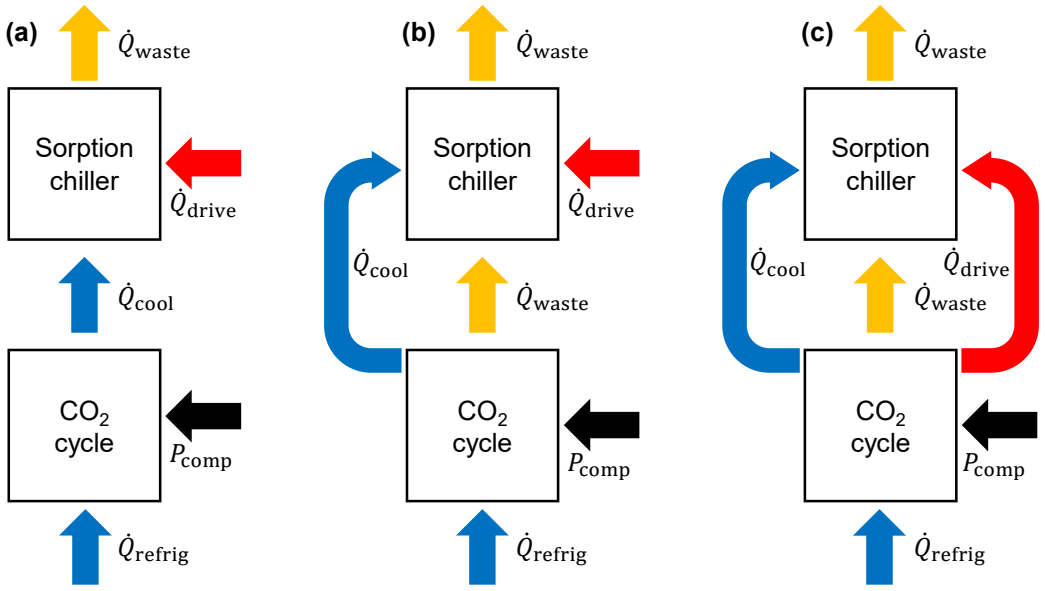

Figure 4.1: Schematic layouts of the potential combinations of CO_2 vapor compression cycle and sorption chiller: (a) cascade system, (b) partially integrated hybrid system and (c) fully integrated hybrid system. Energy flows are shown as arrows. The integrated energy flows are the driving heat flow rate $\dot{Q}_{drive}$ and the cooling heat flow rate $\dot{Q}_{cool}$. The external energy flows are the refrigeration heat flow rate $\dot{Q}_{refrig}$, the compressor power P_{comp} and the waste heat flows to the environment $\dot{Q}_{waste}$.

temperature is released to the environment ($\dot{Q}_{waste}$) in the supercritical gas cooling step of the CO_2 cycle.

Part of the released waste heat from the CO_2 cycle can be recovered to drive the sorption chiller ($\dot{Q}_{drive}$) to allow for a fully integrated hybrid system without external heat source as shown in Figure 4.1 (c) (Arora et al., 2011; Graf et al., 2015). The additional cooling of the sorption chiller ($\dot{Q}_{cool}$) is also integrated into the CO_2 cycle to extend the gas cooling step ($\dot{Q}_{waste}$) as described in the previous paragraph. The major advantage of this hybrid system is that the sorption chiller is fully integrated into the CO_2 cycle, and no separate heat source is required. For this reason, we investigate the integrated hybrid system in the following.

4.1.2 Integrated hybrid system

A scheme of an integrated hybrid system combining a CO_2 cycle and an adsorption chiller is shown in Figure 4.2. The adsorption chiller is integrated into a three-step heat-release process of the CO_2 cycle. In the first step, heat at a high temperature level is recovered in a heat exchanger to drive the adsorption chiller. In the second step, the non-recoverable heat is released to the environment in a gas cooler. In the third step, the additionally generated

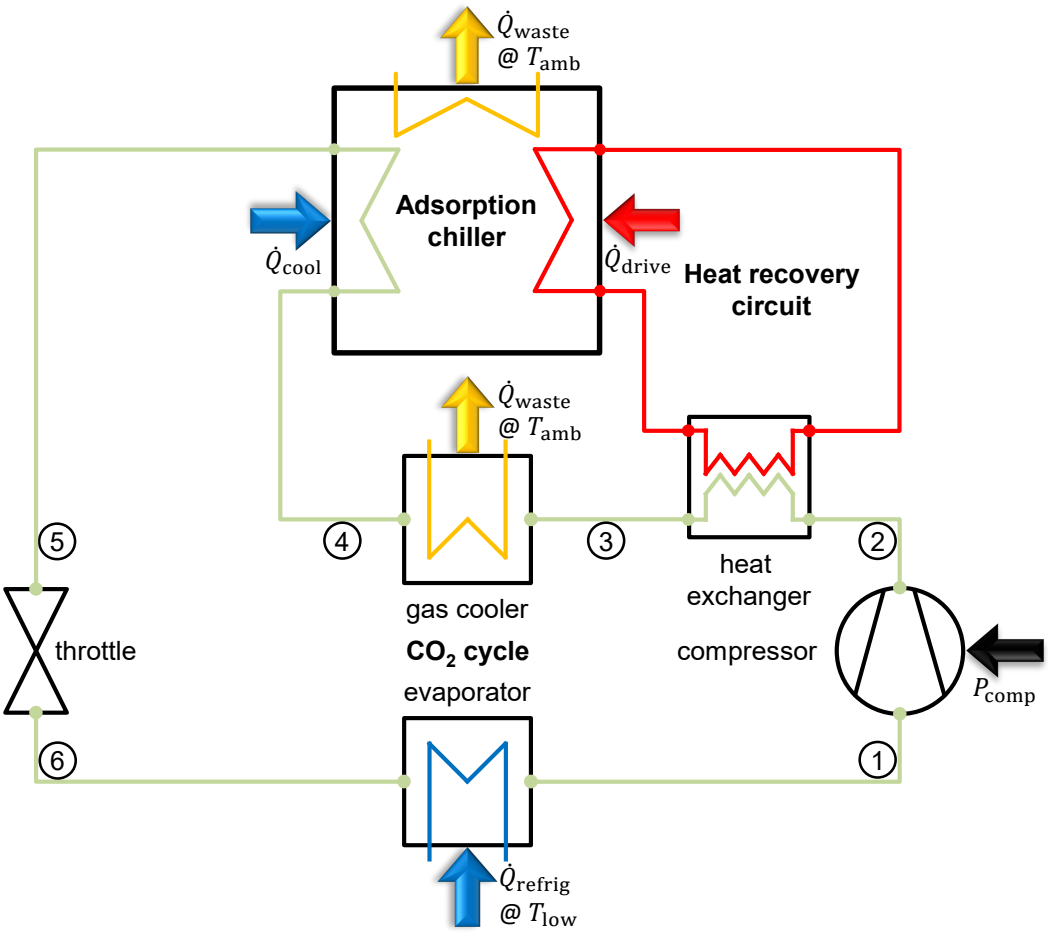

Figure 4.2: Scheme of the integrated hybrid system combining CO_2 cycle and adsorption chiller. Energy flows are shown as arrows. The integrated energy flows are the driving heat flow rate $\dot{Q}_{drive}$ and the cooling heat flow rate $\dot{Q}_{cool}$. The external energy flows are the refrigeration heat flow rate $\dot{Q}_{refrig}$ at the low temperature level T_{low}, the compressor power P_{comp} and the waste heat flows to the environment $\dot{Q}_{waste}$ at ambient temperature T_{amb}.

cooling of the adsorption chiller further cools the CO_2 below ambient temperature. Thus, part of the exergy usually lost during heat rejection at high temperatures is now recovered by the adsorption chiller and re-integrated into the CO_2 cycle.

The efficiency increase by the hybrid system can be illustrated in the thermodynamic cycle. Figure 4.3 shows a pressure–enthalpy diagram with the thermodynamic cycles of the stand-alone CO_2 cycle and the hybrid system. The transcritical stand-alone CO_2 cycle consists of four steps: polytropic compression (state 1 to 2'), isobaric gas cooling (state 2' to 5'), isenthalpic expansion (state 5' to 6') and isobaric evaporation (state 6' to 1). One of the main reasons for the low efficiency of the transcritical cycle is the high exergy loss in the supercritical gas cooling. In contrast to a subcritical cycle, the heat release of the

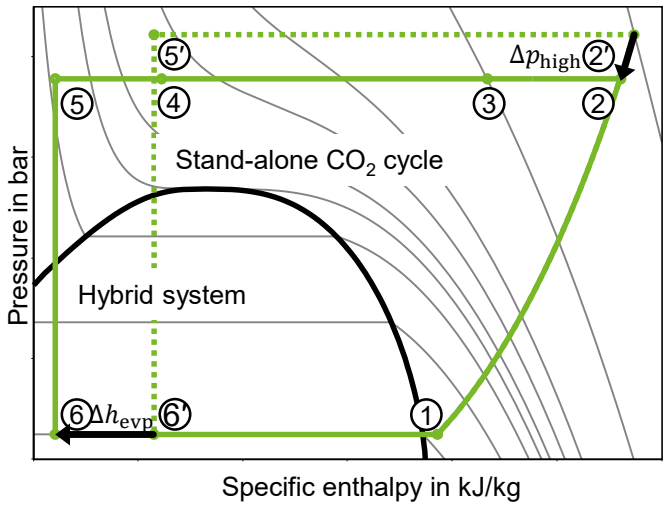

Figure 4.3: Pressure–enthalpy diagram with the thermodynamic cycles of the stand-alone CO_2 cycle (dotted line) and the hybrid system (solid line). The states in the cycle of the hybrid system correspond to the states in the scheme in Figure 4.2. The decreased high pressure level Δp_{high} (state 2' to 2) and the increased difference of specific enthalpy in the evaporator Δh_{evp} (change of state 6' to 6) due to additional cooling increase the efficiency in the hybrid system.

transcritical cycle is non-isothermal leading to a higher mean temperature difference to the heat sink. Due to the higher mean temperature difference to the heat sink, higher exergy losses occur.

The hybrid cycle recovers part of the exergy of the released heat by the adsorption chiller. For this purpose, heat is recovered at a high temperature level to drive the adsorption chiller (state 2 to 3). The adsorption chiller converts the recovered heat into cooling, which can be again integrated as exergy flow into the CO_2 cycle. The integrated cooling further cools the CO_2 below the temperature of the heat sink (state 4 to 5). Thus, the final temperature of the refrigerant after heat release decreases compared to the stand-alone CO_2 cycle (state 5' compared to state 5). The decreased temperature improves the efficiency in two ways: First, the optimal high pressure level of the hybrid system decreases (state 2' to 2) and, thus, the pressure ratio of the compressor decreases. Second, the difference of specific enthalpy between evaporator outlet and inlet increases (state 6' to 6) and, thus, the refrigerant mass flow rate of the compressor decreases for the same refrigeration power. These two effects reduce the electrical energy demand of the compressor and, therefore, lead to energy savings.

4.2 Modeling and optimization framework

In this section, we present a modeling and optimization approach to assess the hybrid system consisting of a CO_2 vapor compression cycle and an adsorption chiller. All models are implemented in the object-oriented language Modelica (Modelica Association, 2017). First, we present the models of the CO_2 cycle (Section 4.2.1) and of the adsorption chiller (Section 4.2.2). Second, we introduce the optimization problem to identify the optimal control parameters and the optimal design (Section 4.2.3).

4.2.1 CO_2 vapor-compression cycle

For the CO_2 cycle, we use quasi-steady-state models described by algebraic equations. The gas cooler and evaporator are modeled as isobaric heat exchangers. The main model equations are summarized in Table 4.1.

Table 4.1: Model equations for the components of the CO_2 cycle (compressor, throttle, gas cooler and evaporator, cf. Figure 4.2). The correlation for the isentropic efficiency of the compressor (Equation (4.4)) is based on Srinivasan et al. (2010).

Mass and energy balances	$\dot{m}_{\text{in}} = \dot{m}_{\text{out}} = \dot{m}_{\text{refrig}}$	(4.1)
	$\dot{m}_{\text{refrig}} \left(h_{\text{out}} - h_{\text{in}}\right) = \sum \dot{Q} + \sum P$	(4.2)
Compressor	$h_{\text{out}} = h_{\text{in}} + \dfrac{h_{\text{out,is}} - h_{\text{in}}}{\eta_{\text{is}}}$	(4.3)
	$\eta_{\text{is}} = 0.567 + 0.0931 \cdot \dfrac{p_{\text{high}}}{p_{\text{low}}} - 0.0164 \cdot \left(\dfrac{p_{\text{high}}}{p_{\text{low}}}\right)^2$	(4.4)
Throttle	$h_{\text{out}} = h_{\text{in}}$	(4.5)
Gas cooler	$T_{\text{out}} = T_{\text{amb}} + \Delta T_{\text{GC}}$	(4.6)
Evaporator	$T_{\text{out}} = T_{\text{sat}} \left(p_{\text{low}}\right) + \Delta T_{\text{sup}}$	(4.7)

Mass and energy balances apply for each component. In all equations, $\dot{m}$ is the mass flow rate, h is the specific enthalpy, and T is the temperature. The subscripts in and out represent the ingoing and the outgoing flows, respectively. In the energy balance, $\dot{Q}$ is the heat flow rate, and P is the mechanical power transferred over the system boundaries of a

component. For the compressor, $h_{\text{out,is}}$ is the outgoing specific enthalpy for an isentropic compression and η_{is} is the isentropic efficiency of the compressor. The isentropic efficiency of the compressor η_{is} is calculated according to an empirical correlation fitted to manufacturer data (Srinivasan et al., 2010). In the correlation, p_{high} is the high pressure level and p_{low} is the low pressure level of the CO_2 cycle. In the gas cooler, ΔT_{gc} is the minimal temperature approach to the ambient temperature T_{amb}. In the evaporator, ΔT_{sup} is the superheating above the saturation temperature at low pressure level $T_{\text{sat}}(p_{\text{low}})$.

The low pressure level of the CO_2 cycle p_{low} is determined by the required refrigeration temperature T_{refrig} through the vapor pressure curve $p_{\text{low}} = p_{\text{sat}}(T_{\text{refrig}})$. The high pressure level p_{high} is a variable control parameter, which can be optimized to achieve maximal efficiency for given operating conditions, e.g., ambient temperature T_{amb} (Yang et al., 2015). With given high and low pressure levels and the equation set from Table 4.1, all states in the CO_2 cycle are fixed. The refrigerant mass flow rate $\dot{m}_{\text{refrig}}$ is determined by the required refrigeration power.

4.2.2 Adsorption chiller

For the adsorption chiller, the experimentally validated lab-scale one-bed model from Section 3.3 is employed. We extended the validated model to a two-bed adsorption chiller by adding a second identical adsorber as for the commercial system in Section 3.4. Thus, the adsorption chiller is described by a differential-algebraic equation (DAE) system. For further information about the adsorption chiller model, the reader is referred to Section 3.1.

To account for the electrical energy consumption of the adsorption chiller, we use the energy efficiency ratio (EER), as introduced in Section 2.1.3, Equation (2.9). We define a nominal EER_0 as ratio between the nominal cooling power of the adsorption chiller $\dot{Q}_{0,\text{AC}}$ and the total electrical energy demand of all auxiliary components $P_{\text{el,AC}}$, such as pumps and fans:

$$\text{EER}_0 = \frac{\dot{Q}_{0,\text{AC}}}{P_{\text{el,AC}}} \tag{4.8}$$

With the nominal EER_0 and the nominal cooling power $\dot{Q}_{0,\text{AC}}$, we calculate the nominal electrical energy demand of the auxiliary components $P_{\text{el,AC}}$. As reference, we use the commercial adsorption chiller *InvenSor LTC 30 e* (Invensor GmbH, 2020), which has a nominal cooling power of 29.5 kW and a nominal EER of 33 resulting in an electrical energy demand of 894 W. This electrical energy demand is assumed to scale linearly with the size of the adsorption chiller and to be constant for all operating conditions, i.e., the control of the auxiliary components is not adapted in part-load. Thus, the EER decreases in part-load since the electrical energy demand remains constant while the cooling power decreases below the nominal value. A decreasing EER in part-load represents a conservative

assumption since the EER can even be increased by up to 25 % in part-load by efficient control (Nienborg et al., 2017).

As shown in Figure 4.2, the chilling and the heating circuit of the adsorption chiller are connected to the CO_2 cycle. Thus, the heat transferred from the CO_2 cycle determines the inlet conditions of the chilling and the heating circuits into the adsorption chiller. In the heat-rejection circuit, heat is released to the environment. As the heat-rejection unit is not modeled in this study, the inlet temperature of the heat-rejection circuit is modeled assuming a constant minimal temperature approach ΔT_{reject} to the ambient temperature.

Inside the two-bed adsorption chiller, each adsorber is alternately connected to the heating circuit (desorption phase) and to the heat-rejection circuit (adsorption phase) to enable a continuous supply of cooling power. The duration of a full cycle consisting of adsorption and desorption phase is the cycle time. The cycle t_{cycle} is a variable control parameter and can be optimized to achieve maximal cooling power for given operating conditions, e.g., inlet temperatures of the heat transfer circuits (Bau, 2018; Bau et al., 2015).

To allow for design variations in the hybrid system, the size of the adsorption chiller can be scaled linearly. Thereby, the size ratio between the CO_2 cycle and the adsorption chiller can be adjusted to optimize the design. We define the size ratio SR as the ratio between the nominal cooling power of the adsorption chiller $\dot{Q}_{0,\text{AC}}$ and the nominal refrigeration power of the CO_2 cycle $\dot{Q}_{0,\text{refrig}}$:

$$\text{SR} = \frac{\dot{Q}_{0,\text{AC}}}{\dot{Q}_{0,\text{refrig}}}. \tag{4.9}$$

4.2.3 Optimization framework

The process model of the hybrid system has two control parameters: the high pressure level of the CO_2 cycle p_{high} and the cycle time of the adsorption chiller t_{cycle}. The high pressure level influences the efficiency of the CO_2 cycle and can be optimized depending on the temperature of the heat sink (Yang et al., 2015). The cycle time influences the power and the thermal efficiency of the adsorption chiller and can be optimized for specific operating points (Bau, 2018; Bau et al., 2015). In the hybrid system, both control parameters also influence each other: the additional cooling of CO_2 by the adsorption chiller reduces the temperature of the heat sink and, thus, influences the optimal high pressure level. The high pressure level determines the temperature level of the released heat to drive the adsorption chiller and, thus, influences the optimal cycle time.

Furthermore, the process model has one design parameter, namely the size ratio SR between the adsorption chiller and the CO_2 cycle. The size ratio SR also influences the

optimal control parameters since SR determines the released heat flow rate to drive the adsorption chiller as well as the provided additional cooling to cool the CO_2 further.

Finally, the optimal control parameters are also influenced by the ambient temperature T_{amb}. The ambient temperature sets the heat-release temperature for the gas cooler as well as for the adsorption chiller.

To compare the actual efficiency of the hybrid system without the effect of poor control, the control parameters have to be optimized for each size ratio SR and each ambient temperature T_{amb}. In the optimization, the coefficient of performance (COP) is used as the objective function. We define the COP of the hybrid system ($\mathrm{COP}_{\mathrm{hyb}}$) as ratio between the refrigeration energy Q_{refrig} and the sum of electrical energy demands of the compressor $W_{\mathrm{el,comp}}$ and of the adsorption chiller $W_{\mathrm{el,AC}}$:

$$\mathrm{COP}_{\mathrm{hyb}} = \frac{Q_{\mathrm{refrig}}}{W_{\mathrm{el,comp}} + W_{\mathrm{el,AC}}}. \tag{4.10}$$

The energy amounts are considered over one full cycle of adsorption and desorption due to the dynamics of the adsorption chiller.

The hybrid system is described by a differential-algebraic equation (DAE) process model. Thus, the resulting optimal control problem reads:

$$\begin{aligned}
\min_{x(\cdot),z(\cdot),t_{\mathrm{cycle}},p_{\mathrm{high}}} \quad & -\mathrm{COP}_{\mathrm{hyb}}\left(x(t_{\mathrm{cycle}}), z(t_{\mathrm{cycle}}), p_{\mathrm{high}}, \mathrm{SR}, T_{\mathrm{amb}}\right) && \text{(Objective functions)} \\
\text{s.t.} \quad & \dot{x} = f\left(x(\cdot), z(\cdot), p_{\mathrm{high}}, \mathrm{SR}, T_{\mathrm{amb}}\right) && \text{(Dynamic model)} \\
& 0 = g\left(x(\cdot), z(\cdot), p_{\mathrm{high}}, \mathrm{SR}, T_{\mathrm{amb}}\right) && \text{(Dynamic model)} \\
& x(t=0) = x(t=t_{\mathrm{cycle}}) && \text{(Cyclic operation)} \\
& \mathrm{SR} = \mathrm{SR}_{\mathrm{i}} && \text{(Size ratio)} \\
& T_{\mathrm{amb}} = T_{\mathrm{amb,i}} && \text{(Ambient temperature)}
\end{aligned}$$

The optimization problem has to be solved subject to (s.t.) the dynamic model equations. The cyclic steady-state constraint ensures that all states of the hybrid system are the same at the beginning of the cycle and the end of the cycle. Furthermore, the optimization problem has to be solved for each size ratio SR_{i}, and each ambient temperature $T_{\mathrm{amb,i}}$ due to the influences on optimal control parameters as discussed above.

To solve the multiple optimization problems, we use the Modelica optimization library developed by the German Aerospace Center (2019). The optimization library provides several numerical optimization algorithms to solve DAE-constrained optimization problems (Pfeiffer, 2012) directly within the Dymola environment (Dassault Systèmes, 2020). Here, we employ the gradient-based sequential quadratic programming (SQP) algorithm. For further information about the optimization methods, the reader is referred to Nocedal and Wright (2006).

4.3 Results

In this section, we present the resulting energy savings by an optimized hybrid system compared to a stand-alone CO_2 vapor-compression cycle. In Section 4.3.1, we show the influence of the hybrid system design on the energy savings for different ambient temperatures. In Section 4.3.2, we present the annual energy savings by the hybrid system for two case studies. The first case study represents a warm climate in Athens, and the second case study represents a moderate climate in Cologne. Furthermore, we show the sensitivity of the energy savings to the energy efficiency ratio (EER) of the adsorption chiller.

4.3.1 Design of the hybrid system

For the investigations in this section, we use a common parameter set for the hybrid system model (cf. Section 4.2). The parameter set is summarized in Table 4.2. The nominal energy efficiency ratio (EER_0) considers the total electrical energy consumption of the adsorption chiller and the three heat transfer circuits (Invensor GmbH, 2020). A minimal temperature approach of 10 K is chosen for both, the heat rejection of the adsorption chiller and the heat rejection of the CO_2 cycle. This temperature approach might be quite high in warm climates and can be reduced by increasing the size or changing the type of the heat-rejection unit. A reduced temperature approach would improve both, the performance of the adsorption chiller, as well as the performance of the stand-alone cycle. Thus, for the comparison, we expect similar results for the energy savings also for a reduced temperature approach.

Table 4.2: Parameter set used for design investigations in Section 4.3.1. Typical ranges are used for the minimal temperature approach, the superheating and the refrigeration temperature (c.f. Gullo et al. (2017) and Sharma et al. (2014)). The nominal energy efficiency ratio (EER_0) was chosen according to manufacturer specifications of a commercial adsorption chiller (Invensor GmbH, 2020).

Minimal temperature approach for gas cooler ΔT_{GC}	10 K
Superheating in the evaporator of the CO_2 cycle ΔT_{sup}	5 K
Refrigeration temperature T_{refrig}	−12 °C
Nominal energy efficiency ratio of the adsorption chiller EER_0	33
Minimal temperature approach for heat rejection of adsorption chiller ΔT_{reject}	10 K

The design of the hybrid system is described by the size ratio SR between the nominal cooling power of the adsorption chiller and the nominal refrigeration power of the CO_2 cycle. To investigate the influence of the design on the energy savings, each design is

evaluated at optimal control parameters, cf. Section 4.2.3. To resolve the effect of different operating conditions, we consider three ambient temperatures. Thus, the energy savings by the hybrid system are a function of both, the size ratio SR and the ambient temperature T_{amb}. We define the relative energy savings as the difference between the electrical energy demand of the stand-alone CO_2 cycle $W_{\mathrm{el,CO_2}}(T_{\mathrm{amb}})$ and the electrical energy demand of the hybrid system $W_{\mathrm{el,hyb}}(\mathrm{SR}, T_{\mathrm{amb}})$, normalized by the demand of the stand-alone CO_2 cycle:

$$\text{energy savings} = \frac{W_{\mathrm{el,CO_2}}(T_{\mathrm{amb}}) - W_{\mathrm{el,hyb}}(\mathrm{SR}, T_{\mathrm{amb}})}{W_{\mathrm{el,CO_2}}(T_{\mathrm{amb}})}. \tag{4.11}$$

The electrical energy demand of the hybrid system includes the demand of the compressor as well as the demand of the adsorption chiller. The energy amount is considered over one cycle for the adsorption chiller.

Figure 4.4 shows the energy savings by the hybrid system as a function of the size ratio for three ambient temperatures (15 °C, 25 °C and 35 °C). A size ratio (SR) of zero

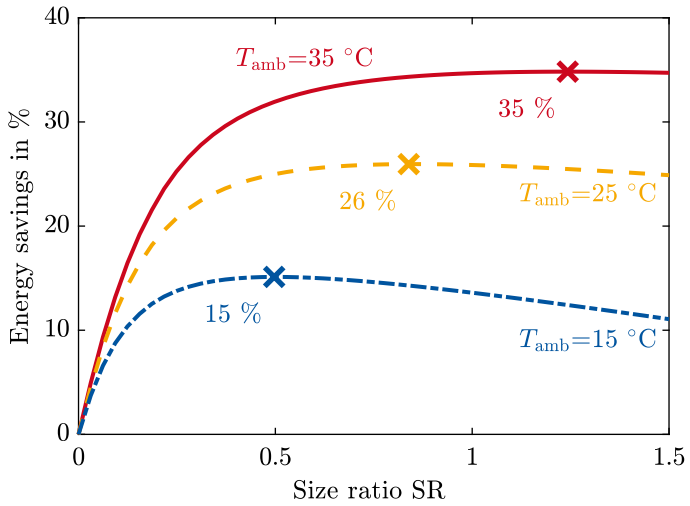

Figure 4.4: Energy savings by the hybrid system as a function of size ratio SR between the adsorption chiller and the CO_2 cycle (see Equation (4.9)) for three ambient temperatures: $T_{\mathrm{amb}} = 15\,°\mathrm{C}$, $T_{\mathrm{amb}} = 25\,°\mathrm{C}$ and $T_{\mathrm{amb}} = 35\,°\mathrm{C}$. The maximal energy savings for each ambient temperature are marked by a cross.

represents the stand-alone CO_2 cycle and, thus, has no energy savings from an adsorption chiller. With increasing size ratio, the nominal cooling power of the adsorption chiller increases. A larger adsorption chiller can recover more waste heat from the CO_2 cycle and can generate more cooling power to cool the CO_2 further. Thus, the energy savings by the hybrid system increase with increasing size ratio. However, with increasing size ratio, the electrical energy consumption of the adsorption chiller also increases. Additionally, with increasing size ratio, the available waste heat to drive the adsorption chiller becomes limiting. Due to the electrical energy consumption of the adsorption chiller, and the

limited waste heat, the increase of the energy savings is degressive. For too high size ratios, the additional electrical energy consumption of the adsorption chiller outweighs the efficiency increase in the CO_2 cycle. For this reason, the energy savings decrease again for high size ratios. Thus, there is an optimal size ratio with maximal energy savings. The maximal energy savings and the corresponding optimal size ratios depend on the ambient temperature (cf. Figure 4.4): for 15 °C, the optimal size ratio is 0.47 and the maximal energy savings are 15 %. For 25 °C, the optimal size ratio is 0.84 and the maximal energy savings are 26 %. For 35 °C, the optimal size ratio is 1.27 and the maximal energy savings are 35 %. The maximal energy savings and the optimal size ratio increase for higher ambient temperatures since the efficiency of the stand-alone CO_2 cycle is lower and more waste heat is available to drive the adsorption chiller. For this reason, higher ambient temperatures allow for higher optimal size ratios.

Figure 4.5 shows the optimal control parameters as a function of the size ratio for the same three ambient temperatures as in Figure 4.4. To check the plausibility of the

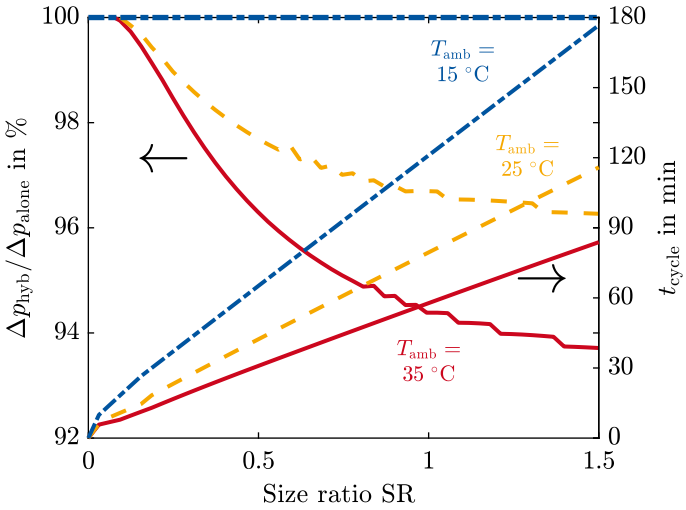

Figure 4.5: Optimal control parameters of the hybrid system as a function of size ratio SR between the adsorption chiller and the CO_2 cycle. Left axis: ratio of pressure differences between optimal high pressure level and low pressure level of the hybrid system Δp_{hyb} and of the stand-alone CO_2 cycle Δp_{alone}. The low pressure level of 25 bar is constant for all configurations due to the defined constant refrigeration temperature. The absolute values for the high pressure level of the stand-alone CO_2 cycle are 64.3 bar at 15 °C, 87.7 bar at 25 °C and 109.1 bar at 35 °C. Right axis: optimal cycle times of adsorption chiller t_{cycle}.

calculated optimum high pressure levels, we compared our values for the stand-alone CO_2 cycle with values calculated by a correlation from literature. Sarkar et al. (2004) derived correlations for the optimum high pressure level as function of the evaporation temperature and the gas cooler outlet temperature. These correlations apply for transcritical operation. Thus, we compare our optimum high pressure levels for $T_{amb} = 25\,°C$ and $T_{amb} = 35\,°C$

which are transcritical. (1) For $T_{amb} = 25\,°C$, our calculated optimum high pressure level is 87.7 bar compared to 88.4 bar according to (Sarkar et al., 2004). (2) For $T_{amb} = 35\,°C$, our calculated optimum high pressure level is 109.1 bar compared to 112.5 bar according to Sarkar et al. (2004). The deviation between the optimal high pressure levels is 0.8 % for $T_{amb} = 25\,°C$ and 3 % for $T_{amb} = 35\,°C$. This slight deviations might result from different compressor efficiencies or from the internal heat exchanger used by Sarkar et al. (2004). This good agreement with literature values supports the plausibility of the optimized high pressure levels.

The pressure difference Δp in Figure 4.5 is the difference between the optimal high pressure level and the low pressure level of the compressor. The low pressure level is constant for all size ratios SR and all ambient temperatures T_{amb}, since the required refrigeration temperature determines the low pressure level. Therefore, changes in the pressure difference result from changes in the optimal high pressure level. For an ambient temperature of 15 °C, the optimal high pressure level of the hybrid system does not change since the CO_2 cycle is subcritical. In a subcritical cycle, the high pressure level is determined by the condensation temperature because pressure and temperature are coupled in the two-phase region (cf. Figure 4.3). Thus, the pressure difference of the hybrid system does not change compared to the stand-alone CO_2 cycle. For ambient temperatures of 25 °C and 35 °C, the optimal high pressure level decreases with increasing size ratio SR due to the additional cooling by the adsorption chiller. Thus, the pressure difference of the hybrid system decreases by up to 4 % at 25 °C and up to 6 % at 35 °C compared to the stand-alone CO_2 cycle. Besides, the additional cooling also reduces the refrigerant mass flow rate of the hybrid system by up to 20 % at 15 °C, up to 28 % at 25 °C, and up to 35 % at 35 °C compared to the stand-alone CO_2 cycle. Both effects, the reduction of the pressure difference and the reduction of the mass flow rate of the refrigerant, lead to energy savings by the hybrid system.

The optimal cycle time t_{cycle} increases with increasing size ratio due to a larger sized adsorption chiller, which requires more time for desorption. In contrast, the optimal cycle time decreases for higher ambient temperatures since a higher heat flow rate is available at a higher desorption temperature to drive the adsorption chiller and, thus, less time is required for desorption. The higher desorption temperature results from a higher pressure level and the corresponding higher outlet temperature of the compressor, which is 76.3 °C at 15 °C ambient temperature, 105.1 °C at 25 °C ambient temperature, and 129 °C at 35 °C ambient temperature. The inlet temperatures for the heat-rejection and the chilling circuit of the adsorption chiller are always 10 K above ambient temperature due to the constant minimal temperature approach (cf. Table 4.2).

In this section, we have investigated the influence of ambient temperature T_{amb} and size ratio SR on the energy savings by the hybrid system. The results show energy savings up

to 35 % for an optimal size ratio SR and an ambient temperature of 35 °C. However, the optimal size ratio and the maximal energy savings depend on the ambient temperature. To evaluate the annual energy savings, in the next step, we consider two case studies with changing ambient temperature over one year.

4.3.2 Case-studies

The first case study represents a warm climate in Athens, and the second case study represents a moderate climate in Cologne. The annual ambient temperature profiles of both case studies are generated with the Meteonorm software (Meteotest AG, 2018). Figure 4.6 shows the duration curves of the ambient temperature for Athens and Cologne. For the following calculations, we assume applications where the refrigeration system runs

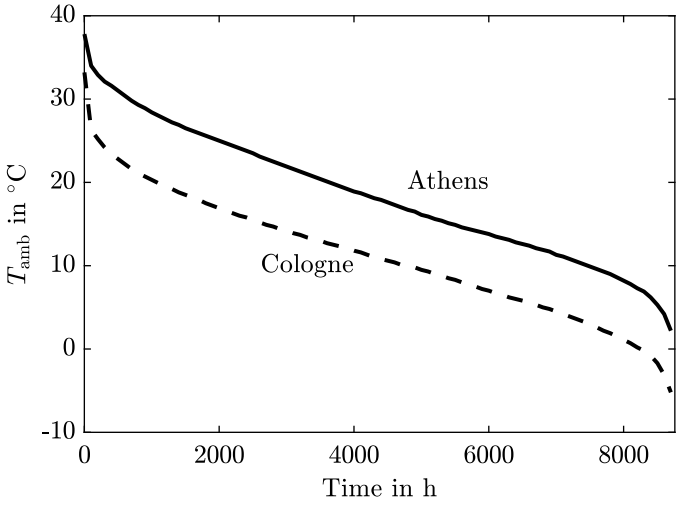

Figure 4.6: Duration curves of the ambient temperature for Athens and Cologne with data generated with the Meteonorm software (Meteotest AG, 2018).

the entire year, such as cold storage units or supermarkets (Gullo et al., 2017). To represent a base-load scenario, the refrigeration load $\dot{Q}_{\text{refrig}}$ is assumed constant over the year, for both, the stand-alone CO_2 cycle and the hybrid system. In many applications, such as supermarkets, the refrigeration load is not constant, since the load is higher during daytime than at night. In this case, the load increases with higher ambient temperatures (Gullo et al., 2017). This increasing load at higher ambient temperatures is beneficial for the hybrid system since the energy savings are particularly high for high ambient temperatures (cf. Figure 4.4). Thus, the annual energy savings by the hybrid system are expected to increase compared to the base-load scenario considered here since operating hours with high ambient temperatures and, consequently, high energy savings would receive a higher weight. Despite this beneficial effect, we use the base-load scenario in the following for simplicity.

The annual energy savings by the hybrid system are calculated with

$$\text{annual energy savings} = \frac{W_{\text{annual,alone}} - W_{\text{annual,hyb}}}{W_{\text{annual,alone}}} \tag{4.12}$$

using the annual electrical energy consumptions of both, the stand-alone CO_2 cycle $W_{\text{annual,alone}}$ and the hybrid system $W_{\text{annual,hyb}}$. The annual electrical energy consumption of the stand-alone CO_2 cycle $W_{\text{annual,alone}}$ is determined from

$$W_{\text{annual,alone}} = \int_0^{8760\,\text{h}} \frac{\dot{Q}_{\text{refrig}}}{\text{COP}^{\text{opt}}_{\text{alone}}(T_{\text{amb}})} \text{d}t, \tag{4.13}$$

and the annual electrical energy consumption of the hybrid system $W_{\text{annual,hyb}}$ is determined from

$$W_{\text{annual,hyb}} = \int_0^{8760\,\text{h}} \frac{\dot{Q}_{\text{refrig}}}{\text{COP}^{\text{opt}}_{\text{hyb}}(T_{\text{amb}}, \text{SR})} \text{d}t. \tag{4.14}$$

Note that for both, the stand-alone CO_2 cycle and the hybrid system, always the optimal COP with optimal control parameters is used. Furthermore, we assume that the adsorption chiller can only be operated above ambient temperatures of 5 °C to avoid freezing in the adsorption chiller since water is used as the refrigerant. Below 5 °C, the energy savings are zero since the hybrid system operates as stand-alone CO_2 cycle. At ambient temperatures above 5 °C, energy is saved by the hybrid system, because energy demand in the CO_2 cycle is reduced more than the additional energy demand of the adsorption chiller. In particular, the energy savings increase with increasing ambient temperature (cf. Figure 4.4) since the higher heat-rejection temperature of the CO_2 cycle increases the driving and cooling temperature of the adsorption chiller. The effect of higher driving and cooling temperature outweighs the effect of higher heat-rejection temperature for the adsorption chiller and, thus, increases the energy savings by the hybrid system.

Figure 4.7 shows the resulting annual energy savings by the hybrid system as a function of the size ratio SR for Athens and Cologne. The annual energy savings for Athens are higher than for Cologne since energy savings increase with increasing ambient temperatures (cf. Figure 4.4). In Athens, high ambient temperatures occur more often than in Cologne, as shown in the duration curves in Figure 4.6. For this reason, energy savings in Athens are up to 22 %, whereas the energy savings in Cologne are up to 16 % compared to the stand-alone CO_2 cycle. To achieve maximal energy savings, there is an optimal size ratio SR for each location. Above this optimal size ratio, the electrical energy consumption of the oversized adsorption chiller outweighs the efficiency increase in the CO_2 cycle and, thus, the energy savings decrease. The optimal size ratio is 0.71 for Athens and 0.5 for Cologne. The optimal size ratio for Athens is higher than for Cologne since higher ambient temperatures favor a higher size ratio (cf. Figure 4.4). However, the optimum is flat:

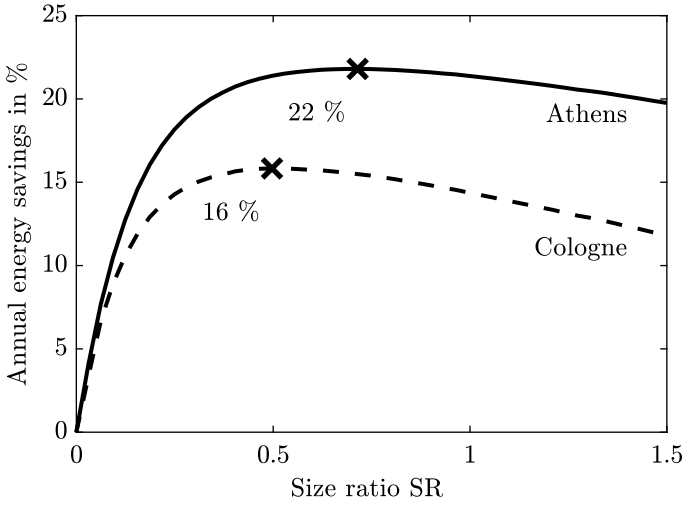

Figure 4.7: Annual energy savings by the hybrid system compared to the stand-alone CO_2 cycle as a function of the size ratio SR for Athens and Cologne. The cross marks the maximal annual energy savings for each case. The energy savings are calculated for a nominal energy efficiency ratio (EER_0) of 33 for the adsorption chiller.

employing the optimal size ratio of Cologne (SR = 0.5) for Athens, the energy savings are still 21.4 %.

Note that the energy savings by the hybrid system depend on the efficiency of the stand-alone CO_2 cycle, which is also affected by the isentropic efficiency of the compressor. The isentropic efficiency might depend on the mass flow rate of the refrigerant, which is reduced by the hybrid system. If the isentropic efficiency decreases for lower mass flows, the energy savings by the hybrid system would also decrease. This effect is neglected in the present assessment but should be considered in future more detailed analyses of the hybrid system. However, applications of CO_2 systems with large capacities, such as supermarkets, cold storage units, or industrial refrigeration, typically employ a compressor rack, consisting of several compressors. In these compressor racks, the single compressors are usually switched on/off to control the mass flow, while only one compressor is speed-controlled for precise adjustment (Hafner et al., 2014). In such a setup, the mass flow variation of one compressor only slightly affects the global efficiency of the compressor rack (Gullo et al., 2017) and a mass-flow-invariant average efficiency is a reasonable approximation for the scope of the present study. Further mechanical or electrical losses of the compressor are also considered neither for the stand-alone CO_2 cycle nor for the hybrid system, which is regarded as a reasonable assumption since our focus is on the comparison of these systems. These additional losses would generally increase the potential energy savings by the hybrid system since the efficiency of the stand-alone CO_2 system decreases. Otherwise, an increase in the compressor efficiency, e.g., due to technical progress, might reduce the potential energy savings, since the efficiency of the stand-alone CO_2 system would increase, and

less waste heat would be available to drive the adsorption chiller. Our analysis employs an empirical correlation for the isentropic efficiency generated from manufacturer data to assess current commercially available CO_2 systems.

The potential energy savings by the hybrid system shown in Figure 4.7 seem very promising to significantly reduce operating costs. However, the adsorption chiller adds to the investment costs. To estimate the economic viability of the hybrid system, we calculated the payback period t_{payback} for the additional investment compared to the stand-alone CO_2 system. The payback period t_{payback} is the additional investment costs of the adsorption chiller divided by the reduced operating costs due to annual energy savings:

$$t_{\text{payback}} = \frac{\text{SR}\ \dot{Q}_{\text{refrig}}\ i_{\text{AC}}}{(W_{\text{annual,alone}} - W_{\text{annual,hyb}})c_{\text{el}}}, \tag{4.15}$$

where i_{AC} are the specific investment costs of the adsorption chiller and c_{el} are the specific electricity costs. For the specific investment costs of the adsorption chiller i_{AC}, we assume a mean value of 900 EUR/kW from literature (Mugnier et al., 2017). For the specific electricity costs c_{el}, we use industrial prices from the Statista portal (Federal Ministry for Economic Affairs and Energy, 2019) with 0.1132 EUR/(kW h) in Greece and 0.1517 EUR/(kW h) in Germany. For the energetically optimum size ratio from Figure 4.7, the payback period is 4.6 years for Athens and 3.3 years for Cologne. Despite the lower annual energy savings, the payback period for Cologne is shorter than for Athens due to the higher electricity costs. This estimate neglects additional costs, e.g., for the heat-rejection unit of the adsorption chiller and the hydraulics. However, there are also compensating cost savings, e.g., due to the smaller sized gas cooler and compressor of the CO_2 system. Furthermore, the payback period is calculated for the energetically optimum size ratio. An economic optimization can further reduce the payback period. However, a detailed economic evaluation is beyond the scope of this study. In summary, the estimated payback period of less than 5 years seems very promising for further investigations of the hybrid system in the future.

The energy savings by the hybrid system also depend on the nominal energy efficiency ratio of the adsorption chiller (EER_0), since the energy savings in the CO_2 cycle are partly reduced by the additional energy consumption of the adsorption chiller. To investigate the sensitivity to EER_0, the maximal annual energy savings are calculated for various EER_0, each at optimal size ratio (cf. cross in Figure 4.7). Figure 4.8 shows the maximal annual energy savings as function of EER_0 for Athens and Cologne. Upper bounds for infinite EER_0 are also shown in Figure 4.8.

For small nominal energy efficiency ratios EER_0, the annual energy savings are very sensitive to EER_0: with decreasing EER_0, also the energy savings decrease. For higher EER_0, the sensitivity decreases since the energy consumption of the adsorption chiller

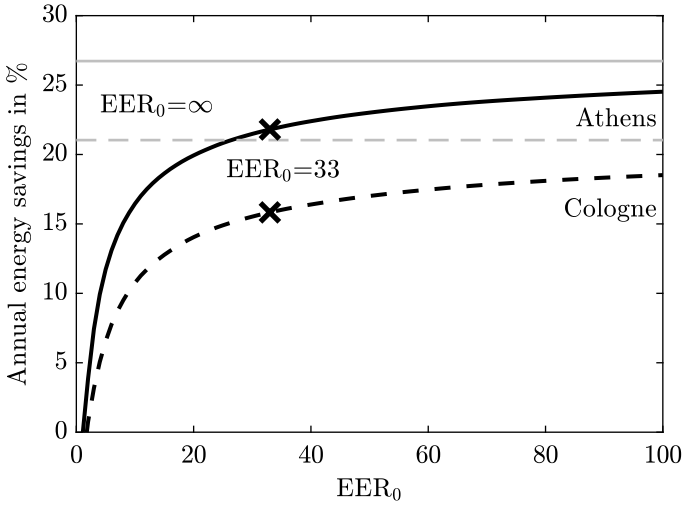

Figure 4.8: maximal annual energy savings at optimal size ratio as function of the nominal energy efficiency ratio of the adsorption chiller (EER_0) for Athens and Cologne. The horizontal lines show the maximal annual energy savings for an infinite EER_0 (no electrical energy consumption by the adsorption chiller). The crosses show the reference case from Figure 4.7 with $EER_0 = 33$.

becomes negligible compared to the energy consumption of the CO_2 cycle. Thus, an efficient adsorption chiller with a high EER_0 is crucial for achieving high energy savings by the hybrid system. Still, for EER_0 of 33 according to manufacturer specifications (Invensor GmbH, 2020), the energy savings are significant with 22 % for Athens and 16 % for Cologne.

The considered EER_0 of 33 considers both, the electricity consumption of the adsorption chiller, e.g., for system controller, and the three pumps for the heating, the chilling, and the heat-rejection circuit. The three circuits include both, the internal pressure drops in the heat exchangers of the adsorption chiller as well as the external pressure drops in the connected devices for heating, heat rejection, and cold distribution (Invensor GmbH, 2020). The electricity consumption of the heat-rejection unit of the adsorption chiller is not considered in the EER_0, since this additional electricity consumption is (at least partly) compensated by the electricity savings of the heat-rejection unit of the CO_2 cycle: as the adsorption chiller absorbs heat from the CO_2 cycle, the amount of heat rejected in the gas cooler decreases. Thus, we expect that the energy savings shown in this study approximate the actual values well. The total energy savings will decrease if the energy consumption for heat rejection of the adsorption chiller is higher than the energy savings for heat rejection of the CO_2 cycle, e.g., due to the lower temperature level. For a conservative estimate of the minimal energy savings, we calculated the additional energy consumption for the heat-rejection unit of the adsorption chiller without considering any energy savings of the gas cooler fan. The average seasonal value for the electricity consumption of the fans

of a dry cooler is 0.0225 kWh_{el}/kWh_{th} (Fugmann et al., 2015). Thus, the EER_0 of the adsorption chiller would decrease to approximately 15. With this EER_0, the minimal energy savings can be determined to 19 % for Athens and 13 % for Cologne (cf. Figure 4.8).

However, there is still potential since the maximal achievable energy savings are up to 27 % for Athens and up to 21 % for Cologne. Thus, up to 5 % more energy could be saved by more efficient adsorption chillers. For the first assessment provided by this study, we use experimentally validated models for the main components, i.e., the adsorption chiller and the compressor of the CO_2 cycle. Experimental data for the hybrid system is not available yet. As the results show a very high potential for energy savings by the hybrid system, the experimental validation of the full hybrid system seems promising in the next step.

4.4 Summary

CO_2 refrigeration systems become increasingly popular due to their environmentally friendly, natural refrigerant. However, low efficiencies at high ambient temperatures pose a challenge for the use of CO_2 systems in warm climates. To overcome this challenge, we propose and model a hybrid system combining a CO_2 cycle with an adsorption chiller.

In the hybrid system, the waste heat of the CO_2 cycle is recovered to drive an adsorption chiller. The cooling power of the adsorption chiller is re-integrated into the CO_2 cycle to increase efficiency. This hybrid system allows for the full integration of the sorption chiller and does not need a separate heat source. The re-integrated cooling from the adsorption chiller increases the efficiency of the CO_2 cycle by two effects: first, the difference between optimal high pressure level and low pressure level decreases by up to 6 % reducing the pressure ratio of the compressor. Second, the mass flow of the refrigerant decreases by up to 35 %. Both, the reduced pressure ratio and the reduced mass flow lead to energy savings in the compressor.

On the other hand, the adsorption chiller also requires some electricity. However, overall, the model identifies energy savings of up to 35 % by the hybrid system at high ambient temperatures. For a full annual cycle, the model finds energy savings of 22 % for Athens and 16 % for Cologne. A first economic analysis yields promising payback periods of less than 5 years for Athens and less than 4 years for Cologne. Economic benefits increase with higher electricity prices. Increasing the electrical efficiency of the adsorption chiller beyond the assumed nominal efficiency of 33 for current technologies could reduce the energy demand further by up to 5 % and thereby further improve the economic viability of the system. Thus, highly efficient adsorption chillers are beneficial for the hybrid system. Our results show the promising potential of the hybrid system to efficiently provide low-temperature refrigeration with environmentally friendly refrigerants at all climates.

CHAPTER 5

Integrated design and control

In this chapter, we propose an efficient method for the integrated optimization of design and control of adsorption chiller systems. The adsorption chiller system includes all main components needed for operation, such as heat source, heat-rejection device and auxiliaries. A literature review of the design and control of adsorption chiller systems is given in Section 2.4. We propose dynamic optimization to identify both, optimal design and optimal control of the system simultaneously for a specific application. The proposed method is illustrated for a case study of a solar-thermally-driven adsorption chiller system.

This chapter is structured as follows: In Section 5.1, we briefly present the main steps of the proposed method for the integrated optimization of design and control. In Section 5.2, each step of the method is exemplified for a case study of a solar-thermally-driven adsorption chiller system. Finally, we summarize the chapter in section Section 5.3.

Contents of this chapter have been reprinted from:

A. Gibelhaus, T. Tangkrachang, U. Bau, J. Seiler, and A. Bardow. "Integrated design and control of full sorption chiller systems". *Energy* 185 (2019), pp. 409–422, with permission from Elsevier. Contributions of the author: Writing the draft as principal author, implementing the models, planning and conducting the simulations, and evaluating the results.

5.1 Method for integrated dynamic optimization of design and control

In this section, we propose a method for the integrated optimization of the design and control of dynamic adsorption chiller systems. The adsorption chiller system consists of the adsorption chiller, the heat source, the heat-rejection unit, and the auxiliaries, such as pumps and fans. The system design sizes the individual system components, while the system control defines the operating points of the components.

The behavior of the system can be described by a dynamic model (differential algebraic equation (DAE) system). Thus, optimization of the system leads to a dynamic optimization problem, which mathematically reads:

$$
\begin{aligned}
\min_{x(\cdot),z(\cdot),u(\cdot),p} \quad & \Phi\left(x(\cdot), z(\cdot), u(\cdot), p\right) && \text{(Objective function)} \\
\text{s.t.} \quad & \dot{x} = f\left(x(t), z(t), u(t), p\right) && \text{(Dynamic model)} \\
& 0 = g\left(x(t), z(t), u(t), p\right) && \\
& 0 \leq c\left(x(t), z(t), u(t), p\right) && \text{(Path constraints)} \\
& 0 \leq r_i\left(x(t_i), z(t_i), u(t_i), p\right) && \text{(Point constraints)} \\
& 0 = x\left(0\right) - x_0 && \text{(Initialization)}
\end{aligned}
$$

In the optimization problem, an objective function Φ, e.g., total costs, is minimized subject to (s.t.): 1) the dynamic model (DAE system), 2) path constraints for the entire time horizon, e.g., technical limitations of components, 3) point constraints at a defined time t_i, e.g., required yield at the end, and 4) initial values x_0 for each differential state. In the equations, t is the independent time variable, x summarizes the differential state variables, z summarizes the algebraic state variables, u summarizes the time-dependent control variables, and p summarizes the time-invariant model parameters. While the differential states x and the algebraic states z result from the model equations, the parameters p and the control variables u are degrees of freedom. These degrees of freedom represent the design and control choices of the dynamic system, respectively. The task is to choose the design and control optimally regarding a defined objective function Φ.

The simultaneous optimization of both, design parameters p and control variables u in one step is computationally demanding for complex dynamic system models (Koller and Ricardez-Sandoval, 2017). Furthermore, most efficient dynamic optimization algorithms are based on local optimization, such that the resulting optimal solution can be only a local optimum (Rao, 2010). To simplify the optimization problem and to investigate the sensitivity of specific design choices, we solve the full large-scale optimization problem above in two steps:

1. The control variables are optimized for a constant set of design parameters p_j.

2. The set of design parameters is modified (p_{j+1}) in an automated loop and step 1) is repeated for the modified design p_{j+1}.

Figure 5.1 shows the entire workflow of the proposed method for the integrated optimization of design and control. The four steps of the proposed workflow are briefly described in the following and illustrated in full detail for a case study in Section 5.2.

Step 1 defines the application and the specifications for which the system design and control shall be optimized. The application sets the required energy demand and the available supply of different forms of energy, the ambient conditions, and the types of components to be used. The specifications define the characteristics of the chosen components, the required auxiliaries, and the interconnection between individual components. With this information, the initial system design can be derived according to design guidelines (Mugnier et al., 2017) and pre-design tools (Semmari et al., 2014).

Based on step 1, step 2 derives and parametrizes a dynamic system model to describe the system behavior. The system model consists of models for the individual components, the required auxiliaries, and the interconnections between individual components. The models for the main components should be calibrated and validated with experimental data (Lanzerath et al., 2015) or manufacturer data (Dalibard, 2013) to ensure reliable results. Furthermore, the individual component models should be variable in size to allow for modifications of the system design. In general, the system model should capture the impact of the investigated design and control choices.

In step 3, the control is optimized with a direct multiple shooting algorithm (Leineweber et al., 2003), an approach for DAE-constrained optimal control. Thereby, we can efficiently identify all optimal control variables simultaneously. Efficient and simultaneous identification is crucial since there are various interdependent control variables for the full-scale system. Thus, many possible combinations exist. The optimization of control is a crucial step because optimal control variables depend on system design. Therefore, different system designs should only be compared under optimal control to distinguish poor design from sub-optimal control (cf. Bau et al. (2017)).

In step 4, we evaluate the system design under optimal control. To evaluate the system design regarding the objective Φ, we apply a feedback loop. The feedback loop modifies the system design and repeats the optimization of control for each design until a termination criterion is fulfilled. The termination criterion can be a given range of design choices or a defined change for the performance indicator. The feedback loop systematically improves the system design until the optimal design under optimal control is identified for the defined application.

The four steps of the proposed workflow are illustrated for a case study of a solar-thermally-driven adsorption chiller system in the following section.

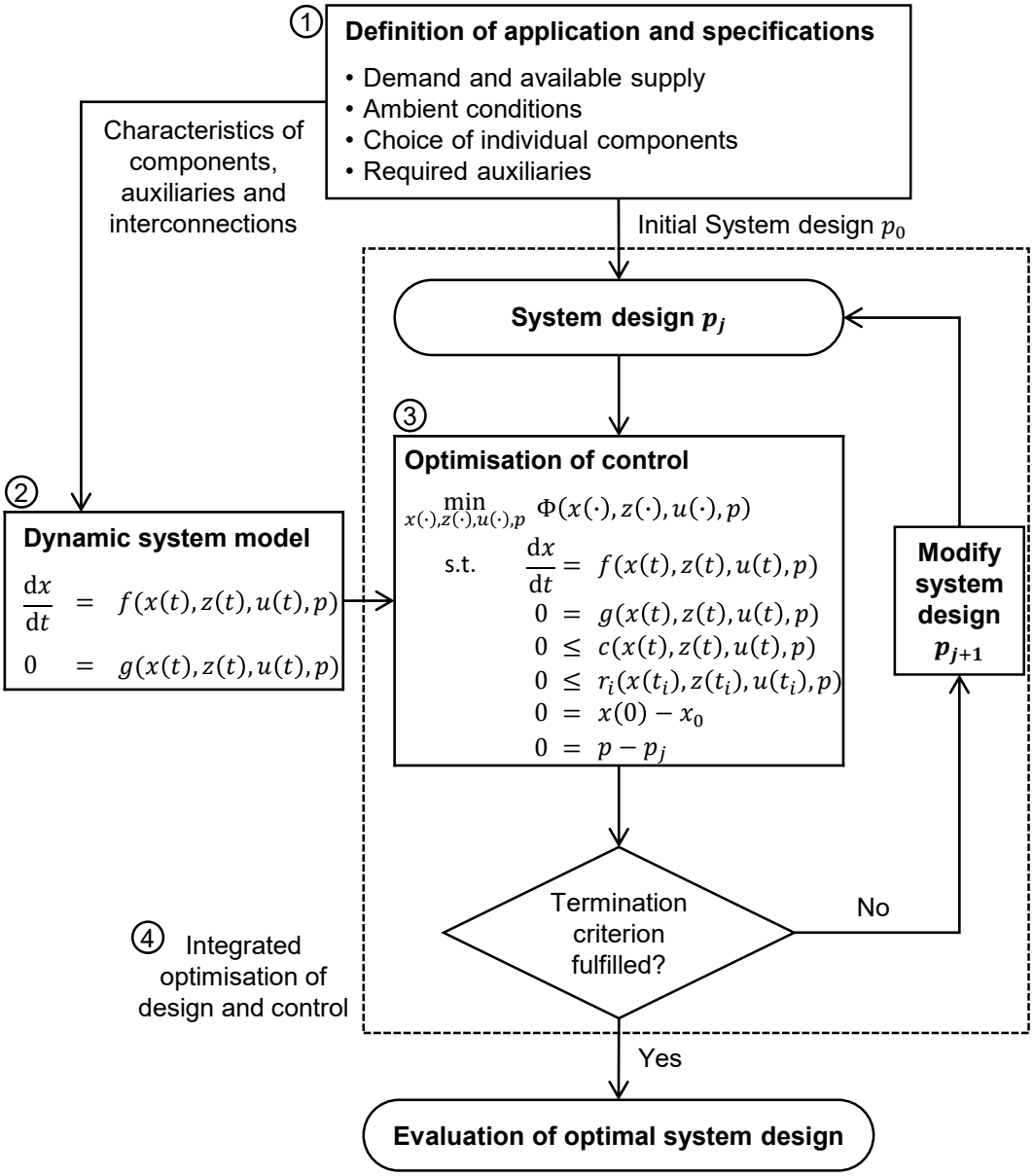

Figure 5.1: Workflow of the proposed method for the integrated optimization of design and control. The workflow has four steps: (1) The application and its specifications are defined. Based on the specifications, an initial system design is chosen. (2) A dynamic model is derived and parametrized for the application. (3) The dynamic system model and the initial system design are used to optimize the control of the system. (4) The optimization of control is repeated for system modified designs in a feedback loop, which runs until a defined termination criterion is fulfilled. Thereby, the modified system designs are evaluated at optimal control to choose the optimal design for the defined application.

5.2 Case-study: solar-thermally-driven adsorption chiller system

In this section, the four steps of the proposed method for the integrated optimization of design and control are illustrated for a case study of a solar-thermally-driven adsorption chiller system (Figure 5.2).

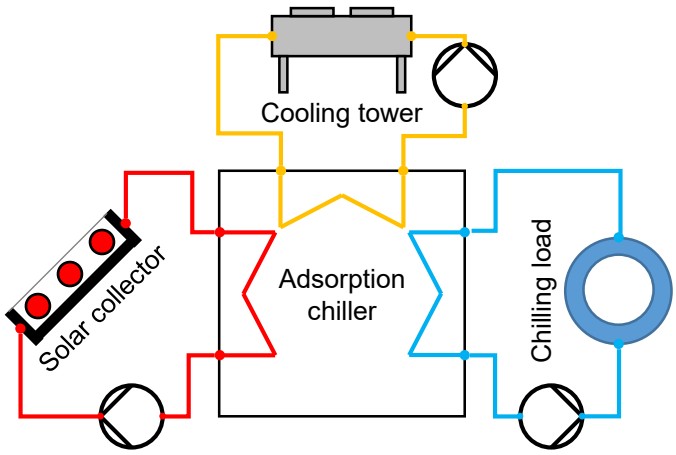

Figure 5.2: Scheme of the solar-thermally-driven adsorption chiller system with four main components: adsorption chiller, solar collector, cooling tower, and chilling load. These main components are interconnected via the heating circuit (red), the heat rejection circuit (yellow) and the chilling circuit (blue).

The degrees of freedom for the system are the system design and control. The system design defines the sizes of adsorption chiller, solar collector, and cooling tower. The system control defines the volume flows of the circulating pumps, the airflow of the cooling tower, and the cycle time of the adsorption chiller. Given an application, the task of a planer is to find the optimal design and control of the system regarding a defined objective. To fulfill this task, we apply the proposed method from Section 5.1 step-by-step to this case study. First, we define the two performance indicators used to evaluate the system design in the following.

5.2.1 Definition of performance indicators

As energetic performance indicator, we use the electrical efficiency of the system, which is described by the energy efficiency ratio (EER), cf. Equation (2.9) in Section 2.1.3. In this case study, the EER results from the ratio between the provided chilling power $\dot{Q}_{\text{chill}}$ and

the total electrical power consumption P_{el} of all system components and auxiliaries, both averaged over the considered time horizon:

$$\mathrm{EER} = \frac{\int \dot{Q}_{\mathrm{chill}} \, \mathrm{d}t}{\int P_{\mathrm{el}} \, \mathrm{d}t}. \tag{5.1}$$

Since the chilling power $\dot{Q}_{\mathrm{chill}}$ is usually set by the application, the energy efficiency ratio (EER) is maximized by minimizing electricity consumption.

As economic performance indicator, we define the total specific costs of the produced chilling C_{tot}. The total specific costs C_{tot} consist of the sum of the annualized investment costs $a \cdot C_{\mathrm{invest}}$ and the annual operating costs C_{op} (Henning et al., 2013), divided by the produced chilling:

$$C_{\mathrm{tot}} = \frac{a \cdot C_{\mathrm{invest}} + C_{\mathrm{op}}}{\int \dot{Q}_{\mathrm{chill}} \, \mathrm{d}t}. \tag{5.2}$$

The investment costs of a medium-size solar chilling system mainly consist of the costs for the main components: the solar collector, the adsorption chiller, and the cooling tower. All other costs, e.g., for the auxiliaries, the storage units, and the planning, are estimated by 30 % of the investment costs for the main components (Mugnier et al., 2017). For these other components, we do not use separate cost correlations, since the design of these components is not regarded in the current study for simplicity reasons. Thus, the investment costs for the considered system are:

$$C_{\mathrm{invest}} = 1.3 \; (C_{\mathrm{coll}} + C_{\mathrm{chiller}} + C_{\mathrm{cooler}}), \tag{5.3}$$

where C_{coll}, C_{chiller} and C_{cooler} are the investment costs of the solar collector, the adsorption chiller and the cooling tower, respectively. For these investment costs, correlations have been derived based on a comprehensive market overview in Task 48 of the Solar Heating and Cooling Programme (SHC) of the International Energy Agency (IEA) (Neyer et al., 2015):

$$C_{\mathrm{coll}} = 760.59 \; A_{\mathrm{coll}}^{0.865} \quad (C_{\mathrm{coll}} \text{ in EUR and } A_{\mathrm{coll}} \text{ in m}^2) \tag{5.4}$$

$$C_{\mathrm{chiller}} = 1680 \; \dot{Q}_{0,\mathrm{chill}}^{0.83} \quad (C_{\mathrm{chiller}} \text{ in EUR and } \dot{Q}_{0,\mathrm{chill}} \text{ in kW}) \tag{5.5}$$

$$C_{\mathrm{cooler}} = 46.8 \; \dot{Q}_{0,\mathrm{cooler}} + 2638 \quad (C_{\mathrm{cooler}} \text{ in EUR and } \dot{Q}_{0,\mathrm{cooler}} \text{ in kW}). \tag{5.6}$$

In the correlations, A_{coll} is the collector area, $\dot{Q}_{0,\mathrm{chill}}$ is the nominal chilling power of the adsorption chiller and $\dot{Q}_{0,\mathrm{cooler}}$ is the nominal cooling power of the dry cooler.

To annualize the investment costs into constant annual quantities over the life-time of the system, we use the annuity a (Henning et al., 2013):

$$a = \frac{i_{\text{eff}}}{1 - (1 + i_{\text{eff}})^{-n}}, \tag{5.7}$$

where i_{eff} is the effective rate of return, which can be calculated as the difference between the average interest rate and the inflation rate. The lifetime of the system is given by n. The values of these parameters are given in Table 5.1.

The annual operating costs C_{op} consist of the costs for electricity consumption, for peak electricity demand and for maintenance (Henning et al., 2013):

$$C_{\text{op}} = \frac{\dot{Q}_{0,\text{chill}}}{\text{EER}} \ (\tau_{\text{FL}} \ c_{\text{el}} + c_{\text{peak,el}}) + C_{\text{maint}}, \tag{5.8}$$

where τ_{FL} are the full load hours, c_{el} are the electricity costs, $c_{\text{peak,el}}$ are the peak electricity costs and C_{maint} are the maintenance costs. The economic parameters for the costs calculations are chosen based on the solar cooling handbook (Henning et al., 2013), shown in Table 5.1.

Table 5.1: Economic parameters for the calculation of the total annualized costs based on the solar cooling handbook (Henning et al., 2013).

Description	Variable	Value
Interest rate	i_{int}	5 %
Inflation rate for energy	i_{inf}	3 %
Lifetime	n	25 a
Full load hours	τ_{FL}	2000 h/a
Electricity price	c_{el}	0.15 EUR/(kW h)
Peak electricity price	$c_{\text{peak,el}}$	50 EUR/(kW a)
Costs for maintenance	C_{maint}	0.015 C_{invest}

5.2.2 Step 1: definition of application, specifications, and initial design

In this section, we first describe the application case for the solar-thermally-driven adsorption chiller system. The application case includes the nominal load, nominal operating conditions, and type of components to be used. Second, we specify the used components. Based on the described application and the specifications of the components, we derive an initial system design.

Application case and specifications of components

A solar-thermally-driven adsorption chiller system shall be designed for the following nominal conditions: The nominal operating conditions are given by a daily average ambient temperature of $T_{\mathrm{amb}} = 25\,°\mathrm{C}$ and a daily average total irradiation of $G_{\mathrm{tot}} = 500\,\mathrm{W/m^2}$ as typical values for a sunny day in southern Europe. We use daily average values since solar chilling systems should be designed to average conditions instead of peak conditions, which should be covered by conventional compression chillers to avoid over-sizing of the more expensive adsorption chiller (Mugnier et al., 2017).

Using daily averages corresponds to assuming that adequately sized storage systems compensate daily fluctuations. However, storage is not in the focus of the present work and, thus, not further analyzed. In this case study, we use one nominal operating point to design the adsorption chiller system since we aim to demonstrate the proposed design method in the most straightforward way. However, the presented design method can also be applied for various operating points to consider different operating conditions of the system. Furthermore, also time-resolved profiles can be used to consider daily or seasonal fluctuations and, thus, to allow for the detailed design of the thermal storage systems. These issues should be investigated in future studies to study potential design modifications.

The key component of the systems is the commercial adsorption chiller *MYCOM ADR-15* (Dalibard, 2017), which shall provide its nominal chilling power of $\dot{Q}_{\mathrm{chill}} = 50\,\mathrm{kW}$. This adsorption chiller was chosen since technical specifications are available in the literature, shown in Table 5.2 (Dalibard, 2017). The nominal temperatures refer to the inlet and

Table 5.2: Technical specifications of the commercial adsorption chiller *MYCOM ADR-15* at nominal operation (Dalibard, 2017).

	Temperature	volume flow	Pressure drop	heat flow
Chilling circuit	14/9 °C	8.6 m³/h	75 Pa	50 kW
Heating circuit	75/70 °C	14.3 m³/h	75 Pa	83 kW
Cooling circuit	29/33 °C	28.6 m³/h	100 Pa	133 kW
COP		0.6		
Electricity demand		0.4 kW		

outlet temperatures of the adsorption chiller. The given nominal volume flows of the heat transfer fluid water lead to the given pressure drops in each circuit. The cooling circuit is split into two parallel flows where 65 % cool the adsorber and 35 % cool the condenser. The Coefficient of Performance (COP) is defined as the ratio of chilling power and driving

power given by the heat input from the heating circuit (cf. Equation (2.6) in Section 2.1.3). The electricity demand accounts for the control electronics of the adsorption chiller.

To drive the adsorption chiller, we use a commercial evacuated-tube solar collector, which has already been used with adsorption chillers. Thus, experimentally validated data for the technical specifications is available, shown in Table 5.3 (Dalibard, 2017).

Table 5.3: Technical specifications of the commercial evacuated-tube collector *CPC 45 Star Azzurro* of the manufacturer Paradigma (Dalibard, 2017). The given parameters are explained in Section 5.2.3.

Description	Variable	Value
Aperture area	A_{ap}	$4.5\,\mathrm{m}^2$
Zero-loss efficiency	$F'(\tau\alpha)_{\mathrm{en}}$	0.644
Linear heat loss coefficient	c_1	$0.749\,\mathrm{W/(m^2\,K)}$
Quadratic heat loss coefficient	c_2	$0.005\,\mathrm{W/(m^2\,K^2)}$
Effective capacitance	c_5	$9180\,\mathrm{J/(m^2\,K)}$
Specific volume flow	$\dot{V}_{0,\mathrm{coll}}/A_{\mathrm{coll}}$	$0.66\,\mathrm{l/(m^2\,min)}$
Pressure drop	$\Delta p_{0,\mathrm{coll}}$	62 mbar

The sizing of the solar collector is realized by the parallel connection of various collectors to reduce the pressure drop. For this reason, the nominal volume flow in Table 5.3 is normalized by the collector area. The nominal volume flow increases linearly with increasing collector area, while the nominal pressure drop remains constant for the higher volume flow.

To reject the waste heat of the adsorption chiller, we use a dry cooler for simplicity reasons. Although wet or hybrid cooling towers are recommended for most solar-thermal chilling systems (Mugnier et al., 2017), dry coolers offer some significant advantages: easy installation, low operational and maintenance costs, and no hygienic problems since spray water is avoided (Henning et al., 2013). The presented design method could also be applied to hybrid or wet cooling towers.

The dry cooler is designed by the Product Calculator of the manufacturer Güntner Group (Güntner Group Europe GmbH, 2018). This tool allows us to design commercial dry coolers of variable size. Furthermore, the tool delivers technical specifications of the dry cooler as well as the part-load behavior to calibrate and validate a dry cooler model. The technical specifications of the dry cooler are given in the next paragraph since the size of the dry cooler has to be specified first.

Initial design of the system

The size of the adsorption chiller is fixed. Thereby, we follow the recommendation of the design guidelines for solar cooling systems (Mugnier et al., 2017) to design adsorption chillers for base-load operation at its nominal capacity. A back-up compression chiller should cover peak-loads. Over-sized adsorption chillers could be beneficial regarding energy efficiency since adsorption chillers have higher efficiency in part-load (Nienborg et al., 2017). Thus, a larger adsorption chiller would allow for smaller sizes of the other components or lower operating costs and vice versa. However, commercial adsorption chillers are generally available in only a few sizes. Therefore, sizing is mainly realized in practice by using multiple adsorption chillers in a modular structure. Sizing of the adsorption chiller is not considered in the current case study since the adsorption chiller shall be operated exactly at its nominal power. For the given adsorption chiller size, the aim is to determine the optimal sizes of both, the solar collector and the dry cooler.

The initial size of the solar collector is determined by a steady-state energy balance as proposed in literature (Henning et al., 2013): The heating supply of the collector $\dot{Q}_{\mathrm{coll}}$ equals the nominal heating demand of the adsorption chiller (cf. Table 5.2). Thus, the required collector area A_{coll} results from the total irradiation G_{tot} and the collector efficiency η_{coll}:

$$A_{\mathrm{coll}} = \frac{\dot{Q}_{\mathrm{coll}}}{G_{\mathrm{tot}}\ \eta_{\mathrm{coll}}}. \tag{5.9}$$

The collector efficiency η_{coll} is determined with the zero-loss efficiency $F'(\tau\alpha)_{\mathrm{en}}$ and the heat loss coefficients c_1 and c_2 from Table 5.3:

$$\eta_{\mathrm{coll}} = F'(\tau\alpha)_{\mathrm{en}} - c_1\ \frac{T_{\mathrm{m}} - T_{\mathrm{amb}}}{G_{\mathrm{tot}}} - c_2\ \frac{(T_{\mathrm{m}} - T_{\mathrm{amb}})^2}{G_{\mathrm{tot}}}. \tag{5.10}$$

The mean temperature of the collector T_{m} is calculated as the arithmetic mean temperature of the heating circuit (cf. Table 5.2). For the ambient temperature T_{amb} and the total irradiation G_{tot}, we use the nominal operating conditions defined above. With the given values, the required collector area A_{coll} is 302.87 m^2. This calculated area is divided by the aperture area of one collector module (cf. Table 5.3) to determine the required number of collector modules of 68 (rounded up).

The initial size of the dry cooler is determined by both, the required heat rejection and the nominal temperatures of the cooling circuit (cf. Table 5.2). With this information and the nominal ambient temperature, the size of the dry cooler can be designed with the Product Calculator of the Güntner Group (Güntner Group Europe GmbH, 2018). The tool suggests the dry cooler *GFHC WD 063* (Table 5.4).

Table 5.4: Technical specifications of the commercial dry cooler *GFHC WD 063*. The specifications are given by the Product Calculator of the Güntner Group (Güntner Group Europe GmbH, 2018).

Description	Variable	Value
Nominal cooling power	$\dot{Q}_{0,\text{cooler}}$	264 kW
Number of fans	n_{fan}	6
Nominal airflow	$\dot{V}_{0,\text{fan}}$	88 368 m^3/h
Nominal electrical power	$P_{0,\text{fan}}$	16.2 kW
Nominal fluid volume flow	$\dot{V}_{0,\text{cooler}}$	28.78 m^3/h
Nominal pressure drop	$\Delta p_{0,\text{cooler}}$	0.77 bar

The nominal cooling power of the dry cooler of 264 kW corresponds to the nominal conditions for dry coolers defined in the European norm Eurovent (Eurovent Certita Certification SAS, 2018): 25 °C ambient temperature and 40 °C inlet temperature of cooling fluid. At the nominal conditions of the adsorption chiller the cooling power of the dry cooler corresponds to the required power of 133 kW (cf. Table 5.2).

The dry cooler is constructed modularly: To increase the size of the dry cooler, the number of fans n_{fan} is increased together with the passes for the cooling fluid. Thus, the nominal airflow $\dot{V}_{0,\text{fan}}$, the nominal electrical power $P_{0,\text{fan}}$, and the nominal volume flow of the cooling fluid $\dot{V}_{0,\text{cooler}}$ increase linearly with size. The nominal pressure drop for the increased volume flow is constant since the fluid passes are connected in parallel.

5.2.3 Step 2: dynamic system model and parametrization

In this section, we describe the models of the individual components: the adsorption chiller, the evacuated-tube collector, and the dry cooler. We parametrize the models with the specifications from Section 5.2.2. Subsequently, we describe the models of the hydraulic circuits and the auxiliaries (pumps and fans). All models are implemented in the object-oriented language Modelica (Modelica Association, 2017).

Adsorption chiller

For the adsorption chiller, the experimentally validated model for the lab-scale one-bed chiller from Section 3.3 is employed. We extended the validated model to a two-bed adsorption chiller by adding a second identical adsorber as for the commercial adsorption chiller in Section 3.4. For further information about the adsorption chiller model, the reader is referred to Section 3.1.

The employed adsorption chiller model is scaled linearly to represent the considered commercial adsorption chiller (Table 5.2): All heat exchanger areas, and the volume of both, adsorbent and VLE were scaled linearly, such that the model provides the same chilling power with the same COP as specified in Table 5.2. The scaling of the heat exchangers was realized with constant Reynolds and Nusselt numbers to maintain the characteristics of the experimentally validated adsorption chiller model.

To operate the adsorption chiller, the adsorber is connected to the solar collector via the heating circuit in the desorption phase. In the adsorption phase, the adsorber is connected to the dry cooler via the cooling circuit (Figure 5.2). The desorption and adsorption phases are switched periodically between both adsorbers. Since one adsorber is in the adsorption phase while the other adsorber is in the desorption phase, the duration of both phases is equal and corresponds to the half-cycle time. The condenser is also connected to the dry cooler, in parallel to the adsorber in the adsorption phase: the cooling circuit leaving the dry cooler is split into two flows, one flow passing the adsorber and the other flow passing the condenser. After passing adsorber and condenser, the two flows are mixed again before entering the dry cooler.

Evacuated-tube collector

We model the evacuated-tube collector according to the Standard DIN EN 12975-2 (German Institute for Standardization, 2006). The energy balance for the collector reads:

$$c_5 \; A_{\mathrm{coll}} \; \frac{\mathrm{d}T_{\mathrm{m}}}{\mathrm{d}t} = \dot{Q}_{\mathrm{irr}} - \dot{Q}_{\mathrm{loss}} - \dot{m}_{\mathrm{coll}} \; (h_{\mathrm{out}} - h_{\mathrm{in}}), \tag{5.11}$$

where c_5 is the effective capacitance, A_{coll} is the collector area, T_{m} is the arithmetic mean temperature of the fluid, $\dot{m}_{\mathrm{coll}}$ is the mass flow of the fluid and h_{out} and h_{in} are the outflowing and the incoming specific enthalpies of the fluid.

The irradiation heat flow $\dot{Q}_{\mathrm{irr}}$ is calculated with the irradiation G_{tot} and the zero-loss efficiency of the collector $F'(\tau\alpha)_{\mathrm{en}}$:

$$\dot{Q}_{\mathrm{irr}} = G_{\mathrm{tot}} \; A_{\mathrm{coll}} \; F'(\tau\alpha)_{\mathrm{en}}. \tag{5.12}$$

The heat loss $\dot{Q}_{\mathrm{loss}}$ is calculated with the heat-loss coefficients c_1 and c_2:

$$\dot{Q}_{\mathrm{loss}} = c_1 \; A_{\mathrm{coll}} \; (T_{\mathrm{m}} - T_{\mathrm{amb}}) + c_2 \; A_{\mathrm{coll}} \; (T_{\mathrm{m}} - T_{\mathrm{amb}})^2. \tag{5.13}$$

For the coefficients $F'(\tau\alpha)_{\mathrm{en}}$, c_1, c_2 and c_5, experimentally determined values by Dalibard (2017) are used (cf. Table 5.3). The total collector area A_{coll} allows to adjust the size of the collector for the system design.

Dry Cooler

To model the dry cooler, we use the effectiveness-NTU (number of transfer units) method based on the work of Stabat and Marchio (2004). The NTU-model approach is suitable for system simulations, since the simplifications are physically consistent and only two fitting parameters are sufficient to achieve good agreement with manufacturer data (Dalibard, 2017). For the dry cooler a steady-state model is employed, since the temperature variations in the dry cooler are comparatively small and the dynamics of the dry cooler are fast compared to the other system components, cf. Dalibard (2017). The energy balance of the dry cooler reads:

$$\dot{Q}_{\text{cooler}} = \dot{m}_{\text{fl}} \ (h_{\text{in}} - h_{\text{out}}), \tag{5.14}$$

where $\dot{m}_{\text{fl}}$ is the mass flow of the fluid and h_{in} and h_{out} are the incoming and the outflowing specific enthalpies of the fluid. The rejected heat flow $\dot{Q}_{\text{cooler}}$ is calculated with the effectiveness of the cooler ε, the minimal heat capacity flow $\dot{C}_{\text{min}}$ and the temperature difference of the incoming fluid $T_{\text{fl,in}}$ and the air $T_{\text{air,in}}$:

$$\dot{Q}_{\text{cooler}} = \varepsilon \ \dot{C}_{\text{min}} \ (T_{\text{fl,in}} - T_{\text{air,in}}). \tag{5.15}$$

The heat capacity flow $\dot{C}$ is defined as product of the mass flow $\dot{m}$ and the specific heat capacity c_p. The minimal heat capacity flow $\dot{C}_{\text{min}}$ is the minimal value of the heat capacity flows of both, fluid and air:

$$\dot{C}_{\text{min}} = \min(\dot{m}_{\text{fl}} \ c_{p,\text{fl}}, \ \dot{m}_{\text{air}} \ c_{p,\text{air}}). \tag{5.16}$$

The effectiveness ε is calculated with the number of transfer units NTU:

$$\varepsilon = \frac{1 - \exp[-\text{NTU} \ (1 - \dot{C}_{\text{min}}/\dot{C}_{\text{max}})]}{1 - \dot{C}_{\text{min}}/\dot{C}_{\text{max}} \ \exp[-\text{NTU} \ (1 - \dot{C}_{\text{min}}/\dot{C}_{\text{max}})]}, \tag{5.17}$$

where the maximal heat capacity flow $\dot{C}_{\text{max}}$ is defined in the same way as the minimal heat capacity flow $\dot{C}_{\text{min}}$ in Equation (5.16), but with the maximal value. The number of transfer units NTU is defined by:

$$\text{NTU} = \frac{UA_{\text{ext}} \ UA_{\text{int}}}{UA_{\text{ext}} + UA_{\text{int}}} \ \frac{1}{\dot{C}_{\text{min}}}. \tag{5.18}$$

Both heat transfer values, the external UA_{ext} and the internal UA_{int}, are functions of the corresponding mass flows of the air $\dot{m}_{\text{air}}$ and of the fluid $\dot{m}_{\text{fluid}}$:

$$UA_{\text{ext}} = \gamma \; c_{p,\text{air}} \; \dot{m}_{\text{air}}^{0.8} \text{ and} \tag{5.19}$$

$$UA_{\text{int}} = \delta \; \frac{\dot{m}_{\text{fl}}^{0.8}}{\mu_{\text{fl}}^{0.8}}, \tag{5.20}$$

where $c_{p,\text{air}}$ is the specific heat capacity of the air, and $\dot{m}_{\text{fl}}$ is the dynamic viscosity of the fluid. The two parameters γ and δ can fit the model to experimental data. To fit the model, we applied the procedure proposed by Dalibard (2013): first, we generated more than 90 different operating points of the selected dry cooler *GFHC WD 063* (Section 5.2.2). The operating points were generated with the Product Calculator of the Güntner Group (Güntner Group Europe GmbH, 2018) by varying both inlet temperatures as well as both volume flows, of the air and the fluid. Second, we chose the parameters γ and δ such that the rejected heat flow $\dot{Q}_{\text{cooler}}$ calculated by the model fits the rejected heat flow given by the manufacturer for all operating points. For this purpose, we minimized the mean square deviation of the rejected heat flow $\dot{Q}_{\text{cooler}}$. The resulting fitting parameters are $\gamma = 4.032$ and $\delta = 606.18$. With these fitting parameters, the standard deviation between the model and manufacturer data is less than 5 %.

To adjust the size of the dry cooler to the system design, the modular structure of the dry cooler allows to increase the number of both, fans and fluid passes (Section 5.2.2).

Hydraulic circuits and auxiliaries

The hydraulic circuits connect the individual components adsorption chiller, evacuated-tube collector, and dry cooler by a heat transfer fluid (Figure 5.2). In the model, the three variables specific enthalpy, pressure, and mass flow are transferred between two connected components: the three variables of the heat transfer fluid flowing out of a component are set equal to those of the heat transfer fluid flowing into the connected component and vice versa. The chilling circuit is modeled by a constant nominal inlet temperature to the evaporator of the adsorption chiller. This modeling approach approximates a buffer storage tank, which smoothens the dynamics of the chilling power over one adsorption chiller cycle as usually employed for practical applications (Nienborg et al., 2017). The storage tank and the cooling load are not modeled in the current study, since we do not consider a specific consumer. If a specific consumer is regarded in a more detailed study, the storage tank could be also modeled to include its sizing to the design optimization.

To improve the thermal efficiency of the system, we implemented a passive heat recovery strategy (Wang et al., 2005): After the switch between the desorption and adsorption phase, the outlet of the hot adsorber 1 remains connected to the collector, while the inlet

is already connected to the dry cooler. Analogously, the outlet of the cooled adsorber 2 remains connected to the dry cooler, while the inlet is already connected to the collector. When the outlet temperature of adsorber 1 drops below the outlet temperature of adsorber 2, the passive heat recovery is terminated, and the outlet of adsorber 1 is switched to the dry cooler. Accordingly, the outlet of adsorber 2 is switched to the collector. The passive heat recovery prevents that hot water is pushed into the cooling circuit and cooled water is pushed into the heating circuit immediately after the switch between the desorption and adsorption phase. Thereby, the internal energy of the heat transfer fluid is recovered and, consequently, the thermal efficiency of the system increases.

To determine the electricity consumption of the pumps, the pressure drops in the hydraulic circuits are modeled by an empirical quadratic correlation between pressure drop Δp and volume flow $\dot{V}$ (Helm, 2015):

$$\Delta p = \Delta p_0 \left(\frac{\dot{V}}{\dot{V}_0} \right)^2 . \tag{5.21}$$

The nominal pressure drops Δp_0 and the nominal volume flow $\dot{V}_0$ for each component are given by the technical specifications (Table 5.2, Table 5.3 and Table 5.4). The actual volume flow $\dot{V}$ of each circuit is a control variable, which can be chosen in the range of a quarter of its nominal value $\dot{V}_0/4$ and the fourfold of its nominal 4 $\dot{V}_0$. Larger volume flows than their nominal values represent larger sized pumps.

To account for the pressure drops due to distribution and piping, we used estimates from literature (Dalibard, 2017): 1) In the heating circuit, 18 % of the total pressure drop is due to the piping. 2) In the cooling circuit, 43 % of the total pressure drop is due to the piping. 3) In the chilling circuit, 53 % of the total pressure drop is due to the distribution and piping. The sizing of the hydraulic circuit (e.g., pipe diameter) is not considered in this study, since it would require a detailed structure of the specific piping network. The detailed piping network is out of the scope of the current study.

The electricity consumption of each pump $P_{\mathrm{P,i}}$ is modelled according to the standard DIN EN 14511-3:2011 with a load-dependent efficiency (Melograno et al., 2015):

$$P_{\mathrm{P,i}} = \frac{\left(\dot{V} \ \Delta p \right)^{0.6817}}{0.0721}. \tag{5.22}$$

The electricity consumption of the dry cooler P_{fan} is modeled by the affinity law as cubic function of the airflow $\dot{V}_{\mathrm{fan}}$ (Heating and Engineers, 2016):

$$P_{\mathrm{fan}} = P_{0,\mathrm{fan}} \left(\frac{\dot{V}_{\mathrm{fan}}}{\dot{V}_{0,\mathrm{fan}}} \right)^3 . \tag{5.23}$$

The nominal electricity consumption $P_{0,\text{fan}}$ and the nominal airflow $\dot{V}_{0,\text{fan}}$ are obtained from Table 5.4. The actual airflow of the dry cooler $\dot{V}_{\text{fan}}$ is a control variable, which can be chosen in the range of a quarter of its nominal value $\dot{V}_{0,\text{fan}}/4$ and its nominal value $\dot{V}_{0,\text{fan}}$.

In sum, the total electricity consumption of the system is:

$$P_{\text{el}} = P_{\text{P,heat}} + P_{\text{P,cool}} + P_{\text{P,chill}} + P_{\text{fan}} + P_{\text{AC}}, \tag{5.24}$$

where P_{AC} is the electricity consumption of the adsorption chiller, given in Table 5.2.

5.2.4 Step 3: optimization of control

In this section, we derive the dynamic optimisation problem to identify optimal control of the full adsorption chiller system. The control of the system is defined by six variables: the five volume flows of 1) the heating circuit $\dot{V}_{\text{heat}}$, 2) the chilling circuit $\dot{V}_{\text{chill}}$, 3) the cooling circuit through the adsorber $\dot{V}_{\text{cool}}^{\text{ads}}$, 4) the cooling circuit through the condenser $\dot{V}_{\text{cool}}^{\text{cond}}$, 5) air in the dry cooler $\dot{V}_{\text{fan}}$ as well as 6) the cycle time of the adsorption chiller t_{cycle}.

The control variables strongly influence both, the thermal and the electrical performance of the system: on the one hand, high volume flows increase the thermal performance since the heat transfer increases. On the other hand, high volume flows decrease electrical performance, since the electricity consumption increases. Thus, optimal control aims at minimizing electricity consumption, while still satisfying the chilling demand for the given system design and operating conditions. To achieve minimal electricity consumption while satisfying the required chilling demand, all control variables are optimized simultaneously. The simultaneous optimization is crucial since the individual control variables can compensate each other: a higher volume flow in one circuit can compensate a lower volume flow in another circuit.

For control optimization, we minimize the electricity consumption. Operation enters the costs of the system only through electricity consumption. Thus, minimizing electricity optimizes both performance indicators, the electrical efficiency EER (Equation (5.1)) and the total specific costs C_{tot} (Equation (5.2)): minimal electricity consumption corresponds to maximal electrical efficiency, since the chilling demand is fixed; minimal electricity consumption corresponds to minimal total costs, since all other costs, such as investment costs, are fixed during control optimization. The resulting dynamic optimization problem

for control reads:

$$
\begin{aligned}
\min_{x(\cdot),z(\cdot),u(\cdot),p,t_\mathrm{f}} \quad & \tau_\mathrm{FL}/t_\mathrm{f} \int_0^{t_\mathrm{f}} P_\mathrm{el}\left(x(t),z(t),u(t),p\right)\ \mathrm{d}t && \text{(Objective function)}\\
\text{s.t.} \quad & \dot{x} = f\left(x(t),z(t),u(t),p\right) && \text{(Dynamic model)}\\
& 0 = g\left(x(t),z(t),u(t),p\right) && \\
& 0 \leq u(t) - u_\mathrm{min} && \text{(Part-load range)}\\
& 0 \leq u_\mathrm{max} - u(t) && \\
& 0 \leq \int_0^{t_\mathrm{f}} \dot{Q}_\mathrm{chill}\ \mathrm{d}t\ /\ t_\mathrm{f} - \dot{Q}_\mathrm{0,chill} && \text{(Chilling demand)}\\
& 0 = x\left(0\right) - x\left(t_\mathrm{f}\right) && \text{(Cyclic operation)}\\
& 0 = p - p_j && \text{(Fixed design)}\\
& t \in \left[0, t_\mathrm{f}\right] && \text{(Time horizon)}
\end{aligned}
$$

The control optimization is performed for the time horizon $[0, t_\mathrm{f}]$. The duration of the time horizon t_f is the half-cycle time of the adsorption chiller t_cycle. The half-cycle time is sufficient to represent the full cycle due to the symmetry of the two identical adsorbers: the states of adsorber 1 after the desorption phase equal the states of adsorber 2 after the adsorption phase and vice versa. This condition for the states of the adsorbers is implemented in the constraint of cyclic operation. As the cycle time t_cycle is a control variable, the duration of the time horizon t_f is also optimized.

The electricity consumption is minimized subject to five types of constraints: 1) The DAE set of the dynamic model; 2) the path constraints for the part-load range of the control variables between a minimal value u_min and a maximal value u_max; 3) a point constraint to provide the nominal chilling demand $\dot{Q}_\mathrm{0,chill}$; 4) the constraint of cyclic operation to ensure that the differential states at the beginning of the time horizon are the same as at the end of the time horizon; and 5) an equality constraint to fix the design parameters p_j during optimization of control.

To solve the optimization problem, we employ the Modelica optimization library developed by the German Aerospace Center (2019). The library provides tools and methods to solve DAE-constrained (dynamic) optimization problems (Pfeiffer, 2012) directly within the Dymola environment (Dassault Systèmes, 2020). For this purpose, the dynamic infinite-dimensional optimization problem is transformed into a finite-dimensional non-linear program (NLP) by discretizing path constraints and state trajectories. The resulting large-scale but structured NLP is solved by a sequential quadratic programming (SQP) algorithm. For detailed information about the numerical algorithms and techniques, the reader is referred to the literature (Nocedal and Wright, 2006).

The described optimization library can also identify optimal trajectories for the control variables $u(t)$ over the time horizon using a single-shooting algorithm. In the following, we optimized the control variables as time-invariant values ($u(t) = u$). We found that

time-dependent optimal trajectories have not significantly improved the results compared to time-invariant optimal values, but have worsened the robustness of the optimization algorithm. We expect that for varying operating conditions, the benefits due to optimal trajectories would become significant.

Figure 5.3 compares the optimal control to the nominal control for the initial system design (cf. Section 5.2.2). The nominal volume flows of both, the heat transfer circuits and

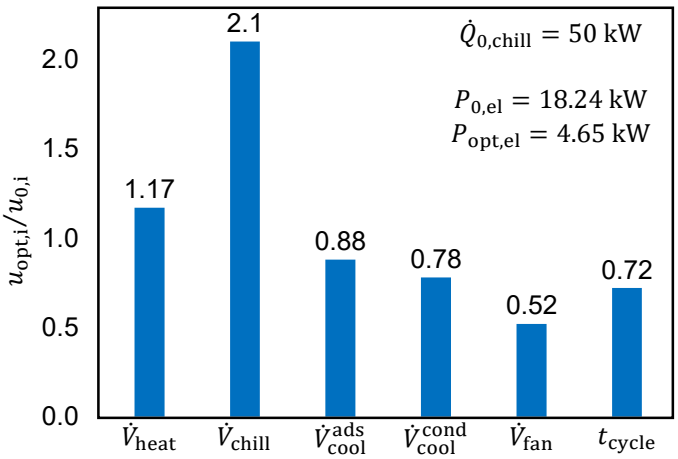

Figure 5.3: Ratio of optimal control variables $u_{\mathrm{opt,i}}$ and nominal control variables $u_{0,\mathrm{i}}$ for the initial design defined in Section 5.2.2. The control variables are the volume flows of the heat transfer circuits $\dot{V}$ and the cycle time of the adsorption chiller t_{cycle}. The system provides a nominal chilling power of $\dot{Q}_{0,\mathrm{chill}} = 50\,\mathrm{kW}$ with an electricity consumption of $P_{0,\mathrm{el}} = 18.24\,\mathrm{kW}$ for nominal control variables and of $P_{\mathrm{opt,el}} = 4.56\,\mathrm{kW}$ for optimal control variables.

the dry cooler, correspond to the technical specifications (Table 5.2 and Table 5.4). The nominal cycle time results from a control heuristic presented by Bau and Bardow (2019) applied at nominal volume flows. This control heuristic has shown good performance by switching between the adsorption and desorption phase when the average chilling power of the current cycle drops below the required chilling power.

The control optimization increases the volume flows by 17 % for the heating circuit and by 110 % for the chilling circuit compared to the nominal volume flows (Table 5.2). In contrast, the optimal volume flows decrease by 12 % for the cooling circuit through the adsorber and by 22 % for the cooling circuit through the condenser. The optimal airflow of the dry cooler also decreases by 48 %. Thus, the increased optimal volume flows in both, the chilling circuit and the heating circuit, compensate the decreased optimal volume flows in the cooling circuit and the decreased airflow of the dry cooler. The optimal cycle time decreases by 28 % to adjust the chilling power to the required chilling demand with the changed volume flows.

The increase of the volume flow in the chilling circuit is particularly high because we assume a fixed inlet temperature to the evaporator of the adsorption chiller independent of the volume flow: For a fixed inlet temperature, the volume flow increases the capacity flow of the heat transfer fluid proportionally. The increased capacity flow leads to a higher outlet temperature of the evaporator if the same amount of heat is transferred. The higher outlet temperature and the fixed inlet temperature increase the driving force in the evaporator and, thereby, increase the thermal efficiency of the adsorption chiller. In contrast, higher volume flows in the heating and cooling circuits increase the capacity flows of the heat transfer fluid less than in the chilling circuit, since the inlet temperatures are not fixed but depend on the solar collector and the dry cooler, respectively. Therefore, the increase of the volume flow in the chilling circuit is particularly beneficial.

At optimal control, the required chilling load is provided using 75.5 % less electricity than for nominal control. The electrical efficiency of the system EER (Equation (5.1)) increases by a factor of four from 2.7 to 10.8. The total specific costs C_{tot} (Equation (5.2)) decrease by 28 % from 0.18 EUR/(kW h) to 0.13 EUR/(kW h). Thus, the control already shows a large optimization potential. The determined optimal control variables are specific for the initial system design. E.g., a larger dry cooler would allow for lower optimal volume flows due to the increased heat transfer area. Thus, only system designs under optimal control should be compared to investigate the influence of design choices without the effect of poor control. To investigate the system design in the next step, we apply the optimization of control for each modified system design (cf. Section 5.1). Solving the optimization of control takes a few minutes on an Intel Core i5-6600 desktop CPU with 3.3 GHz. Thus, this efficient solution method allows for multiple design variations.

5.2.5 Step 4: evaluation of system design under optimal control

In this section, we evaluate the design of the adsorption chiller system under optimal control. For this purpose, we apply the proposed method for the integrated optimization of design and control (Section 5.1): we modify the size of the solar collector and the size of the dry cooler. For each design modification, we optimize the control (cf. Section 5.2.4). Under optimal control, we evaluate the system design regarding the two performance indicators: (1) electrical efficiency EER (Equation (5.1)) and (2) total specific costs C_{tot} (Equation (5.2)). In the following, the size of the collector is quantified by the collector area, and the size of the dry cooler is quantified by the nominal cooling power (cf. Table 5.4).

Design optimization regarding electrical efficiency EER

Figure 5.4 (a) shows the electrical efficiency EER as function of system design. Each design is evaluated under optimal control. Figure 5.4 (b) compares the corresponding optimal control to nominal control.

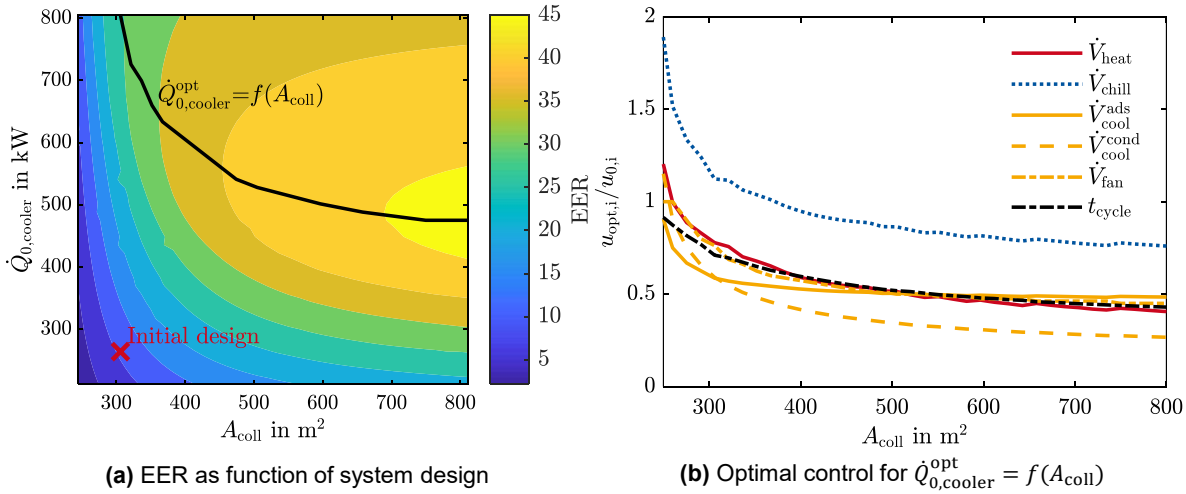

(a) EER as function of system design

(b) Optimal control for $\dot{Q}^{opt}_{0,cooler} = f(A_{coll})$

Figure 5.4: Results of the design optimization under optimal control for electrical efficiency EER. (a) EER as function of both, the collector area A_{coll} and the nominal cooling power of the dry cooler $\dot{Q}_{0,cooler}$. The initial design (Section 5.2.2) is marked by a red cross. The black curve shows the optimal nominal power of the dry cooler as function of the collector area $\dot{Q}^{opt}_{0,cooler} = f(A_{coll})$. (b) Ratio of optimal control variables $u_{opt,i}$ and nominal control variables $u_{0,i}$ corresponding to $\dot{Q}^{opt}_{0,cooler} = f(A_{coll})$. The control variables are the volume flows of the heat transfer circuits $\dot{V}$ and the cycle time of the adsorption chiller t_{cycle}.

The electrical efficiency EER of the initial system design is 10.8 under optimal control. This EER is already 4 times higher than at nominal control (Section 5.2.4). By optimizing the design, the EER further increases by more than factor four up to more than 45 (Figure 5.4 (a)). The EER increases since larger components (solar collector and dry cooler) provide larger heat flows. These larger heat flows increase driving forces in the heat transfer circuits and, thus, allow to decrease the volume flows, as shown in Figure 5.4 (b). To achieve the highest EER, we have to increase the sizes of both components, the collector and the dry cooler.

The collector has no optimal size regarding electrical efficiency EER. A larger collector always increases the EER (Figure 5.4 (a)) due to 1) a direct effect and 2) an indirect effect. 1) The direct effect is that a larger-sized collector increases the driving temperature in the heating circuit due to the larger heat flow. The higher driving temperature leads to both, higher thermodynamic efficiency and a higher driving force for the heat transfer. Higher

thermodynamic efficiency and the higher driving force allow for lower volume flows to transfer the required heat flow and, thus, reduce electricity consumption. 2) Furthermore, a large collector also allows to reduce the volume flows in the other circuits due to the indirect effect: Lower volume flows decrease electricity consumption, but at the same time also decrease the thermal efficiency of the adsorption chiller (cf. Section 5.2.3). However, the lower thermal efficiency can be compensated by the larger collector, since more heat is available to provide the required chilling demand. Therefore, a larger collector provides the required chilling demand with lower volume flows in all components (Figure 5.4 (b)) and, consequently, with higher electrical efficiency EER.

For the size of the dry cooler, there is an optimum regarding electrical efficiency EER (Figure 5.4 (a)). On the one hand, a larger dry cooler rejects the required heat with lower volume flows for both, the cooling circuit and the airflow due to a larger heat transfer area. Furthermore, a larger dry cooler can provide the same airflow as a smaller dry cooler with less electricity consumption: while both, the nominal airflow and the nominal electricity consumption increase linearly with dry cooler size (Table 5.4), the electricity consumption in part-load decreases cubically (Equation (5.23)). On the other hand, the minimal electricity consumption of the dry cooler is limited by its minimal part-load (Section 5.2.3). This minimal electricity consumption also increases linearly with the dry cooler size, such that an over-sized dry cooler also decreases the electrical efficiency EER.

Figure 5.4 (b) illustrate the importance of the integrated optimization of design and control. Modifying the system design influences the choice of optimal control significantly: for different designs, all optimal control variables significantly decrease by up to 50 % below their initial optimal value. If the designs would be compared at the same control, the difference between poor design and poor control could not be distinguished.

Design optimization regarding the total specific costs C_{tot}

Figure 5.5 shows the specific costs at optimal control as function of the system design. There is an optimal system design with minimal total specific costs C_{tot} (white cross in Figure 5.4 (a)). The optimal design results from the trade-off between operating costs and investment costs: On the one hand, the operating costs decrease for a larger collector and dry cooler due to the higher electrical efficiency (Figure 5.4). On the other hand, the investment costs increase for larger components. This trade-off is illustrated in Figure 5.4 (b) and (c).

Furthermore, Figure 5.5 shows that the investment costs are dominated by the costs for the collector: total costs increase more strongly with increasing collector area (Figure 5.5 (b)) than with nominal power of the dry cooler (Figure 5.5 (c)). For this reason, it is cheaper to decrease the operating costs by a larger dry cooler than by a larger collector: the

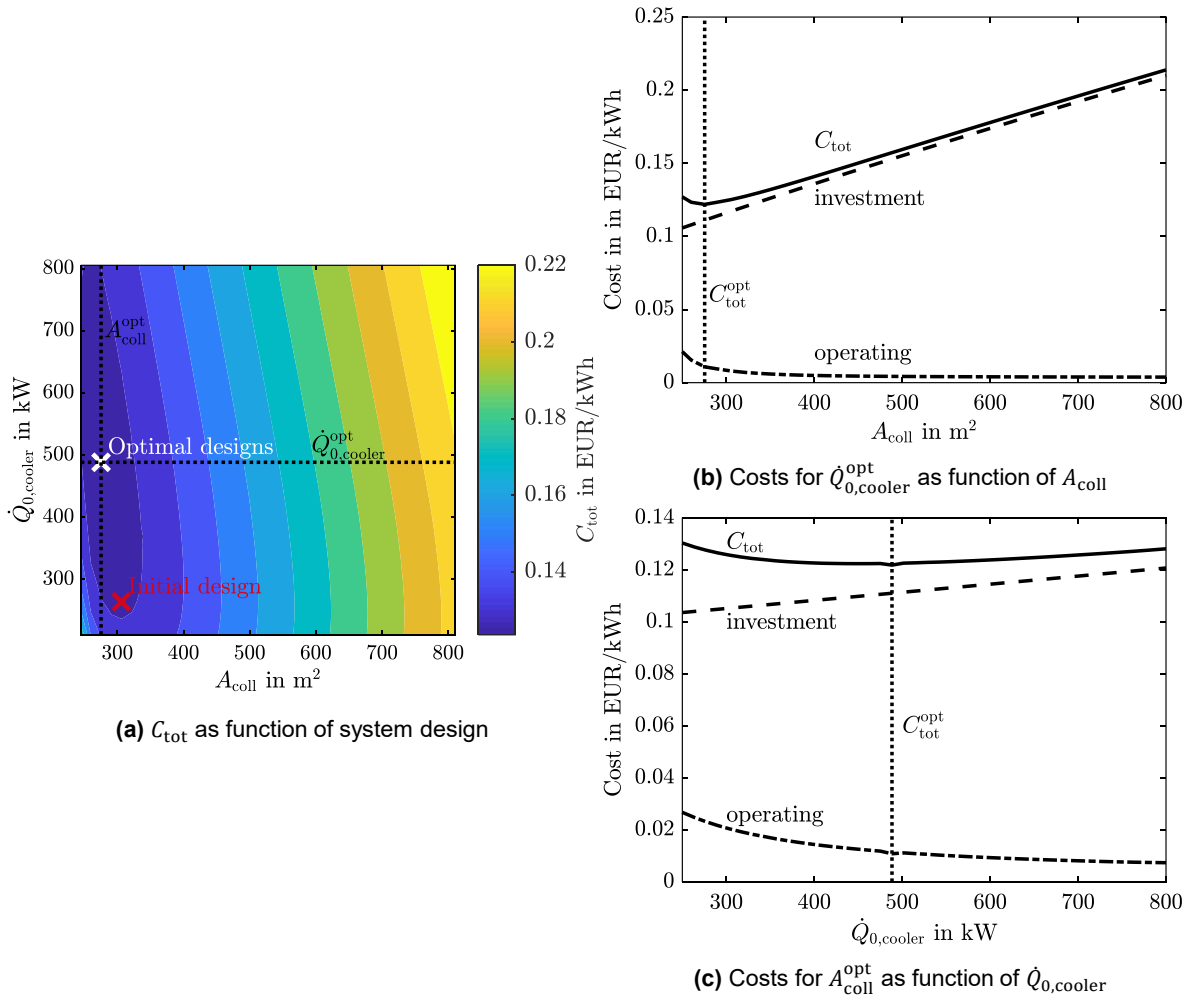

(a) C_{tot} as function of system design

(b) Costs for $\dot{Q}_{0,\text{cooler}}^{\text{opt}}$ as function of A_{coll}

(c) Costs for $A_{\text{coll}}^{\text{opt}}$ as function of $\dot{Q}_{0,\text{cooler}}$

Figure 5.5: Results of the design optimization under optimal control for total specific costs C_{cost}. (a) Total specific costs C_{tot} as function of both, the collector area A_{coll} and the nominal cooling power of the dry cooler $\dot{Q}_{0,\text{cooler}}$. The initial design (Section 5.2.2) is marked by a red cross. The optimal design regarding the total costs C_{tot} is marked by a white cross. Total specific costs C_{tot}, specific investment costs and specific operating costs (b) as function of the collector area A_{coll} for the optimal nominal cooling power of the dry cooler $\dot{Q}_{\text{o,cooler}}^{\text{opt}}$ (horizontal dotted line in (a)); and (c) as function of the nominal cooling power of the dry cooler $\dot{Q}_{0,\text{cooler}}$ for the optimal collector area $A_{\text{coll}}^{\text{opt}}$ (vertical dotted line in (a)).

cost-optimal dry cooler size $\dot{Q}_{0,\text{cooler}}^{\text{opt}} = 488.4\,\text{kW}$ is 85 % larger than the initial dry cooler size $\dot{Q}_{0,\text{cooler}}^{\text{init}} = 264\,\text{kW}$ (Section 5.2.2) while the cost-optimal collector size $A_{\text{coll}}^{\text{opt}} = 275.4\,\text{m}^2$ is 10 % smaller than the initial collector size $A_{\text{coll}}^{\text{init}} = 306\,\text{m}^2$ (Section 5.2.2). The cost-optimal design increases the electrical efficiency by 50 % to EER = 16.2 compared to the initial design at optimal control (EER = 10.8, cf. Figure 5.4). Even though a very high electrical efficiency (EER) of more than 40 is possible (Figure 5.4), it is suboptimal

since the decreased operating costs are not sufficient to compensate the higher costs for the collector. Thus, lower collector costs or higher electricity costs would lead to higher electrical efficiency EER for the cost-optimal design.

The cost-optimal design decreases the total specific costs by 8 % compared to the initial design, from 0.13 EUR/(kW h) to 0.12 EUR/(kW h). The decrease of total specific costs for the cost-optimal design is rather small due to the low contribution of operating costs to total costs (Figure 5.5 (b)). Therefore, the increase in electrical efficiency only slightly decreases the total costs. In future scenarios, the increase in electrical efficiency might become more important if the electricity costs increase and if the investment costs of the system components decrease due to higher technical maturity. In these cases, the contribution of the operating costs to the total costs would increase, and higher electrical efficiencies would be more beneficial from an economic point of view. Furthermore, the environmental benefits from higher electrical efficiencies can lead to economic benefits, e.g., through emissions trading or white certificates. Thus, the cost-optimal design would move to larger sized system components, which would allow for higher electrical efficiencies.

5.3 Summary

Design and control of adsorption chiller systems are key to achieve high electrical and economic performance. The interdependency of design and control requires the simultaneous optimization of both, which is challenging due to the many degrees of freedom.

In this study, we propose a method for the integrated optimization of design and control employing dynamic optimization. The method decomposes the optimization of design and control in two steps: In the first step, the control is optimized for a fixed design. In the second step, the design is modified, and the first step is repeated for the modified design. Thus, all different designs are compared under optimal control to distinguish between poor design and poor control.

We apply the proposed method to a case study of a solar-thermally-driven adsorption chiller system. The results are compared to an established design method and nominal control according to manufacturer specifications: 1) Optimization of control for the reference design, increases the electrical efficiency by factor four from 2.7 to 10.8. The total specific costs decrease by 28 % from 0.18 EUR/(kW h) to 0.13 EUR/(kW h). 2) The cost-optimal design further increases the electrical efficiency by 50 % to 16.2 and further decreases the total specific costs by 8 % to 0.12 EUR/(kW h). For an energetically-optimal design, even higher electrical efficiencies of more than 40 are possible such that higher benefits are expected for high electricity costs or lower investment costs.

The case study shows that the proposed method provides an efficient approach to improve both, electrical and economic performance of adsorption chiller systems.

CHAPTER 6

Summary, conclusion and future perspective

This thesis aims to shift the focus of the evaluation and optimization of adsorption chillers to the systems integration since the system-level performance is crucial for the competitiveness and the market penetration of adsorption chillers. To move towards optimal systems integration, this thesis provides the essential models and methods. Furthermore, this thesis proposes a comprehensive framework for optimal systems integration. In the following, the key results of this thesis are summarized, and the main conclusions are drawn in Section 6.1. Based on the results and conclusions, possible future research topics are derived in Section 6.2.

6.1 Summary and conclusion

The systems integration of adsorption chillers is crucial since the main benefit of adsorption chillers is to substitute electricity with thermal energy. However, this benefit is often nullified by connected system components and auxiliaries, such as the heat-rejection unit and the pumps. Optimal systems integration is a challenging task due to the intrinsic dynamic behavior of adsorption chillers, the close interaction between many system components, and the strong dependency of design, control, and operating conditions. Thus, there are many interdependent degrees of freedom, which are difficult to determine. To account for all these challenges and to capture all significant effects, this thesis pursues a model- and optimization-based approach for the systems integration of adsorption chillers. To this end, the thesis covers three important topics of systems integration: 1) model development and validation, 2) integration in hybrid systems, and 3) integration within the auxiliaries. The major contributions of each topic are highlighted in the following.

Efficient and validated adsorption chiller model

We developed an efficient model that achieves the same accuracy as a state-of-the-art model but with increased computational efficiency by up to 70 %. The increased computational efficiency is achieved by avoiding the computationally expensive discretization of the heat exchangers and applying an operator splitting approach instead. Thereby, the proposed model is well suited for the complex task of systems integration. We demonstrated the applicability of the model by calibrating and validating the model for two types of adsorption chillers: (1) a lab-scale two-bed adsorption chiller, and (2) a commercial, two-bed adsorption chiller.

Integration in hybrid systems

We integrated an adsorption chiller into a CO_2 vapor compression cycle to provide low-temperature refrigeration with natural refrigerants only. The hybrid system revealed a high energy savings potential compared to a stand-alone CO_2 cycle: Particularly for warm climates, as in Athens, annual energy savings of 22 % were shown. But also for moderate climates, as in Cologne, annual energy savings of 16 % were achieved. A first economic analysis also yielded promising results with payback periods of less than five years. The energy savings obtained in the study largely depend on the electrical efficiency of the adsorption chiller, which highlights the importance of optimal integration. The case study was based on the nominal electrical efficiency of a commercial adsorption chiller. If the electrical efficiency decreases, the energy savings will also decrease, while even up to 5 % more energy could be saved if the electrical efficiency is improved.

Integration within the auxiliaries

We proposed a method for the integrated optimization of design and control of adsorption chiller systems, including all main system components and auxiliaries. We demonstrated the method for a case-study of a solar-thermally-driven cooling system, consisting of the adsorption chiller, a solar-thermal collector, a dry cooler, and the pumps. The results showed that the proposed method can increase the electrical efficiency of the system by a factor of six and to decrease the specific costs of cooling by up to 33 % for a cost-optimal design and control compared to an established design method and nominal control. The results of the case study show that the detailed systems integration provides a powerful tool to improve the system-level performance of adsorption chillers by optimizing the design and the control of the system.

In summary, this thesis can also be used as a comprehensive framework for optimal systems integration of adsorption chillers, consisting of the three topics described above:

1. **Model validation:** As basis for model-based systems integration, we propose to derive an reliable model of the considered adsorption chiller by parameterizing, calibrating, and validating the model developed in this thesis with experimental data.
2. **Conceptual integration:** Having the validated model and a potential application, we propose to evaluate whether or under which circumstances the integration of the adsorption chiller is beneficial by quantifying the expected benefit as demonstrated for the hybrid refrigeration system in this thesis.
3. **Detailed integration:** If the conceptual integration revealed a high potential, we propose to optimize the design and control of all system components and auxiliaries in detail, using the proposed method for integrated optimization of design and control.

6.2 Future research

Based on the presented methods and findings, suggestions for further research are derived in the following.

Further development of the calibration and validation method

The calibration of the adsorption chiller was performed by employing one operating point, which was derived from typical operating conditions. To make the calibration more efficient and potentially more accurate, statistical methods could be employed to determine a suitable operating point for calibration. Furthermore, also more than one operating point could be used for calibration to improve the accuracy of the model in a broader range. A promising possibility to improve the calibration method is to apply optimal experimental design methods (Franceschini and Macchietto, 2008), which allow for a theoretically justified selection of operating conditions for calibration with minimal experimental effort. A first work on this topic was done by Postweiler (2019) in his master's thesis.

Experimental validation of promising hybrid refrigeration system

The conceptual integration showed that the integration of an adsorption chiller into a CO_2 vapor compression cycle provides a promising hybrid system to provide low-temperature refrigeration with natural refrigerants efficiently. Although for the individual components of the hybrid system validated models were employed, the actual combination of the components in the hybrid system was shown only theoretically. To validate the theoretical

results and to derive further practical research topics, a prototype of the hybrid system would be helpful in the next step. Based on the prototype, the model of the hybrid system could be validated and further improved to support the rigorous optimization of design and control.

Including component and working pair design into systems integration

In this thesis, the systems integration of a fixed, given adsorption chiller was considered, which is, e.g., the case for the integration of a specific adsorption chiller available on the market. In the next step, the design of the adsorption chiller itself, its components, and the employed working pair could be included in the systems integration. As the proposed models are based on physical laws, the models can also capture the effect of component and working pair design. Furthermore, the proposed models and methods are computationally sufficiently efficient to allow for holistic optimization of working pair, component, and system design. This holistic optimization would bridge the gap between component design and systems integration, and thereby, support the use of adsorption chillers.

Transient load profiles and operating conditions for rigorous systems integration

The rigorous systems integration was demonstrated for nominal, average operating points, which is a reasonable assumption for base case scenarios. However, the presented models and methods can also be used with transient profiles for load and operating conditions. These transient profiles would consider daily or seasonal fluctuations for the design and control of the system. Furthermore, a detailed design of thermal storage units could be included in the system design.

Consideration of environmental and systemic benefits of adsorption chillers for systems integration

In this thesis, only energetic and economic objectives were considered for the systems integration of adsorption chillers. However, from a purely economic point of view, adsorption chillers currently can hardly compete with conventional technologies in many applications, such as solar cooling, due to their lower market maturity and their more complex technology. Instead, adsorption chillers offer some further environmental advantages, such as environmentally friendly working pairs, including refrigerants with zero global warming potential, and systemic advantages, such as relieving the power grid. These advantages could be included in the objective function of systems integration to support the efficient use of adsorption chillers. There are first works, which quantify the ecological impacts and consider the life cycle assessment of adsorption-based technologies (Beccali

et al., 2015; Nienborg et al., 2018). These life cycle assessment methods can be integrated into the systems integration methods presented in this thesis to allow for a more holistic evaluation of adsorption chillers.

APPENDIX A

Adsorption equilibrium of silica gel 123 / water

In this appendix, the adsorption equilibrium of the employed working pair silica gel 123 / water is documented. Besides to the adsorption equilibrium, also the specific heat capacity of the adsorbent is given.

The adsorption equilibrium is described by a characteristic curve (cf. Section 2.2.1), which was experimentally determined and fitted by an inverse tangent (arctan) function by (Schawe, 1999):

$$W = d + \frac{a}{\pi}\left[\arctan\left(\frac{A-b}{c}\right) + \frac{\pi}{2}\right] , \tag{A.1}$$

with the coefficients

$$\begin{aligned} a &= 5.072\,313 \times 10^{-1} , \\ b &= 1.305\,531 \times 10^{2} , \\ c &= -8.492\,403 \times 10^{1} , \\ d &= 4.128\,962 \times 10^{3} . \end{aligned}$$

The validity of the fitted characteristic curve $W = f(A)$ is reported in the range of $A > 17\,\mathrm{kJ/kg} < A < 1940\,\mathrm{kJ/kg}$.

The specific heat capacity of the adsorbent was also reported by Schawe (1999) as:

$$c_{\mathrm{sor}} = 1000\,\mathrm{J/(kg\,K)} . \tag{A.2}$$

APPENDIX B

Parametrization of the lab-scale one-bed adsorption chiller

In this appendix, the lab-scale one-bed adsorption chiller, which was employed for the calibration and validation of the models (cf. Section 3.3), is briefly described. Furthermore, the parametrization of the corresponding component models is given. The lab-scale one-bed adsorption chiller was constructed by Lanzerath (2013), where more details about the experimental setup can be found.

The one-bed adsorption chiller has a modular structure and consists of three main components: an adsorber, an evaporator, and a condenser (Figure B.1). These three components are pictured in Figure B.2:

1. The adsorber heat exchanger consists of 13 longitudinally-finned tubes, which are connected in series. Between the longitudinal fins, the adsorbent particles are filled and fixed by a vapor-permeable net.
2. The evaporator heat exchanger consists of four cross-finned tubes, which are connected in series. The low fins of the evaporator allow for an efficient, capillary-assisted vaporization at vacuum conditions (Lanzerath et al., 2016).
3. The condenser consists of a copper helix with 17.5 coils. The outer surface of the condenser helix is not structured to allow for a free drain of the condensed water.

The parametrization of each component of the adsorption chiller model (cf. Section 3.3) is summarized in Table B.1.

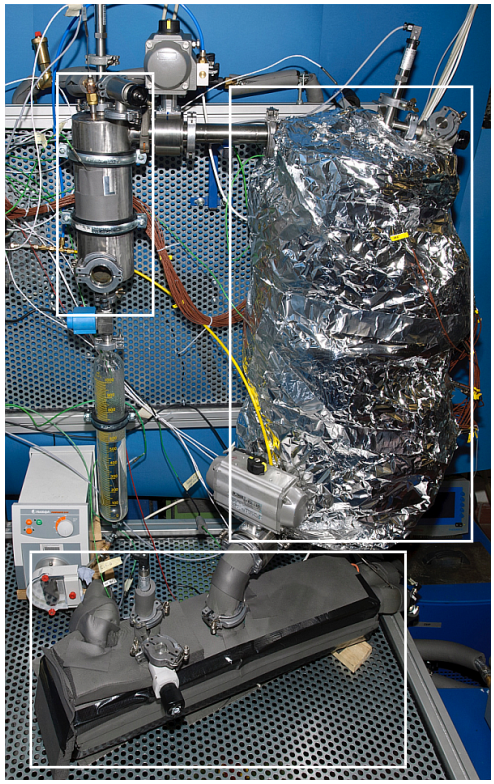

Figure B.1: Picture of the modular, one-bed adsorption chiller, constructed by Lanzerath (2013). The three main components, adsorber, evaporator, and condenser are marked in the picture.

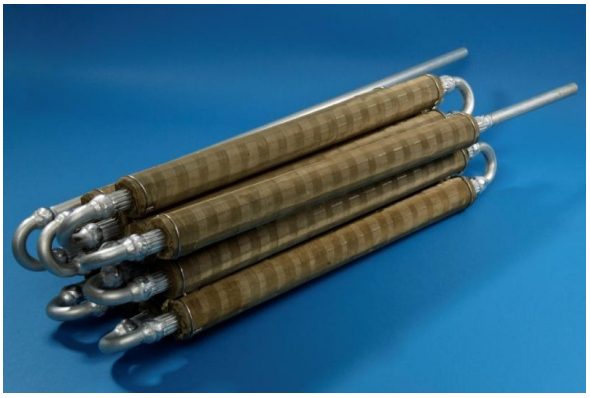

(a) Longitudinally-finned-tube adsorber

(b) Cross-finned-tube evaporator

(c) Helix condenser

Figure B.2: Pictures of the components of the modular, one-bed adsorption chiller, constructed by Lanzerath (2013): (a) longitudinally-finned-tube adsorber, (b) cross-finned-tube evaporator, and (c) helix condenser.

Table B.1: Parametrization of the three main components of the adsorption chiller model: adsorber, evaporator and condenser.

Parameters of the adsorber model		
material of the tube and the fins		aluminum
length of the adsorber tube	L_{tube}	7.355 m
inner diameter of the adsorber tube	$d_{\mathrm{tube,i}}$	12.85 mm
outer diameter of the adsorber tube	$d_{\mathrm{tube,o}}$	15.71 mm
heat transfer value inside the tube	$(hA)_{\mathrm{i}}$	Sieder and Tate (1936)
heat transfer value outside the tube	$(hA)_{\mathrm{o}}$	calibration parameter
Sieder parameter	C_{ST}	0.033885
working pair		silica gel 123/water (Schawe, 1999)
mass of adsorbent	m_{sor}	2.236 kg
particle radius	r_{particle}	0.45 mm
Parameters of the evaporator model		
material of the tube		copper
length of the evaporator tube	L_{tube}	2.31 m
inner diameter of the evaporator tube	$d_{\mathrm{tube,i}}$	14.67 mm
outer diameter of the evaporator tube	$d_{\mathrm{tube,o}}$	17.72 mm
heat transfer value inside the tube	$(hA)_{\mathrm{i}}$	Sieder and Tate (1936)
heat transfer value outside the tube	$(hA)_{\mathrm{o}}$	calibration parameter
Sieder parameter	C_{ST}	0.05
Parameters of the condenser model		
material of the tube		copper
length of the condenser tube	L_{tube}	4.55 m
inner diameter of the condenser tube	$d_{\mathrm{tube,i}}$	8.0 mm
outer diameter of the condenser tube	$d_{\mathrm{tube,o}}$	10.0 mm
heat transfer value inside the tube	$(hA)_{\mathrm{i}}$	Schmidt (1967)
heat transfer value outside the tube	$(hA)_{\mathrm{o}}$	calibration parameter
average diameter of the helix	d_{helix}	75 mm

APPENDIX C

Discretization of the adsorber model

To test grid independence of the discretized adsorber model, we systematically varied the discretization between 2 and 200 discretization elements. For this purpose, we employed the adsorber model with ideal models for condenser and evaporator from Section 3.5. As measure for the change in the simulation results with increasing number of discretization elements, we calculated the coefficient of variation (cf. Section 3.2.1) of the adsorber between the current simulation with n discretization elements and the subsequent simulation with $n+1$ discretization elements (CV_{n+1}):

$$\mathrm{CV}_{n+1} = \frac{1}{Q^{\mathrm{A}}_{n+1}/\Delta t}\sqrt{\frac{1}{\Delta t}\int_0^{\Delta t}\left(\dot{Q}^{\mathrm{A}}_{n+1} - \dot{Q}^{\mathrm{A}}_{\mathrm{n}}\right)^2 \mathrm{d}t}. \tag{C.1}$$

Figure C.1 shows the CV_{n+1} as function of the number of discretization elements.

For high numbers of discretization elements, the change in the simulation results (CV_{n+1}) becomes negligible (Figure C.1) and, thus, the model can be assumed as grind independent. For discretizations with more than 34 elements the CV_{n+1} is below 1 %. Thus, the fine discretization of the adsorber with 40 elements in Section 3.3 is sufficient to achieve grid independence with a CV_{n+1} of less than 0.7 %. In contrast, the coarse discretization with 5 elements still reveals a significant grid dependence with a CV_{n+1} of more than 26 %. Consequently, the coarse discretization is not suitable to achieve accurate simulation results (cf. Section 3.3.2), since the discretization already causes a considerable error.

In Section 3.5, we even employed a finer discretization of 100 elements as benchmark models to test the validity of the proposed plug-flow-based model. Figure C.1 proves that for 100 discretization elements the simulation results are nearly grid independent, since the CV_{n+1} is even below 0.1 %.

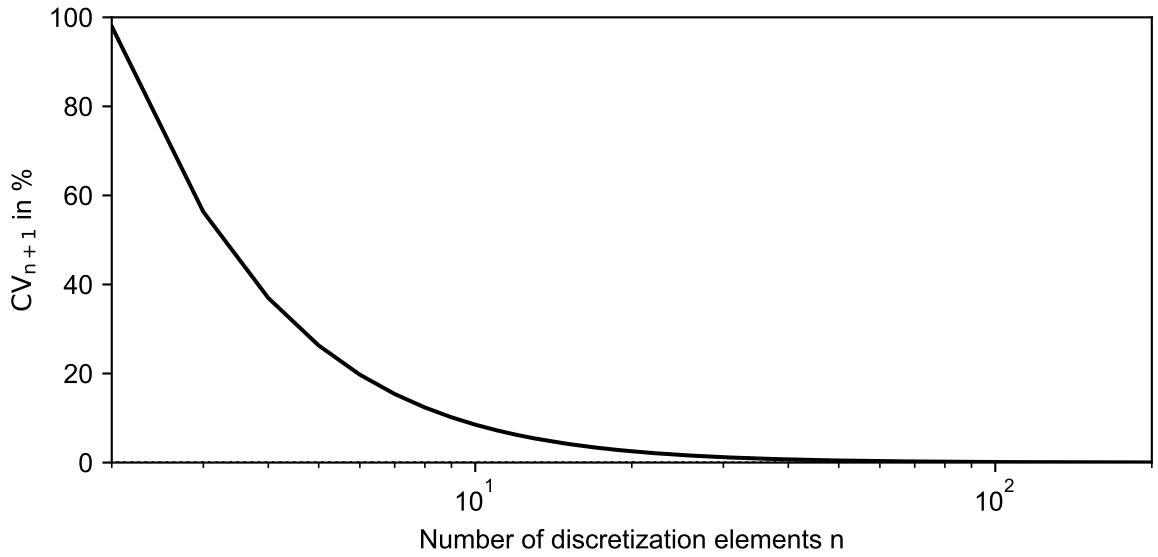

Figure C.1: Change in the simulation results of the adsorber in dependence of the discretization resolution: Coefficient of variation of the adsorber (CV_{n+1}) between the simulation with n discretization elements and the simulation with $n + 1$ discretization elements as function of the number of discretization elements n.

APPENDIX D

Publications and Student Theses

List of publications

Journal contributions

A. Gibelhaus, N. Fidorra, F. Lanzerath, L. Schnabel, J. Köhler, and A. Bardow. "Effiziente Kältebereitstellung durch Kopplung von Adsorptions- und CO_2-Kompressionskälteanlage". *KI – Kälte • Luft • Klimatechnik* 12 (2016), pp. 46–50.

G.Tjarks, A. Gibelhaus, F. Lanzerath, M. Müller, A. Bardow, and D. Stolten. "Energetically-optimal PEM electrolyzer pressure in power-to-gas plants". *Applied Energy* 218 (2018), pp. 192–198.

A. Gibelhaus, N. Fidorra, F. Lanzerath, U. Bau, J. Köhler, and A. Bardow. "Hybrid refrigeration by CO_2 vapour compression cycle and water-based adsorption chiller: An efficient combination of natural working fluids". *International Journal of Refrigeration* 103 (2019), pp. 204–214.

A. Gibelhaus, T. Tangkrachang, U. Bau, J. Seiler, and A. Bardow. "Integrated design and control of full sorption chiller systems". *Energy* 185 (2019), pp. 409–422.

M. Engelpracht, A. Gibelhaus, J. Seiler, S. Graf, N. Nasruddin and A. Bardow. "Upgrading Waste Heat from 90 °C to 110 °C: The Potential of Adsorption Heat Transformation". *Energy Technology* (2020)

Conference contributions

U. Bau, A. Gibelhaus, F. Lanzerath, and A. Bardow. "Optimal operation of two-bed adsorption chillers by combining heat recovery and reallocation of adsorption/desorption times". *International Sorption Heat Pump Conference*, Tokyo, Japan (2017).

A. Gibelhaus, N. Fidorra, F. Lanzerath, L. Schnabel, J. Köhler, and A. Bardow. "Effiziente Kältebereitstellung durch Kopplung von Adsorptions- und CO_2-Kompressionskälteanlage". *Deutsche-Kälte-Klima-Tagung (DKV-Tagung)*, Kassel, Germany (2016).

A. Gibelhaus, G. Tjarks, F. Lanzerath, M. Müller, D. Stolten, and A. Bardow. "Energieeffiziente Produktion und Nachbehandlung von Wasserstoff für Power-to-Gas Anwendungen". *VDI Thermodynamik-Kolloquium*, Kaiserslautern, Germany (2016).

A. Gibelhaus, N. Fidorra, F. Lanzerath, U. Bau, L.Schnabel, J. Köhler, and A. Bardow. "Hybrid refrigeration with CO_2 vapor compression cycle and adsorption chiller: Anefficient combination of natural working fluids". *International Sorption Heat Pump Conference*, Tokyo, Japan (2017).

A. Gibelhaus, T. Tangkrachang, U. Bau, and A. Bardow. "Design and control of adsorption cooling systems based on dynamic optimization". *Heat Powered Cycles Conference*, Bayreuth, Germany (2018).

A. Gibelhaus, U. Bau, F. Lanzerath, and A. Bardow. "Auslegung und Steuerung von Adsorptionskühlsystemen mittels dynamischer Optimierung". *Deutsche-Kälte-Klima-Tagung (DKV-Tagung)*, Aachen, Germany (2018).

S. Graf, A. Gibelhaus, U. Bau, F. Lanzerath, and A. Bardow. "Honey, I shrunk the sorption Lab - Model-based scale-up of adsorption systems". *Heat Powered Cycles Conference*, Bayreuth, Germany (2018).

D. Tillmanns, C. Gertig, J. Schilling, A. Gibelhaus, U. Bau, F. Lanzerath, and A. Bardow. "Integrated design of ORC process and working fluid using PC-SAFT and Modelica". *4th International Seminar on ORC Power Systems*, Milano, Italy (2017).

Student theses supervised during this work

L. Balhorn. "Simplified model of an additively manufactured molten salt to supercritical carbon dioxide heat exchanger". Bachelor's thesis, RWTH Aachen University (2019).

P. Dossow. "Model-based Design and Control of Adsorption Cooling Systems Employing Dynamic Optimization and Time Series for Operating Conditions". Master's thesis, RWTH Aachen University (2018).

T. Gülker. “Experimentelle Untersuchung von Desorptionskonzepten für offene Adsorptionssysteme (in German)”. Bachelor’s thesis, RWTH Aachen University (2017).

P. Postweiler. “Experimental validation of a dynamic adsorption chiller model using dynamic optimisation for parameter estimation and optimal experimental design”. Master’s thesis, RWTH Aachen University (2019).

R. Seeger. “Modellgestützte Betriebs- und Designoptimierung eines hybriden Kältesystems mit CO_2-Kompressionskältemaschine und Adsorptionskältemaschine (in German)”. Bachelor’s thesis, RWTH Aachen University (2018).

T. Tangkrachang. “Cost Estimation and Economic Optimization of Solar-Driven Adsorption Chiller”. Master’s thesis, RWTH Aachen University (2017).

Bibliography

Alam, K. C. A., Akahira, A., Hamamoto, Y., Akisawa, A., and Kashiwagi, T. (2004). "A four-bed mass recovery adsorption refrigeration cycle driven by low temperature waste/renewable heat source". *Renewable Energy* 29.9, pp. 1461–1475.

Albers, J. (2014). "New absorption chiller and control strategy for the solar assisted cooling system at the German federal environment agency". *International Journal of Refrigeration* 39, pp. 48–56.

Albers, J., Kemmer, H., and Ziegler, F. (2009). "Solar driven absorption chiller controlled by hot and cooling water temperature". *3rd International Conference Solar Air-Conditioning*. Palermo, Italy, pp. 338–343.

Allouhi, A., Kousksou, T., Jamil, A., and Zeraouli, Y. (2014). "Modeling of a thermal adsorber powered by solar energy for refrigeration applications". *Energy* 75, pp. 589–596.

Aprea, C. and Maiorino, A. (2009). "Transcritical CO2 refrigerator and sub-critical R134a refrigerator: A comparison of the experimental results". *International Journal of Energy Research* 33.12, pp. 1040–1047.

Aprea, C., Greco, A., and Maiorino, A. (2013). "The substitution of R134a with R744: An exergetic analysis based on experimental data". *International Journal of Refrigeration* 36.8, pp. 2148–2159.

Aprile, M., Freni, A., Toppi, T., and Motta, M. (2020). "Modelling and Performance Assessment of a Thermally-Driven Cascade Adsorption Cycle Suitable for Cooling Applications". *Thermal Science and Engineering Progress*.

Aristov, Y. I., Dawoud, B., Glaznev, I. S., and Elyas, A. (2008). "A new methodology of studying the dynamics of water sorption/desorption under real operating conditions of adsorption heat pumps: Experiment". *International Journal of Heat and Mass Transfer* 51.19-20, pp. 4966–4972.

Aristov, Y. I. (Aug. 2020). "Dynamics of adsorptive heat conversion systems: Review of basics and recent advances". *Energy* 205, p. 117998.

Aristov, Y. I., Tokarev, M. M., Freni, A., Glaznev, I. S., and Restuccia, G. (2006). "Kinetics of water adsorption on silica Fuji Davison RD". *Microporous and Mesoporous Materials* 96.1, pp. 65–71.

Aristov, Y. I. (2013). "Challenging offers of material science for adsorption heat transformation: A review". *Applied Thermal Engineering* 50.2, pp. 1610–1618.

Arora, A., Singh, N. K., Monga, S., and Kumar, O. (2011). "Energy and exergy analysis of a combined transcritical CO2 compression refrigeration and single effect H2O-LiBr vapour absorption system". *International Journal of Exergy* 9.4, p. 453.

Askalany, A. A., Saha, B. B., Kariya, K., Ismail, I. M., Salem, M., Ali, A. H. H., and Morsy, M. G. (2012). "Hybrid adsorption cooling systems–An overview". *Renewable and Sustainable Energy Reviews* 16.8, pp. 5787–5801.

Bansal, P. (2012). "A review – Status of CO2 as a low temperature refrigerant: Fundamentals and R&D opportunities". *Applied Thermal Engineering* 41, pp. 18–29.

Batchelor, G. K. (2000). *An Introduction to Fluid Dynamics*. Cambridge Mathematical Library. Cambridge: Cambridge University Press.

Bau, U. (2018). "From Dynamic Simulation to Optimal Designand Control of Adsorption Energy Systems". PhD Thesis. RWTH Aachen University.

Bau, U. and Bardow, A. (2019). "Pareto-optimal performance of one-bed adsorption chillers by easy-to-implement heat-flow-based control". *Applied Thermal Engineering* 159.

Bau, U., Braatz, A.-L., Lanzerath, F., Herty, M., and Bardow, A. (2015). "Control of adsorption chillers by a gradient descent method for optimal cycle time allocation". *International Journal of Refrigeration* 56, pp. 52–64.

Bau, U., Hoseinpoori, P., Graf, S., Schreiber, H., Lanzerath, F., Kirches, C., and Bardow, A. (2017). "Dynamic optimisation of adsorber-bed designs ensuring optimal control". *Applied Thermal Engineering* 125, pp. 1565–1576.

Bau, U., Baumgärtner, N., Seiler, J., Lanzerath, F., Kirches, C., and Bardow, A. (2019). "Optimal operation of adsorption chillers: First implementation and experimental evaluation of a nonlinear model-predictive-control strategy". *Applied Thermal Engineering* 149, pp. 1503–1521.

Beccali, M., Cellura, M., Longo, S., Finocchiaro, P., and Selke, T. (2015). *Task 48: Quality Assurance and Support Measures for Solar Cooling -Report on Life cycle analysis*. Report. International Energy Agency, Solar Heating and Cooling Programme.

Bering, B. P., Dubinin, M. M., and Serpinsky, V. V. (1966). "Theory of volume filling for vapor adsorption". *Journal of Colloid and Interface Science* 21.4, pp. 378–393.

Beshr, M., Aute, V., Abdelaziz, O., Fricke, B., and Radermacher, R. (2016). "Potential emission savings from refrigeration and air conditioning systems by using low GWP refrigerants". *The International Journal of Life Cycle Assessment* 22.5, pp. 675–682.

Brown, G. O. (2002). "Environmental and Water Resources History". *Environmental and Water Resources History*. American Society of Civil Engineers. Chap. The History of the Darcy-Weisbach Equation for Pipe Flow Resistance, pp. 34–43.

Brunauer, S., Emmett, P. H., and Teller, E. (1938). "Adsorption of Gases in Multimolecular Layers". *Journal of the American Chemical Society* 60.2, pp. 309–319.

Buonomano, A., Calise, F., and Palombo, A. (2018). "Solar heating and cooling systems by absorption and adsorption chillers driven by stationary and concentrating photovoltaic/thermal solar collectors: Modelling and simulation". *Renewable and Sustainable Energy Reviews* 82, pp. 1874–1908.

Cacciola, G. and Restuccia, G. (1995). "Reversible adsorption heat pump: a thermodynamic model". *International Journal of Refrigeration* 18.2, pp. 100–106.

Calabrese, L., Bruzzaniti, P., Palamara, D., Freni, A., and Proverbio, E. (2020). "New SAPO-34-SPEEK composite coatings for adsorption heat pumps: Adsorption performance and thermodynamic analysis". *Energy* 203.

Cao, N. V. and Chung, J. D. (2019). "Exergy Analysis of Adsorption Cooling Systems Based on Numerical Simulation". *Energy Technology* 7.1, pp. 153–166.

Chakraborty, A., Saha, B. B., Koyama, S., and Ng, K. C. (2007). "Specific heat capacity of a single component adsorbent-adsorbate system". *Applied Physics Letters* 90.17.

Chen, W. D. and Chua, K. J. (2020). "Parameter analysis and energy optimization of a four-bed, two-evaporator adsorption system". *Applied Energy* 265, p. 114842.

Chen, Y., Han, W., and Jin, H. (2017). "Proposal and analysis of a novel heat-driven absorption–compression refrigeration system at low temperatures". *Applied Energy* 185, pp. 2106–2116.

Choudhury, B., Saha, B. B., Chatterjee, P. K., and Sarkar, J. P. (2013). "An overview of developments in adsorption refrigeration systems towards a sustainable way of cooling". *Applied Energy* 104, pp. 554–567.

Chua, H. T., Ng, K. C., Malek, A., Kashiwagi, T., Akisawa, A., and Saha, B. B. (2001). "Multi-bed regenerative adsorption chiller — improving the utilization of waste heat

and reducing the chilled water outlet temperature fluctuation". *International Journal of Refrigeration* 24.2, pp. 124–136.

Chua, H. T., Ng, K. C., Wang, W., Yap, C., and Wang, X. L. (2004). "Transient modeling of a two-bed silica gel–water adsorption chiller". *International Journal of Heat and Mass Transfer* 47.4, pp. 659–669.

Ciconkov, R. (2018). "Refrigerants: There is still no vision for sustainable solutions". *International Journal of Refrigeration* 86, pp. 441–448.

Colorado, D. and Rivera, W. (2015). "Performance comparison between a conventional vapor compression and compression-absorption single-stage and double-stage systems used for refrigeration". *Applied Thermal Engineering* 87, pp. 273–285.

Colorado, D. and Velázquez, V. M. (2013). "Exergy analysis of a compression–absorption cascade system for refrigeration". *International Journal of Energy Research* 37.14, pp. 1851–1865.

Coulomb, D. (2016). "Statement given by Didier Coulomb, Director General of the International Institute of Refrigeration (IIR)". *22nd United Nations Climate Change Conference (COP 22)*. Marrakesh, Marocco.

Critoph, R. E. (1988). "Performance limitations of adsorption cycles for solar cooling". *Solar Energy* 41.1, pp. 21–31.

Critoph, R. E. (1999). "Forced convection adsorption cycle with packed bed heat regeneration: Cycle à adsorption à convection forcée avec régénération thermique du lit fixe". *International Journal of Refrigeration* 22.1, pp. 38–46.

Cyklis, P. (2014). "Two stage ecological hybrid sorption–compression refrigeration cycle". *International Journal of Refrigeration* 48, pp. 121–131.

Dalibard, A. (2013). *TRNSYS Type 821 - Closed wet cooling tower model for TRNSYS*. Report. Research Center for Sustainable Energy Technology.

Dalibard, A. (2017). "Advanced control strategies of solar driven adsorption chillers". PhD Thesis. Technische Universität Berlin.

Dalibard, A., Gürlich, D., Schneider, D., and Eicker, U. (2016). "Control Optimization of Solar Thermally Driven Chillers". *Energies* 9.11, pp. 864–878.

Dassault Systèmes (2020). *DYMOLA (Dynamic Modeling Laboratory) Systems Engineering: Multi-Engineering Modeling and Simulation based on Modelica and FMI*. `https://www.3ds.com/de/produkte-und-services/catia/produkte/dymola/`.

Dawoud, B., Vedder, U., Amer, E. H., and Dunne, S. (2007). "Non-isothermal adsorption kinetics of water vapour into a consolidated zeolite layer". *International Journal of Heat and Mass Transfer* 50.11, pp. 2190–2199.

Demir, H., Mobedi, M., and Ülkü, S. (2008). "A review on adsorption heat pump: Problems and solutions". *Renewable and Sustainable Energy Reviews* 12.9, pp. 2381–2403.

Deng, J., Wang, R. Z., and Han, G. Y. (2011). "A review of thermally activated cooling technologies for combined cooling, heating and power systems". *Progress in Energy and Combustion Science* 37.2, pp. 172–203.

Do, D. D. (1998). *Adsorption Analysis: Equilibria and Kinetics*. Vol. Volume 2. Series on Chemical Engineering. London: Imperial Collage Press.

Douss, N. and Meunier, F. (1989). "Experimental study of cascading adsorption cycles". *Chemical Engineering Science* 44.2, pp. 225–235.

Douss, N., Meunier, F. E., and Sun, L. M. (1988). "Predictive model and experimental results for a two-adsorber solid adsorption heat pump". *Industrial & Engineering Chemistry Research* 27.2, pp. 310–316.

Dubinin, M. M. (1960). "Theory of the physical adsorption of gases and vapors and adsorption properties of adsorbents of various natures and porous structures". *Bulletin of the Academy of Sciences of the USSR, Division of chemical science* 9.7, pp. 1072–1078.

Dubinin, M. M. (1967). "Adsorption in micropores". *Journal of Colloid and Interface Science* 23.4, pp. 487–499.

Dubinin, M. M. and Astakhov, V. A. (1971). "Description of Adsorption Equilibria of Vapors on Zeolites over Wide Ranges of Temperature and Pressure". *Molecular Sieve Zeolites-II*. Vol. 102. Advances in Chemistry. AMERICAN CHEMICAL SOCIETY. Chap. 44, pp. 69–85.

Dubinin, M. M. and Stoeckli, H. F. (1980). "Homogeneous and heterogeneous micropore structures in carbonaceous adsorbents". *Journal of Colloid and Interface Science* 75.1, pp. 34–42.

Eisentraut, A. and Brown, A. (2014). *Heating Without Global Warming: Market Developments and Policy Considerations for Renewable Heat*. Report. International Energy Agency.

Eurovent Certita Certification SAS (2018). *Eurovent Rating Standard for DX Air Coolers, Air Cooled Condensers, Dry Coolers*.

Federal Ministry for Economic Affairs and Energy (2019). *Eurostat - International comparison of electricity prices for industry*.

Fernández-Seara, J., Sieres, J., and Vázquez, M. (2006). "Compression–absorption cascade refrigeration system". *Applied Thermal Engineering* 26.5-6, pp. 502–512.

Franceschini, G. and Macchietto, S. (2008). "Model-based design of experiments for parameter precision: State of the art". *Chemical Engineering Science* 63.19, pp. 4846–4872.

Frazzica, A., Füldner, G., Sapienza, A., Freni, A., and Schnabel, L. (2014). "Experimental and theoretical analysis of the kinetic performance of an adsorbent coating composition for use in adsorption chillers and heat pumps". *Applied Thermal Engineering* 73.1, pp. 1022–1031.

Freni, A., Maggio, G., Cipitì, F., and Aristov, Y. I. (2012). "Simulation of water sorption dynamics in adsorption chillers: One, two and four layers of loose silica grains". *Applied Thermal Engineering* 44, pp. 69–77.

Freni, A., Bonaccorsi, L., Calabrese, L., Caprì, A., Frazzica, A., and Sapienza, A. (2015). "SAPO-34 coated adsorbent heat exchanger for adsorption chillers". *Applied Thermal Engineering* 82, pp. 1–7.

Frolov, T. and Mishin, Y. (2015). "Phases, phase equilibria, and phase rules in low-dimensional systems". *J Chem Phys* 143.4, p. 044706.

Fugmann, H., Nienborg, B., Trommler, G., Dalibard, A., and Schnabel, L. (2015). "Performance Evaluation of Air-Based Heat Rejection Systems". *Energies* 8.2, pp. 714–741.

Garimella, S., Brown, A. M., and Nagavarapu, A. K. (2011). "Waste heat driven absorption/vapor-compression cascade refrigeration system for megawatt scale, high-flux, low-temperature cooling". *International Journal of Refrigeration* 34.8, pp. 1776–1785.

Gerber, R. (2011). "Waste heat recovery of a transcritical CO2 system with adsorption technology". *ATMOsphere Europe 2011*. Brussels, Belgium.

German Aerospace Center (2019). *Optimization Library for Dymola (Version 2.2.4): Tutorial*. `https://www.systemcontrolinnovationlab.de/the-dlr-optimization-library/`.

German Institute for Standardization (2006). *DIN EN 12975-2:2006-06: Thermal solar systems and components - Solar collectors - Part 2: Test methods*.

Glueckauf, E. (1955). "Theory of chromatography Part 10.—Formulae for diffusion into spheres and their application to chromatography". *Transactions of the Faraday Society* 51, pp. 1540–1551.

Güntner Group Europe GmbH (2018). *Güntner Product Calculator (GPC)*. https://www.guentner.de/know-how/product-calculator-gpc/.

Goldsworthy, M. J. (2014). "Measurements of water vapour sorption isotherms for RD silica gel, AQSOA-Z01, AQSOA-Z02, AQSOA-Z05 and CECA zeolite 3A". *Microporous and Mesoporous Materials* 196, pp. 59–67.

Gong, L. X., Wang, R. Z., Xia, Z. Z., and Chen, C. J. (2011). "Design and performance prediction of a new generation adsorption chiller using composite adsorbent". *Energy Conversion and Management* 52.6, pp. 2345–2350.

Graf, R., Fidorra, N., Schröder, A., Ciganda, J. L. C., Ziegler, F., and Köhler, J. (2015). "Untersuchung der Kopplung von Absorptionskältemaschinen und CO2 Dampfkompressionsanlagen zur effizienten Kältebereitstellung". *Deutsche Kälte- und Klimatagung*. Dresden, Germany.

Graf, S., Eibel, S., Lanzerath, F., and Bardow, A. (2020). "Validated Performance Prediction of Adsorption Chillers: Bridging the Gap from Gram-Scale Experiments to Full-Scale Chillers". *Energy Technology* 8.5.

Gräber, M., Kirches, C., Bock, H. G., Schlöder, J. P., Tegethoff, W., and Köhler, J. (2011). "Determining the optimum cyclic operation of adsorption chillers by a direct method for periodic optimal control". *International Journal of Refrigeration* 34.4, pp. 902–913.

Gullo, P., Hafner, A., and Cortella, G. (2017). "Multi-ejector R744 booster refrigerating plant and air conditioning system integration – A theoretical evaluation of energy benefits for supermarket applications". *International Journal of Refrigeration* 75, pp. 164–176.

Hafner, A., Forsterling, S., and Banasiak, K. (2014). "Multi-ejector concept for R-744 supermarket refrigeration". *International Journal of Refrigeration* 43, pp. 1–13.

Hamamoto, Y., Amanul Alam, K. C., Akisawa, A., and Kashiwagi, T. (2005). "Performance evaluation of a two-stage adsorption refrigeration cycle with different mass ratio". *International Journal of Refrigeration* 28.3, pp. 344–352.

Hassan, A. A., Elwardany, A. E., Ookawara, S., Ahmed, M., and El-Sharkawy, I. I. (2020). "Integrated adsorption-based multigeneration systems: A critical review and future trends". *International Journal of Refrigeration* 116, pp. 129–145.

Hauer, A. (2002). "Beurteilung fester Adsorbentien in offenen Sorptionssystemen für energetische Anwendungen (in German)". Doctoral Thesis. Technische Universität Berlin.

Heating, R. American Society of and Engineers, A.-C. (2016). *Ashrae Handbook: HVAC Systems and Equipment: SI Edition*. ASHRAE.

Heijde, B. van der, Fuchs, M., Ribas Tugores, C., Schweiger, G., Sartor, K., Basciotti, D., Müller, D., Nytsch-Geusen, C., Wetter, M., and Helsen, L. (2017). "Dynamic equation-based thermo-hydraulic pipe model for district heating and cooling systems". *Energy Conversion and Management* 151, pp. 158–169.

Helm, M. (2015). *Task 48: Quality Assurance and Support Measures for Solar Cooling - Pump Efficiency and Adaptability*. Report. International Energy Agency, Solar Heating and Cooling Programme.

Henning, H., Motta, M., and Mugnier, D. (2013). *Solar Cooling Handbook: A Guide to Solar Assisted Cooling and Dehumidification Processes*. 3rd. Vienna: Ambra |5.

Huber, M. L., Perkins, R. A., Laesecke, A., Friend, D. G., Sengers, J. V., Assael, M. J., Metaxa, I. N., Vogel, E., Mareš, R., and Miyagawa, K. (2009). "New International Formulation for the Viscosity of H2O". *Journal of Physical and Chemical Reference Data* 38.2, pp. 101–125.

Huber, M. L., Perkins, R. A., Friend, D. G., Sengers, J. V., Assael, M. J., Metaxa, I. N., Miyagawa, K., Hellmann, R., and Vogel, E. (2012). "New International Formulation for the Thermal Conductivity of H2O". *Journal of Physical and Chemical Reference Data* 41.3, p. 033102.

Institute of Technical Thermodynamics, RWTH Aachen (2020). *SorpLib - Adsorption Energy Systems Library*. `https://www.git.rwth-aachen.de/ltt/SorpLib`.

Intergovernmental Panel on Climate Change (2018). "Special report on the impacts of gloabal warming of 1.5 °C". *24st Conference of the Parties*.

International Energy Agency (2015). *Solar Heating and Cooling Programme Task 48: Quality Assurance and Support Measures for Solar Cooling*. `https://www.task48.iea-shc.org/`.

Invensor GmbH (2020). *Adsorption Chiller InvenSor LTC 30 e plus*. `https://www.invensor.com/en/products/invensor-ltc-30-e-plus/`.

Jaehnig, D. and Thuer, A. (2011). *Task 38: Solar Air-Conditioning and Refrigeration - Monitoring Results*. Report. International Energy Agency, Solar Heating and Cooling Programme.

Jain, V., Sachdeva, G., and Kachhwaha, S. S. (2015). "Energy, exergy, economic and environmental (4E) analyses based comparative performance study and optimization of vapor compression-absorption integrated refrigeration system". *Energy* 91, pp. 816–832.

Karagiorgas, M. and Meunier, F. (1987). “The dynamics of a solid-adsorption heat pump connected with outside heat sources of finite capacity”. *Heat Recovery Systems and CHP* 7.3, pp. 285–299.

Kast, W. (1988). *Adsorption aus der Gasphase: Ingenieurwissenschaftliche Grundlagen und technische Verfahren*. Vol. 1. Weinheim: VCH Verlagsgesellschaft.

Keller, J. U. and Staudt, R. (2005). *Gas Adsorption Equilibria - Experimental Methods and Adsorptive Isotherms*. Boston: Springer Science + Business Media.

Kojok, F., Fardoun, F., Younes, R., and Outbib, R. (2016). “Hybrid cooling systems: A review and an optimized selection scheme”. *Renewable and Sustainable Energy Reviews* 65, pp. 57–80.

Koller, R. W. and Ricardez-Sandoval, L. A. (2017). “A dynamic optimization framework for integration of design, control and scheduling of multi-product chemical processes under disturbance and uncertainty”. *Computers & Chemical Engineering* 106, pp. 147–159.

Krzywanski, J., Grabowska, K., Herman, F., Pyrka, P., Sosnowski, M., Prauzner, T., and Nowak, W. (2017). “Optimization of a three-bed adsorption chiller by genetic algorithms and neural networks”. *Energy Conversion and Management* 153, pp. 313–322.

Langmuir, I. (1918). “The adsorption of gases on plane surfaces of glass, mica and platinum”. *Journal of the American Chemical Society* 40.9, pp. 1361–1403.

Lanzerath, F. (2013). “Modellgestützte Entwicklung von Adsorptionswärmepumpen (in German)”. PhD Thesis. RWTH Aachen University.

Lanzerath, F., Bau, U., Seiler, J., and Bardow, A. (2015). “Optimal design of adsorption chillers based on a validated dynamic object-oriented model”. *Science and Technology for the Built Environment* 21.3, pp. 248–257.

Lanzerath, F., Seiler, J., Erdogan, M., Schreiber, H., Steinhilber, M., and Bardow, A. (2016). “The impact of filling level resolved: Capillary-assisted evaporation of water for adsorption heat pumps”. *Applied Thermal Engineering* 102.5, pp. 513–519.

Lazrak, A., Boudehenn, F., Bonnot, S., Fraisse, G., Leconte, A., Papillon, P., and Souyri, B. (2016). “Development of a dynamic artificial neural network model of an absorption chiller and its experimental validation”. *Renewable Energy* 86, pp. 1009–1022.

Le Denn, A., Boudehenn, F., Mugnier, D., and Papillon, P. (2013). “A simple predesign tool for solar cooling, heating and domestic hot water production systems”. *13th Conference of International Building Performance Simulation*. Chambéry, France, pp. 1031–1038.

Lee, J.-G., Bae, K. J., and Kwon, O. K. (2020). “Performance Investigation of a Two-Bed Type Adsorption Chiller with Various Adsorbents”. *Energies* 13.10.

Leineweber, D. B., Bauer, I., Bock, H. G., and Schlöder, J. P. (2003). "An efficient multiple shooting based reduced SQP strategy for large-scale dynamic process optimization. (Parts I and II)". *Computers & Chemical Engineering* 27.2, pp. 157–174.

Lemmon, E. W., McLinden, M. O., and Friend, D. G. (2013). *Thermophysical properties of fluid systems*. NIST Standard Reference Database. Gaithersburg: NIST.

Leong, K. C. and Liu, Y. (2004a). "Numerical modeling of combined heat and mass transfer in the adsorbent bed of a zeolite/water cooling system". *Applied Thermal Engineering* 24.16, pp. 2359–2374.

Leong, K. C. and Liu, Y. (2004b). "Numerical study of a combined heat and mass recovery adsorption cooling cycle". *International Journal of Heat and Mass Transfer* 47.22, pp. 4761–4770.

Leong, K. C. and Liu, Y. (2006). "System performance of a combined heat and mass recovery adsorption cooling cycle: A parametric study". *International Journal of Heat and Mass Transfer* 49.15-16, pp. 2703–2711.

Li, X. H., Hou, X. H., Zhang, X., and Yuan, Z. X. (2015). "A review on development of adsorption cooling—Novel beds and advanced cycles". *Energy Conversion and Management* 94, pp. 221–232.

Liaw, C. H., Wang, J. S. P., Greenkorn, R. A., and Chao, K. C. (1979). "Kinetics of fixed-bed adsorption: A new solution". *AIChE Journal* 25.2, pp. 376–381.

Luberti, M., Di Santis, C., and Santori, G. (2020). "Ammonia/Ethanol Mixture for Adsorption Refrigeration". *Energies* 13.4.

MacNamara, S. and Strang, G. (2016). "Operator Splitting". *Splitting Methods in Communication, Imaging, Science, and Engineering*. Ed. by R. Glowinski, S. J. Osher, and W. Yin. Cham: Springer International Publishing, pp. 95–114.

Maggio, G., Freni, A., and Restuccia, G. (2006). "A dynamic model of heat and mass transfer in a double-bed adsorption machine with internal heat recovery". *International Journal of Refrigeration* 29.4, pp. 589–600.

Mahdavikhah, M. and Niazmand, H. (2013). "Effects of plate finned heat exchanger parameters on the adsorption chiller performance". *Applied Thermal Engineering* 50.1, pp. 939–949.

Marimón, M. A., Arias, J., Lundqvist, P., Bruno, J. C., and Coronas, A. (2011). "Integration of trigeneration in an indirect cascade refrigeration system in supermarkets". *Energy and Buildings* 43.6, pp. 1427–1434.

Marletta, L., Maggio, G., Freni, A., Ingrasciotta, M., and Restuccia, G. (2002). "A non-uniform temperature non-uniform pressure dynamic model of heat and mass transfer in compact adsorbent beds". *International Journal of Heat and Mass Transfer* 45.16, pp. 3321–3330.

Melograno, P. N., Vasta, S., Boudehenn, F., Fedrizzi, R., and Doell, J. (2015). *Task 48: Quality Assurance and Support Measures for Solar Cooling - Chiller Characterization*. Report. International Energy Agency, Solar Heating and Cooling Programme.

Metcalf, S. J., Critoph, R. E., and Tamainot-Telto, Z. (2012). "Optimal cycle selection in carbon-ammonia adsorption cycles". *International Journal of Refrigeration* 35.3, pp. 571–580.

Meteotest AG (2018). *Meteonorm Software - Global irradiation and climate data*. `https://www.meteonorm.com/`.

Meunier, F. (2013). "Adsorption heat powered heat pumps". *Applied Thermal Engineering* 61.2, pp. 830–836.

Meunier, F., Neveu, P., and Castaing-Lasvignottes, J. (1998). "Equivalent Carnot cycles for sorption refrigeration: Cycles de Carnot équivalents pour la production de froid par sorption". *International Journal of Refrigeration* 21.6, pp. 472–489.

Mhimid, A. (1998). "Theoretical study of heat and mass transfer in a zeolite bed during water desorption: validity of local thermal equilibrium assumption". *International Journal of Heat and Mass Transfer* 41.19, pp. 2967–2977.

Miyazaki, T. and Akisawa, A. (2009). "The influence of heat exchanger parameters on the optimum cycle time of adsorption chillers". *Applied Thermal Engineering* 29.13, pp. 2708–2717.

Modelica Association (2017). *Modelica ® - A Unified Object-Oriented Language for Systems Modeling, Language Specification Version 3.4*. `https://www.modelica.org/documents/ModelicaSpec34.pdf`.

Mohammadi, S. M. H. and Ameri, M. (2016). "Energy and exergy performance comparison of different configurations of an absorption-two-stage compression cascade refrigeration system with carbon dioxide refrigerant". *Applied Thermal Engineering* 104, pp. 104–120.

Mohammed, R. H., Mesalhy, O., Elsayed, M. L., and Chow, L. C. (2019). "Assessment of numerical models in the evaluation of adsorption cooling system performance". *International Journal of Refrigeration* 99, pp. 166–175.

Mugnier, D., Neyer, D., and White, S. (2017). *The Solar Cooling Design Guide: Case Studies of Successful Solar Air Conditioning Design*. 1st. Berlin: Wilhelm Ernst & Sohn.

Mugnier, D. (2015). *Task 48: Quality Assurance and Support Measures for Solar Cooling - Solar Cooling Position Paper*. Report. International Energy Agency, Solar Heating and Cooling Programme.

Mugnier, D. and Jakob, U. (2015). "Status of solar cooling in the World: markets and available products". *Wiley Interdisciplinary Reviews: Energy and Environment* 4.3, pp. 229–234.

Nöding, M., Fidorra, N., Gräber, M., and Köhler, J. (2016). "Operation strategy for heat recovery of transcritical CO2 refrigeration systems with heat storages". *29th International Conference on Efficiency, Cost, Optimization, Simulation and Environmental Impact of Energy systems*. Portorož, Slovenia.

Neyer, D., Neyer, J., Thür, A., Fedrizzi, R., Vittoriosi, A., White, S., and Focke, H. (2015). *Task 48: Quality Assurance and Support Measures for Solar Cooling - Collection of criteria to quantify the quality and cost competitiveness for solar cooling systems*. Report. International Energy Agency, Solar Heating and Cooling Programme.

Núñez, T. (2001). "Charakterisierung und Bewertung von Adsorbentien für Wärmetransformationsanwendungen (in German)". PhD Thesis. Albert-Ludwigs-Universität Freiburg.

Núñez, T., Mittelbach, W., and Henning, H.-M. (2007). "Development of an adsorption chiller and heat pump for domestic heating and air-conditioning applications". *Applied Thermal Engineering* 27.13, pp. 2205–2212.

Niazmand, H., Talebian, H., and Mahdavikhah, M. (2012). "Bed geometrical specifications effects on the performance of silica/water adsorption chillers". *International Journal of Refrigeration* 35.8, pp. 2261–2274.

Nienborg, B., Dalibard, A., Schnabel, L., and Eicker, U. (2017). "Approaches for the optimized control of solar thermally driven cooling systems". *Applied Energy* 185, pp. 732–744.

Nienborg, B., Helling, T., Fröhlich, D., Horn, R., Munz, G., and Schossig, P. (2018). "Closed Adsorption Heat Storage—A Life Cycle Assessment on Material and Component Levels". *Energies* 11.12, p. 3421.

Nocedal, J. and Wright, S. J. (2006). *Numerical optimization*. 2nd. Springer series in operations research. New York: Springer Science+Business Media, LLC.

Okunev, B. N., Gromov, A. P., Heifets, L. I., and Aristov, Y. I. (2008). "Dynamics of water sorption on a single adsorbent grain caused by a large pressure jump: Modeling of coupled heat and mass transfer". *International Journal of Heat and Mass Transfer* 51.25, pp. 5872–5876.

Oppelt, T., Urbaneck, T., Gross, U., and Platzer, B. (2016). “Dynamic thermo-hydraulic model of district cooling networks”. *Applied Thermal Engineering* 102, pp. 336–345.

Palomba, V., Ferraro, M., Frazzica, A., Vasta, S., Sergi, F., and Antonucci, V. (2018). “Experimental and numerical analysis of a SOFC-CHP system with adsorption and hybrid chillers for telecommunication applications”. *Applied Energy* 216, pp. 620–633.

Palomba, V., Wittstadt, U., Bonanno, A., Tanne, M., Harborth, N., and Vasta, S. (2019a). “Components and design guidelines for solar cooling systems: The experience of ZEOSOL”. *Renewable Energy* 141, pp. 678–692.

Palomba, V., Varvagiannis, E., Karellas, S., and Frazzica, A. (2019b). “Hybrid Adsorption-Compression Systems for Air Conditioning in Efficient Buildings: Design through Validated Dynamic Models”. *Energies* 12.6.

Palomba, V., Dino, G. E., and Frazzica, A. (2020). “Coupling sorption and compression chillers in hybrid cascade layout for efficient exploitation of renewables: Sizing, design and optimization”. *Renewable Energy* 154, pp. 11–28.

Passos, E. F., Escobedo, J. F., and Meunier, F. (1989). “Simulation of an intermittent adsorptive solar cooling system”. *Solar Energy* 42.2, pp. 103–111.

Pesaran, A., Lee, H., Hwang, Y., Radermacher, R., and Chun, H.-H. (2016). “Review article: Numerical simulation of adsorption heat pumps”. *Energy* 100, pp. 310–320.

Pfeiffer, A. (2012). “Optimization Library for Interactive Multi-Criteria Optimization Tasks”. *Proceedings of the 9th International Modelica Conference*. Munich, Germany, pp. 669–679.

Polanyi, M. (1916). “Adsorption von Gasen (Dämpfen) durch ein festes nichtflüchtiges Adsorbens”. *Verhandlungen der DEutschen Physikalischen Gesellschaft* 18, pp. 55–60.

Polanyi, M. (1932). “Section III.—Theories of the adsorption of gases. A general survey and some additional remarks. Introductory paper to section III”. *Transactions of the Faraday Society* 28.0, pp. 316–333.

Pons, M. and Poyelle, F. (1999). “Adsorptive machines with advanced cycles for heat pumping or cooling applications: Cycles á adsorption pour pompes á chaleur ou machines frigor: figues”. *International Journal of Refrigeration* 22.1, pp. 27–37.

Postweiler, P. (2019). “Experimental validation of a dynamic adsorption chiller model using dynamic optimisation for parameter estimation and optimal experimental design”. MA thesis. RWTH Aachen University.

Qian, S., Gluesenkamp, K., Hwang, Y., Radermacher, R., and Chun, H.-H. (2013). "Cyclic steady state performance of adsorption chiller with low regeneration temperature zeolite". *Energy* 60, pp. 517–526.

Radu, A. I., Defraeye, T., Ruch, P., Carmeliet, J., and Derome, D. (2017). "Insights from modeling dynamics of water sorption in spherical particles for adsorption heat pumps". *International Journal of Heat and Mass Transfer* 105, pp. 326–337.

Rao, A. V. (2010). "A Survey of Numerical Methods for Optimal Control". *Advances in the Astronautical Sciences* 135, pp. 497–528.

Raymond, A. and Garimella, S. (2011). "Intraparticle Mass Transfer in Adsorption Heat Pumps: Limitations of the Linear Driving Force Approximation". *Journal of Heat Transfer* 133.4.

Restuccia, G., Freni, A., and Maggio, G. (2002). "A zeolite-coated bed for air conditioning adsorption systems: parametric study of heat and mass transfer by dynamic simulation". *Applied Thermal Engineering* 22.6, pp. 619–630.

Rezk, A. R. M. and Al-Dadah, R. K. (2012). "Physical and operating conditions effects on silica gel/water adsorption chiller performance". *Applied Energy* 89.1, pp. 142–149.

Riffel, D. B., Wittstadt, U., Schmidt, F. P., Núñez, T., Belo, F. A., Leite, A. P. F., and Ziegler, F. (2010). "Transient modeling of an adsorber using finned-tube heat exchanger". *International Journal of Heat and Mass Transfer* 53.7, pp. 1473–1482.

Roetzel, W., Luo, X., and Chen, D. (2020). "Design and Operation of Heat Exchangers and their Networks". *Design and Operation of Heat Exchangers and their Networks*. Elsevier Inc. Chap. Dynamic analysis of heat exchangers and their networks, pp. 319–390.

Ruthven, D. M. (1984). *Principles of Adsorption and Adsorption Processes*. Vol. 1. Edition. New York: John Wiley & Sons.

Sah, R. P., Choudhury, B., Das, R. K., and Sur, A. (2017). "An overview of modelling techniques employed for performance simulation of low–grade heat operated adsorption cooling systems". *Renewable and Sustainable Energy Reviews* 74, pp. 364–376.

Sakoda, A. and Suzuki, M. (1986). "Simultaneous Transport of Heat and Adsorbate in Closed Type Adsorption Cooling System Utilizing Solar Heat". *Journal of Solar Energy Engineering* 108.3, pp. 239–245.

Sakoda, A. and Suzuki, M. (1984). "Fundamental study on solar powered adsorption cooling system". *Journal of Chemical Engineering of Japan* 17.1, pp. 52–57.

Salajeghe, M. and Ameri, M. (2016). “Effects of further cooling the gas cooler outlet refrigerant by an absorption chiller, on a transcritical CO2-compression refrigeration system”. *International Journal of Exergy* 21.1, p. 110.

Santori, G., Sapienza, A., and Freni, A. (2012). “A dynamic multi-level model for adsorptive solar cooling”. *Renewable Energy* 43, pp. 301–312.

Sapienza, A., Santamaria, S., Frazzica, A., and Freni, A. (2011). “Influence of the management strategy and operating conditions on the performance of an adsorption chiller”. *Energy* 36.9, pp. 5532–5538.

Sarkar, J., Bhattacharyya, S., and Gopal, M. R. (2004). “Optimization of a transcritical CO2 heat pump cycle for simultaneous cooling and heating applications”. *International Journal of Refrigeration* 27.8, pp. 830–838.

Sarkar, J., Bhattacharyya, S., and Ramgopal, M. (2008). “A transcritical CO2 heat pump for simultaneous water cooling and heating: Test results and model validation”. *International Journal of Energy Research* 33.1, pp. 100–109.

Sartor, K. and Dewalef, P. (2017). “Experimental validation of heat transport modelling in district heating networks”. *Energy* 137, pp. 961–968.

Sawalha, S. (2013). “Investigation of heat recovery in CO2 trans-critical solution for supermarket refrigeration”. *International Journal of Refrigeration* 36.1, pp. 145–156.

Sawant, P., Bürger, A., Doan, M. D., Felsmann, C., and Pfafferott, J. (2020). “Development and experimental evaluation of grey-box models of a microscale polygeneration system for application in optimal control”. *Energy and Buildings* 215.

Schawe, D. (1999). “Theoretical and experimental investigations of an adsorption heat pump with heat transfer between two adsorbers”. PhD Thesis. University of Stuttgart.

Scherle, M. and Nieken, U. (2020). “Simultaneous Optimization of Process Operational and Material Parameters for a 2-Bed Adsorption Refrigeration Process”. *ChemEngineering* 4.2.

Schicktanz, M. and Núñez, T. (2009). “Modelling of an adsorption chiller for dynamic system simulation”. *International Journal of Refrigeration* 32.4, pp. 588–595.

Schmidt, E. F. (1967). “Wärmeübergang und Druckverlust in Rohrschlangen”. *Chemie Ingenieur Technik - CIT* 39.13, pp. 781–789.

Schnabel, L. (2009). “Experimentelle und numerische Untersuchung der Adsorptionskinetik von Wasser an Adsorbens-Metallverbundstrukturen (in German)”. PhD Thesis. Technische Universität Berlin.

Schulze, C. W. (2013). "A Contribution to Numerically Efficient Modelling of Thermodynamic Systems". PhD Thesis. Technical University of Braunschweig.

Söderlind, G. and Wang, L. (2006). "Evaluating numerical ODE/DAE methods, algorithms and software". *Journal of Computational and Applied Mathematics* 185.2, pp. 244–260.

Semmari, H., Marc, O., Praene, J.-P., Le Denn, A., Boudéhenn, F., and Lucas, F. (2014). "Sensitivity Analysis of the New Sizing Tool "PISTACHE" for Solar Heating, Cooling and Domestic Hot Water Systems". *Energy Procedia* 48, pp. 997–1006.

Sharafian, A. and Bahrami, M. (2014). "Assessment of adsorber bed designs in waste-heat driven adsorption cooling systems for vehicle air conditioning and refrigeration". *Renewable and Sustainable Energy Reviews* 30, pp. 440–451.

Sharafian, A. and Bahrami, M. (2015). "Critical analysis of thermodynamic cycle modeling of adsorption cooling systems for light-duty vehicle air conditioning applications". *Renewable and Sustainable Energy Reviews* 48, pp. 857–869.

Sharafian, A., McCague, C., and Bahrami, M. (2015). "Impact of fin spacing on temperature distribution in adsorption cooling system for vehicle A/C applications". *International Journal of Refrigeration* 51, pp. 135–143.

Sharma, V., Fricke, B., and Bansal, P. (2014). "Comparative analysis of various CO2 configurations in supermarket refrigeration systems". *International Journal of Refrigeration* 46, pp. 86–99.

Shelton, S. V., Wepfer, W. J., and Miles, D. J. (1989). "Square wave analysis of the solid-vapor adsorption heat pump". *Heat Recovery Systems and CHP* 9.3, pp. 233–247.

Sieder, E. N. and Tate, G. E. (1936). "Heat Transfer and Pressure Drop of Liquids in Tubes". *Industrial & Engineering Chemistry* 28.12, pp. 1429–1435.

Sircar, S. and Hufton, J. R. (2000). "Why Does the Linear Driving Force Model for Adsorption Kinetics Work?" *Adsorption* 6.2, pp. 137–147.

Speerforck, A. and Schmitz, G. (2015). "Integration of an adsorption chiller in an open-cycle desiccant-assisted air-conditioning system". *Science and Technology for the Built Environment* 21.3, pp. 375–383.

Srinivasan, K., Sheahen, P., and Sarathy, C. S. P. (2010). "Optimum thermodynamic conditions for upper pressure limits of transcritical carbon dioxide refrigeration cycle". *International Journal of Refrigeration* 33.7, pp. 1395–1401.

Stabat, P. and Marchio, D. (2004). "Simplified model for indirect-contact evaporative cooling-tower behaviour". *Applied Energy* 78.4, pp. 433–451.

Teng, W. S., Leong, K. C., and Chakraborty, A. (2016). "Revisiting adsorption cooling cycle from mathematical modelling to system development". *Renewable and Sustainable Energy Reviews* 63, pp. 315–332.

Thome, J. (2010). *The Heat Transfer Engineering Data Book III: Enhanced heat transfer design methods for tubular heat exchangers*. 3rd. Ulm: Wieland-Werke AG.

Tso, C. Y., Chao, C. Y. H., and Fu, S. C. (2012). "Performance analysis of a waste heat driven activated carbon based composite adsorbent – Water adsorption chiller using simulation model". *International Journal of Heat and Mass Transfer* 55.25-26, pp. 7596–7610.

Tummescheit, H. (2002). "Design and Implementation of Object-Oriented Model Libraries using Modelica". PhD Thesis. Lund University.

United Nations (2015). "Adoption of the Paris Agreement". *21st Conference of the Parties*.

Vasta, S., Palomba, V., La Rosa, D., and Mittelbach, W. (2018). "Adsorption-compression cascade cycles: An experimental study". *Energy Conversion and Management* 156, pp. 365–375.

Verde, M., Cortés, L., Corberán, J. M., Sapienza, A., Vasta, S., and Restuccia, G. (2010). "Modelling of an adsorption system driven by engine waste heat for truck cabin A/C. Performance estimation for a standard driving cycle". *Applied Thermal Engineering* 30.13, pp. 1511–1522.

Wagner, W. and Pruß, A. (2002). "The IAPWS Formulation 1995 for the Thermodynamic Properties of Ordinary Water Substance for General and Scientific Use". *Journal of Physical and Chemical Reference Data* 31.2, pp. 387–535.

Wang, X. and Chua, H. T. (2007). "Two bed silica gel–water adsorption chillers: An effectual lumped parameter model". *International Journal of Refrigeration* 30.8, pp. 1417–1426.

Wang, X., Chua, H. T., and Ng, K. C. (2005). "Experimental investigation of silica gel–water adsorption chillers with and without a passive heat recovery scheme". *International Journal of Refrigeration* 28.5, pp. 756–765.

Wang, X., He, Z., and Chua, H. T. (2015). "Performance simulation of multi-bed silica gel-water adsorption chillers". *International Journal of Refrigeration* 52, pp. 32–41.

Weber, C., Mehling, F., Fregin, A., Daßler, I., and Schossig, P. (2014). "On Standardizing Solar Cooling – Field Test in the Small Capacity Range". *Energy Procedia* 48, pp. 1027–1035.

Wu, J. Y., Wang, R. Z., and Xu, Y. X. (2000). "Dynamic simulation and experiments of a heat regenerative adsorption heat pump". *Energy Conversion and Management* 41.10, pp. 1007–1018.

Wu, X., Hu, S., and Mo, S. (2013). "Carbon footprint model for evaluating the global warming impact of food transport refrigeration systems". *Journal of Cleaner Production* 54, pp. 115–124.

Yaïci, W. and Entchev, E. (2019). "Coupled unsteady computational fluid dynamics with heat and mass transfer analysis of a solar/heat-powered adsorption cooling system for use in buildings". *International Journal of Heat and Mass Transfer* 144, p. 118648.

Yang, L., Li, H., Cai, S.-W., Shao, L.-L., and Zhang, C.-L. (2015). "Minimizing COP loss from optimal high pressure correlation for transcritical CO2 cycle". *Applied Thermal Engineering* 89, pp. 656–662.

Yong, L. and Sumathy, K. (2002). "Review of mathematical investigation on the closed adsorption heat pump and cooling systems". *Renewable and Sustainable Energy Reviews* 6.4, pp. 305–338.

Zhang, L. Z. and Wang, L. (1999). "Effects of coupled heat and mass transfers in adsorbent on the performance of a waste heat adsorption cooling unit". *Applied Thermal Engineering* 19.2, pp. 195–215.

Zhao, Y., Hu, E., and Blazewicz, A. (2012). "Dynamic modelling of an activated carbon–methanol adsorption refrigeration tube with considerations of interfacial convection and transient pressure process". *Applied Energy* 95, pp. 276–284.

Ziegler, F. (2009). "Sorption heat pumping technologies: Comparisons and challenges". *International Journal of Refrigeration* 32.4, pp. 566–576.

Zolcer Skačanová, K. and Battesti, M. (2019). "Global market and policy trends for CO2 in refrigeration". *International Journal of Refrigeration* 107, pp. 98–104.

Aachener Beiträge zur Technischen Thermodynamik

ABTT 1
Philip Voll
Automated Optimization-Based Synthesis of Distributed Energy Supply Systems
1. Auflage 2014
ISBN 978-3-86130-474-6

ABTT 2
Johannes Jung
Comparative Life Cycle Assessment of Industrial Multi-Product Processes
1. Auflage 2014
ISBN 978-3-86130-471-5

ABTT 3
Franz Lanzerath
Modellgestützte Entwicklung von Adsorptionswärmepumpen
1. Auflage 2014
ISBN 978-3-86130-472-2

ABTT 4
Thorsten Brands
Einfluss der Gemischzusammensetzung auf die Verbrennung im Diesel- und GCAI-Motor
1. Auflage 2014
ISBN 978-3-95886-006-3

ABTT 5
Dominique Dechambre
Efficient Measurement of Liquid-Liquid Equilibria using Automation and Optimal Experimental Design
1. Auflage 2016
ISBN 978-395886-077-3

ABTT 6
Niklas von der Aßen
From Life-Cycle Assesement towards life-Cycle Design of Carbon Dioxide Capture and Utilization
1. Auflage 2016
ISBN 978-3-95886-080-3

ABTT 7
Matthias Lampe
Integrated Process and Organic Rankine Cycle Working Fluid Design in the Continuous-Molecular Targeting Framework
1. Auflage 2016
ISBN 978-3-95886-086-5

ABTT 8
Thomas Hülser
Optische Untersuchung der Zündvorgänge und deren Auswirkung auf die Verbrennung in PKW-Motoren
1. Auflage 2016
ISBN 978-3-95886-090-2

Aachener Beiträge zur Technischen Thermodynamik

ABTT 9
Malte Döntgen
Reaction Models from Reactive Molecular Dynamics and High-Level Kinetics Predictions
1. Auflage 2016
ISBN 978-3-95886-156-5

ABTT 10
Heike Schreiber
Experiments and Validated Models for Adsorption Thermal Energy Storage in Industrial and Residential Application
1. Auflage 2017
ISBN 978-3-95886-178-7

ABTT 11
André Dirk Sternberg
System-Wide Perspective for Life Cycle Assesment of CO_2-based C1-Chemicals
1. Auflage 2017
ISBN 978-3-95886-193-0

ABTT 12
Uwe Bau
From Dynamic Simulation to Optimal Design and Control of Adsorption Energy Systems
1. Auflage 2018
ISBN 978-3-95886-216-6

ABTT 13
Christian Jens
Modellbasiertes Design von Produkt, Lösungsmittel und Prozess für die Ameisensäure-synthese aus CO_2 und H_2
1. Auflage 2018
ISBN 978-3-95886-231-9

ABTT 14
Jan David Scheffczyk
Integrated Computer-Aided Design of Molecules and Processes using COSMO-RS
1. Auflage 2018
ISBN 978-3-95886-236-4

ABTT 15
Björn Bahl
Optimization-Based Synthesis of Large-Scale Energy Systems by Time-Series Aggregation
1. Auflage 2018
ISBN 978-3-95886-240-1

Aachener Beiträge zur Technischen Thermodynamik

ABTT 16
Bastian Liebergesell
A Milliliter-Scale Setup for the Efficient Characterization of Multicomponent Vapor-Liquid Equilibria Using Raman Spectroscopy
1. Auflage 2018
ISBN 978-3-95886-247-0

ABTT 17
Stefan Wilhelm Graf
A Design Approach for Adsorption Energy Systems Integrating Dynamic Modeling with Small-Scale Experiments
1. Auflage 2018
ISBN 978-3-95886-258-6

ABTT 18
Sebastian Kaminski
Quantum-Mechanics-Based Prediction of SAFT Parameters for Non-Associating and Associating Molecules Containing Carbon, Hydrogen, Oxygen and Nitrogen
1. Auflage 2019
ISBN 978-3-95886-270-8

ABTT 19
Maike Renate Hennen
Decision Support for the Synthesis of Energy Systems by Analysis of the Near-Optimal Solution Space
1. Auflage 2019
ISBN 978-3-95886-277-7

ABTT 20
Peyman Yamin
COSMO-RS-Based Methods for Improved Modelling of Complex Chemical Systems
1. Auflage 2019
ISBN 978-3-95886-288-3

ABTT 21
Meltem Erdogan
Assessement of Adsorbents for Drying by Experiments and Dynamic Simulations
1. Auflage 2019
ISBN 978-3-95886-303-3

ABTT 22
Christian Schulz
SRS/LIF-Messungen zur Charakterisierung rußarmer dieselähnlicher Flammen von alternativen Kraftstoffen und n-Heptan
1. Auflage 2019
ISBN 978-3-91886-310-1

Aachener Beiträge zur Technischen Thermodynamik

ABTT 23
Peter Beumers
Physically-Based Models for the Analysis of Raman Spectra
1. Auflage 2019
ISBN 978-3-95886-319-4

ABTT 24
Arne Kätelhön
Technology Choice Model for Consequential Life Cycle Assessment
1. Auflage 2019
ISBN 978-3-95886-324-8

ABTT 25
Christine Peters
Measurement of Multicomponent Diffusion in Liquids Using Raman Microspectroscopy and Microfluidics
1. Auflage 2020
ISBN 978-3-95886-337-8

ABTT 26
Dinah Elena Hollermann
Reliable and Robust Optimal Design of Sustainable Energy Systems
1. Auflage 2020
ISBN 978-3-95886-346-0

ABTT 27
Thomas Raffius
Laserspektroskopische Analyse von selbstzündenden motorischen Einspritzstrahlen alternativer Biokraftstoffe
1. Auflage 2020
ISBN 978-3-95886-358-3

ABTT 28
Johannes Schilling
Integrated Thermo-Economic Design of Processes and Molecules Using PC-SAFT
1. Auflage 2020
ISBN 978-3-95886-368-2

ABTT 29
Nils Julius Baumgärtner
Optimization of Low-Carbon Energy Systems from Industrial to National Scale
1. Auflage 2020
ISBN 978-3-95886-385-9

ABTT 30
Ludger Wolff
From Model-based Experimental Design and Analysis of Diffusion and Liquid-Liquid Equilibria to Process Applications
1. Auflage 2020
ISBN 978-3-95886-402-3

Aachener Beiträge zur Technischen Thermodynamik

ABTT 31
Andrej Gibelhaus
A Model-based Framework for Optimal Systems Integration of Adsorption Chillers
1. Auflage 2021
ISBN 978-3-95886-406-1